Naval Research Laboratory

Washington, DC 20375-5320

NRL/MR/5650--12-9456

Design and Performance of Ka-Band Fiber-Optic Delay Lines

Vincent J. Urick
Joseph M. Singley
Christopher E. Sunderman
John F. Diehl
Keith J. Williams

Photonics Technology Branch
Optical Sciences Division

December 28, 2012

REPORT DOCUMENTATION PAGE

Form Approved
OMB No. 0704-0188

1. REPORT DATE *(DD-MM-YYYY)*	2. REPORT TYPE	3. DATES COVERED *(From - To)*
28-12-2012	Memorandum	09 March 2012 - 27 September 2012

4. TITLE AND SUBTITLE

Design and Performance of Ka-Band Fiber-Optic Delay Lines

5a. CONTRACT NUMBER
N0001912WX07123

5b. GRANT NUMBER

5c. PROGRAM ELEMENT NUMBER
0204136N

6. AUTHOR(S)

Vincent J. Urick, Joseph M. Singley, Christopher E. Sunderman,
John F. Diehl, and Keith J. Williams

5d. PROJECT NUMBER
2065

5e. TASK NUMBER

5f. WORK UNIT NUMBER
4400

7. PERFORMING ORGANIZATION NAME(S) AND ADDRESS(ES)

Naval Research Laboratory, Code 5650
4555 Overlook Avenue, SW
Washington, DC 20375-5320

8. PERFORMING ORGANIZATION REPORT NUMBER

NRL/MR/5650--12-9456

9. SPONSORING / MONITORING AGENCY NAME(S) AND ADDRESS(ES)

NAVAIR, PEOTACAIR PMA265
47123 Buse Road, Suite 445
Patuxent River, MD 20670-1547

10. SPONSOR / MONITOR'S ACRONYM(S)

NAVAIR

11. SPONSOR / MONITOR'S REPORT NUMBER(S)

12. DISTRIBUTION / AVAILABILITY STATEMENT

Approved for public release; distribution is unlimited.

13. SUPPLEMENTARY NOTES

14. ABSTRACT

The principles of fiber-optic delay lines (FODLs) are summarized and an example design is provided. The performance of two packaged FODLs is detailed including four-port S Parameters, noise figure, single-sideband phase noise, single-sideband amplitude noise, compression dynamic range and spurious-free dynamic range (SFDR).

15. SUBJECT TERMS

Fiber optics
Fiber-optic delay lines
Analog photonics

16. SECURITY CLASSIFICATION OF:			17. LIMITATION OF ABSTRACT	18. NUMBER OF PAGES	19a. NAME OF RESPONSIBLE PERSON
a. REPORT	b. ABSTRACT	c. THIS PAGE			Vincent J. Urick
Unclassified Unlimited	Unclassified Unlimited	Unclassified Unlimited	Unclassified Unlimited	64	19b. TELEPHONE NUMBER *(include area code)* (202) 767-9352

Standard Form 298 (Rev. 8-98)
Prescribed by ANSI Std. Z39.18

TABLE OF CONTENTS

EXECUTIVE SUMMARY

The principles of fiber-optic delay lines (FODLs) are summarized and an example design is provided. The performance of two packaged FODLs is detailed including four-port S Parameters, noise figure, single-sideband phase noise, single-sideband amplitude noise, compression dynamic range and spurious-free dynamic range (SFDR). A photograph of the front panel for one of the FODLs is shown below. Between the two FODLs, there are eight possible configurations as listed in the table below.

Frequency (GHz)	Delay (μs)	SFDR (dB·Hz$^{2/3}$)
10	67	107
10	125	105
40	67	107
40	125	106
10	100	105
10	200	103
40	100	107
40	200	103

DESIGN AND PERFORMANCE OF KA-BAND FIBER-OPTIC DELAY LINES

1 INTRODUCTION

Fiber-optic delay lines (FODLs) exhibit unique capabilities for use as wideband radio-frequency memory (WRFM) modules. The principle of a FODL is simple: encode radio-frequency (RF) onto an optical carrier, use the finite speed of light to store the analog information in a fiber-optic medium and decode the optical signal back into a RF signal. A typical optical loss for standard single-mode fiber is 0.2 dB/km, which translates to 0.4 dB/km for a RF signal modulated onto light in a dual-sideband format. With an index of refraction of about 1.5, the RF loss in fiber is 0.08 dB/μs and is independent of the RF signal. This figure accounts for propagation loss in the fiber only, not the electrical-to-optical-to-electrical (EOE) conversion (see Section 2.1). Wideband EOE components are readily available up to 40 GHz with research-grade devices surpassing 110 GHz. Given such bandwidth and low-loss delay capability, FODL technology is incredibly useful as a buffer for signal processing tasks or to simulate range in radar testing.

A large-scale commercial need for high-end FODL technology is lacking, leaving those with the requirement for high-fidelity analog delay modules little options. There are some commercial-off-the-shelf (COTS) FODLs available from a small number of companies but these units do not meet the requirements for all applications. Delaying a radar signal in a FODL to simulate propagation delay is an example of an application of the technology that cannot always be satisfied with COTS solutions. The performance of a FODL will have strict requirements that are tied to the radar system(s) under consideration. For example, the spurious- and compression-free dynamic range of the FODL will be linked to range of input powers into the FODL. If a wide range of radiated powers and/or stand-off distances are required, the dynamic range asked of the FODL can be quite high. High signal-to-noise ratios will be required at the output of the FODL to ensure that the radar return signal can be processed. This can require the FODL to have low baseband noise and negligible up-converted noise to the radar signal frequency. The latter requirement can be especially difficult to achieve in long FODLs, particularly in terms of RF phase noise. The operational bandwidth of the radar must not be neglected because fiber effects in long delay lines can degrade the RF response. The design of a high-performance FODL requires balancing the electro-optic front and back end performance with issues in the optical domain. Designing a "one-off" FODL tailored to a particular radar system is a viable solution but severely restricts the utility of the FODL unit. The long-term need for a high-performance FODL that is widely applicable to a large range of radar testing scenarios is the motivation of this work.

This report describes a novel Ka-Band FODL design including the performance of two packaged rack-mount units for radar testing applications. The design employs COTS components and can therefore be implemented by others versed in the state of the art. The design carefully addresses the aforementioned trades between RF performance and feasibly of the optical architecture. An article on long-haul analog photonics [1] covers much of the basic principles for FODL design; those applicable to this implementation are reviewed in Section 2. The specific design for the Ka-Band FODL is detailed in Section 3. The measured performance of the two units is documented in Section 4, followed by diagrams and operational notes in Section 5. Concluding remarks are provided in Section 6.

Manuscript approved November 16, 2012.

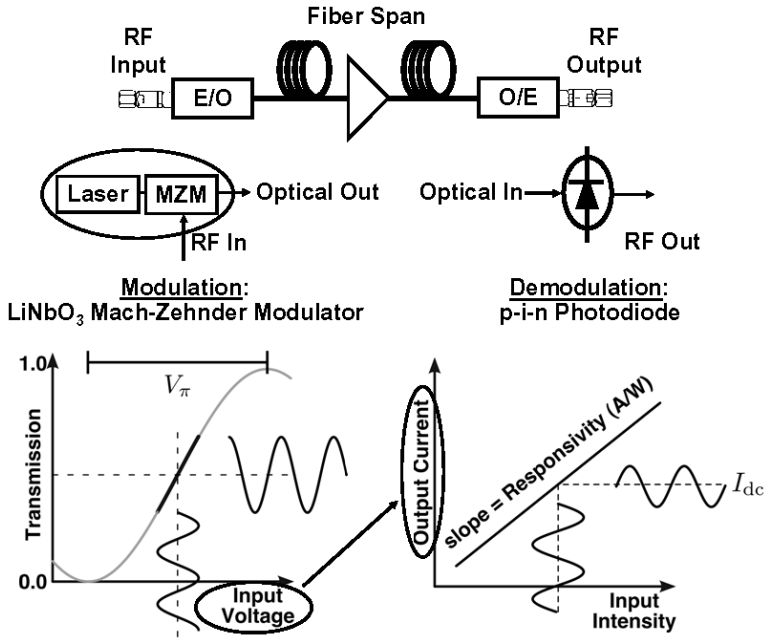

Fig. 1: Basic concept of an intensity-modulation direct detection (IMDD) photonic link employing a quadrature-biased Mach-Zehnder modulator (MZM) with a half-wave voltage V_π and a p-i-n photodiode operating at an average photocurrent $I_{\rm dc}$.

2 DESIGN CONSIDERATIONS

The basic principles of FODL design are provided in this section. A large portion of the material is covered thoroughly from basic principles in a review article [1]. Therefore, the focus here will be primarily on the results. The design assumes that an intensity-modulation direct detection (IMDD) architecture employing a quadrature-biased Mach-Zehnder modulator (MZM) and a single ideal p-i-n photodiode is used (see Fig. 1). Distortion from off-quadrature biasing of the MZM and photodiode nonlinearities are not covered here but are analyzed in [2]. The governing equations will be provided with little derivation, noting that detail is provided in [1]. However, the equations presented here include a factor of four reduction in RF output power for the link due to loss in the impedance-matching circuit of the photodiode, as opposed to [1] where it is assumed that all of the RF power is delivered to the load. Finally, a more detailed treatment will be provided for material not covered in [1], such as in the case of RF phase noise.

2.1 RF Performance Metrics

The RF performance for an IMDD link can be expressed in terms of a manageable number of parameters given the above assumptions. The analysis here assumes that the input to the MZM comprises a DC portion to hold the MZM at quadrature and a sinusoidal signal of the form $V\sin(\Omega t)$, where Ω is the angular drive frequency. The average RF output power for the link is

$$P_{\text{out}} = \frac{1}{2} I_{\text{dc}}^2 J_1^2\left(\phi_{\text{rf}}\right) R_{\text{out}}, \tag{1}$$

where I_{dc} is the DC photocurrent, J_1 is a Bessel function of the first kind and R_{out} is the output resistance assumed to be matched to the load. In (1) $\phi_{\text{rf}} = \pi V / V_\pi$, where V_π is the MZM half-wave voltage. The maximum of (1) is

$$\max\left(P_{\text{out}}\right) = \frac{1}{2} I_{\text{dc}}^2 R_{\text{out}} \max\left(J_1^2\left(\phi_{\text{rf}}\right)\right) \approx 0.1693 \cdot I_{\text{dc}}^2 R_{\text{out}}. \tag{2a}$$

Equation (2a) can be written in decibel (dB) form as

$$P_{\max}\left[\text{dBm}\right] = -20.7 + 20\log\left(I_{\text{dc}}\left[\text{mA}\right]\right), \tag{2b}$$

for R_{out} = 50 Ω. Using the small-signal approximation $J_1\left(\phi_{\text{rf}}\right) \approx \phi_{\text{rf}}/2$, the small-signal output power is obtained from (1) as

$$P_{\text{out,ss}} = \frac{\pi^2 I_{\text{dc}}^2 V^2 R_{\text{out}}}{8 V_\pi^2}. \tag{3}$$

Finally, the output power at 1-dB compression is given by

$$P_{\text{out,1dB}} = \frac{1}{2} I_{\text{dc}}^2 J_1^2\left(\phi_{\text{1dB}}\right) R_{\text{out}} \approx 0.08968 \cdot I_{\text{dc}}^2 R_{\text{out}}, \tag{4a}$$

which can be written in dB form as

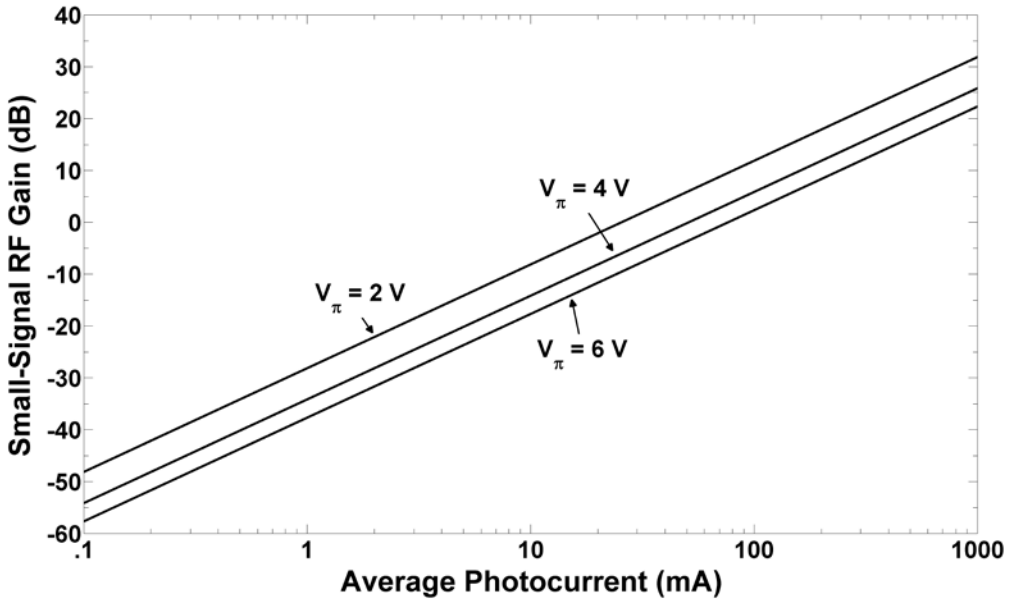

Fig. 2: Calculated small-signal RF gain (6a) as a function of I_{dc} for three values of MZM half-wave voltage.

$$P_{\text{out,1dB}}\left[\text{dBm}\right] = -23.5 + 20\log\left(I_{\text{dc}}\left[\text{mA}\right]\right) \tag{4b}$$

for $R_{\text{out}} = 50\ \Omega$.

The gain factor is defined as

$$g \equiv \frac{P_{\text{out}}}{P_{\text{in}}}, \tag{5}$$

where P_{in} is the average RF input power. For the analysis here, $P_{\text{in}} = V^2/\left(2R_{\text{in}}\right)$, and the small-signal gain for an IMDD link is

$$g = \frac{\pi^2}{4}\left(\frac{I_{\text{dc}}^2}{V_\pi^2}\right)R_{\text{in}}R_{\text{out}}, \tag{6a}$$

where R_{in} is the input resistance. For $R_{\text{in}} = R_{\text{out}} = 50\ \Omega$, (6a) can be written as

$$G\left[\text{dB}\right] = -22.1 + 20\log\left(I_{\text{dc}}\left[\text{mA}\right]\right) - 20\log\left(V_\pi\left[\text{V}\right]\right). \tag{6b}$$

Equation (6b) is plotted in Fig. 2 as a function of I_{dc} for three values of V_π. The input 1-dB compression point is given by $P_{\text{in,1dB}} = P_{\text{out,1dB}} \times 10^{0.1}/g$. Inserting (4) and (6) into this expression yields

$$P_{\text{in,1dB}} = \frac{0.04576 \cdot V_\pi^2}{R_{\text{in}}}. \tag{7a}$$

With $R_{in=}$ = 50 Ω (7a) becomes

$$P_{\text{in,1dB}}\left[\text{dBm}\right] = -0.4 + 20\log\left(V_\pi\left[\text{V}\right]\right). \tag{7b}$$

The standard RF noise factor is defined as [3]

$$F \equiv \frac{N_{\text{out}}}{g k_{\text{B}} T}, \tag{8}$$

where N_{out} is the output noise power spectral density, k_{B} is Boltzmann's constant and T = 290 K, the standard temperature for measuring noise. Inserting (6a) into (8) yields the noise factor for an IMDD link:

$$F = \frac{4V_\pi^2 N_{\text{out}}}{I_{\text{dc}}^2 \pi^2 R_{\text{in}} R_{\text{out}} k_{\text{B}} T}. \tag{9a}$$

The noise figure (NF) is the decibel version of F; for an IMDD link with $R_{\text{in}} = R_{\text{out}}$ = 50 Ω the noise figure is

$$\text{NF}\left[\text{dB}\right] = 196.1 - 20\log\left(I_{\text{dc}}\left[\text{mA}\right]\right) + 20\log\left(V_\pi\left[\text{V}\right]\right) + N_{\text{out}}\left[\text{dBm/Hz}\right]. \tag{9b}$$

Equation (9b) is plotted in Fig. 3 for various conditions on N_{out} that will be clarified in Section 2.2.

The 1-dB compression dynamic range is defined as

$$\text{CDR} \equiv \frac{P_{\text{out,1dB}} \times 10^{0.1}}{N_{\text{out}} B}, \tag{10}$$

or, equivalently,

$$\text{CDR} \equiv \frac{P_{\text{in,1dB}}}{F B k_{\text{B}} T}, \tag{11}$$

where B is the RF bandwidth. The CDR for an IMDD link is obtained by inserting (4a) into (10) or by inserting (7a) and (9a) into (11):

$$\text{CDR} = \frac{0.1129 \cdot I_{\text{dc}}^2 R_{\text{out}}}{N_{\text{out}} B}. \tag{12a}$$

In dB form

$$\text{CDR}\left[\text{dB} \cdot \text{Hz}\right] = -22.5 + 20\log\left(I_{\text{dc}}\left[\text{mA}\right]\right) - N_{\text{out}}\left[\text{dBm/Hz}\right], \tag{12b}$$

where R_{out} = 50 Ω and the CDR was normalized to B = 1 Hz, as is often the convention. Equation (12b) is plotted in Fig. 4.

The n^{th}-order spur-free dynamic range is defined as

$$\mathrm{SFDR}_n \equiv \left(\frac{\mathrm{OIP}n}{N_{\text{out}} B} \right)^{(n-1)/n}, \tag{13a}$$

where OIPn is the n^{th} -order output intercept point. Normalized to B = 1 Hz, (13a) can be written as

$$\mathrm{SFDR}_n \left[\mathrm{dB} \cdot \mathrm{Hz}^{(n-1)/n} \right] = \frac{n-1}{n} \left(\mathrm{OIP}n \left[\mathrm{dBm} \right] - N_{\text{out}} \left[\mathrm{dBm/Hz} \right] \right). \tag{13b}$$

The SFDR_n can be defined in terms of the n^{th} -order input intercept point as

$$\mathrm{SFDR}_n \equiv \left(\frac{\mathrm{IIP}n}{FBk_{\mathrm{B}}T} \right)^{(n-1)/n}, \tag{14a}$$

$$\mathrm{SFDR}_n \left[\mathrm{dB} \cdot \mathrm{Hz}^{(n-1)/n} \right] = \frac{n-1}{n} \left(174.0 + \mathrm{IIP}n \left[\mathrm{dBm} \right] - \mathrm{NF} \left[\mathrm{dB} \right] \right). \tag{14b}$$

Given the assumptions above, an IMDD link will be limited by 3$^{\text{rd}}$-order nonlinearities. The OIP3 for such a link is

$$\mathrm{OIP3} = I_{\text{dc}}^2 R_{\text{out}}. \tag{15a}$$

For R_{out} = 50 Ω

$$\mathrm{OIP3} \left[\mathrm{dBm} \right] = -13.0 + 20 \log \left(I_{\text{dc}} \left[\mathrm{mA} \right] \right). \tag{15b}$$

The IIP3 for an IMDD link is

$$\mathrm{IIP3} = \frac{4V_\pi^2}{\pi^2 R_{\text{in}}}. \tag{16a}$$

For R_{in} = 50 Ω

$$\mathrm{IIP3} \left[\mathrm{dBm} \right] = 9.1 + 20 \log \left(V_\pi \left[\mathrm{V} \right] \right). \tag{16b}$$

The SFDR for an IMDD link is obtained by inserting (15a) into (13a) or by inserting (9a) and (16a) into (14a):

$$\mathrm{SFDR}_3 = \left(\frac{I_{\text{dc}}^2 R_{\text{out}}}{N_{\text{out}} B} \right)^{2/3}, \tag{17a}$$

or

$$\mathrm{SFDR}\left[\mathrm{dB}\cdot\mathrm{Hz}^{2/3}\right] = -8.7 + \frac{40}{3}\log\left(I_{\mathrm{dc}}\left[\mathrm{mA}\right]\right) - \frac{2}{3}N_{\mathrm{out}}\left[\mathrm{dBm/Hz}\right]. \tag{17b}$$

for R_{out} = 50 Ω and B = 1 Hz. Plots of (17b) are provided in Fig. 5, noting that Section 2.2 must be consulted to describe how N_{out} is handled.

The basic design equations for an IMDD link have been listed. As can be seen in Figs. 2 and 3, G and NF both improve with increasing I_{dc} and decreasing V_{π}. It is evident from Figs. 4 and 5 that CDR and SDFR improve with increasing I_{dc} and are independent of V_{π} except at large I_{dc} where amplified thermal noise can clamp the dynamic range (see Section 2.2).

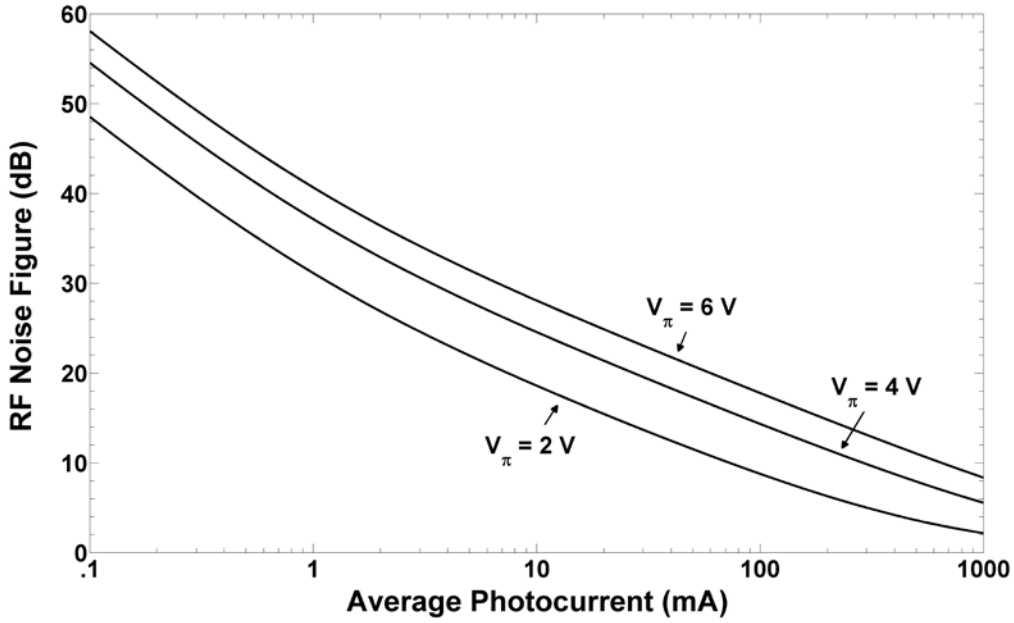

(a)

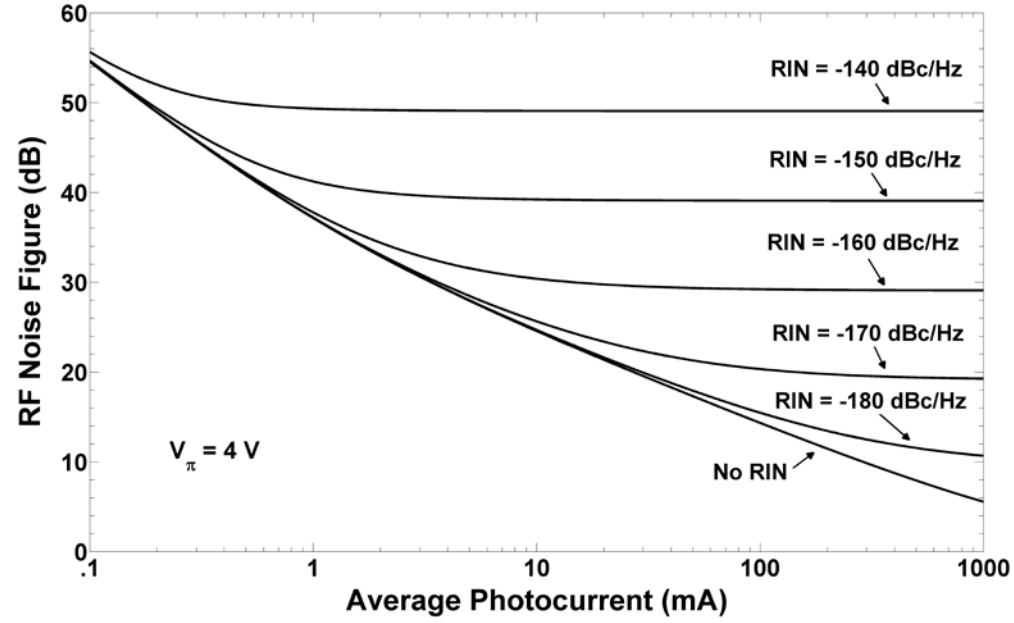

(b)

Fig. 3: Calculated RF noise figure (9) as a function of I_{dc} (a) for three values of MZM half-wave voltage without any excess relative intensity noise (RIN) and (b) for six values of RIN with a fixed 4-V half-wave voltage.

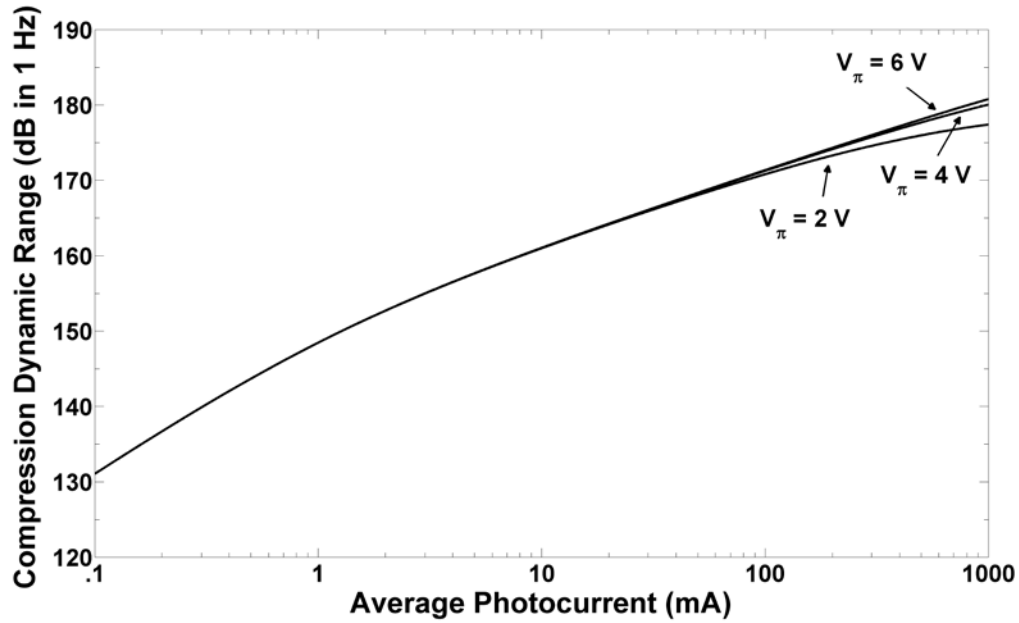

(a)

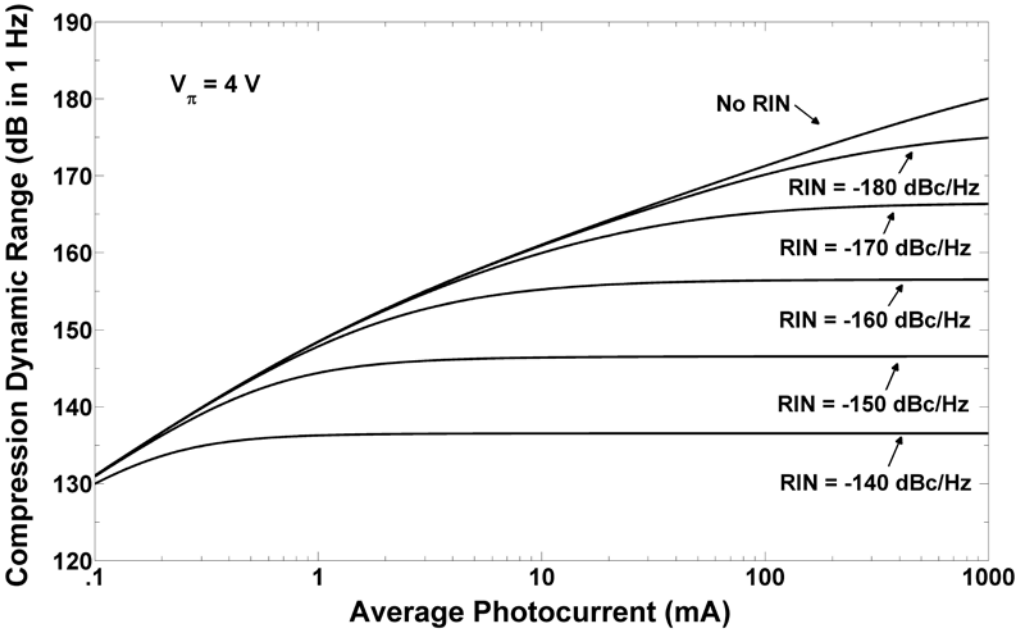

(b)

Fig. 4: Calculated 1-dB compression dynamic range (12) as a function of I_{dc} (a) for three values of MZM half-wave voltage without any excess relative intensity noise (RIN) and (b) for six values of RIN with a fixed 4-V half-wave voltage.

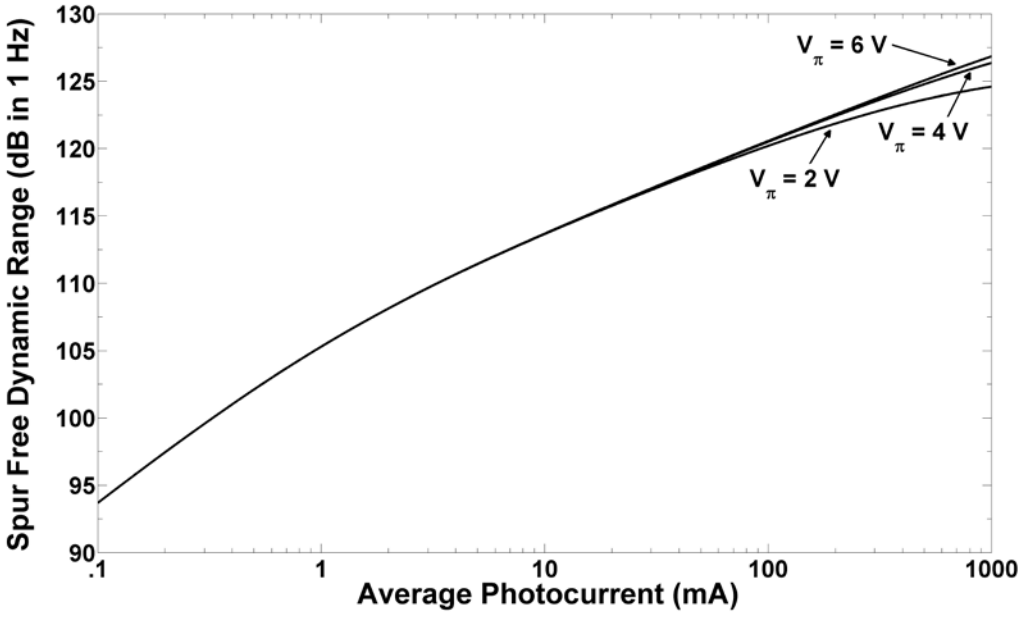

(a)

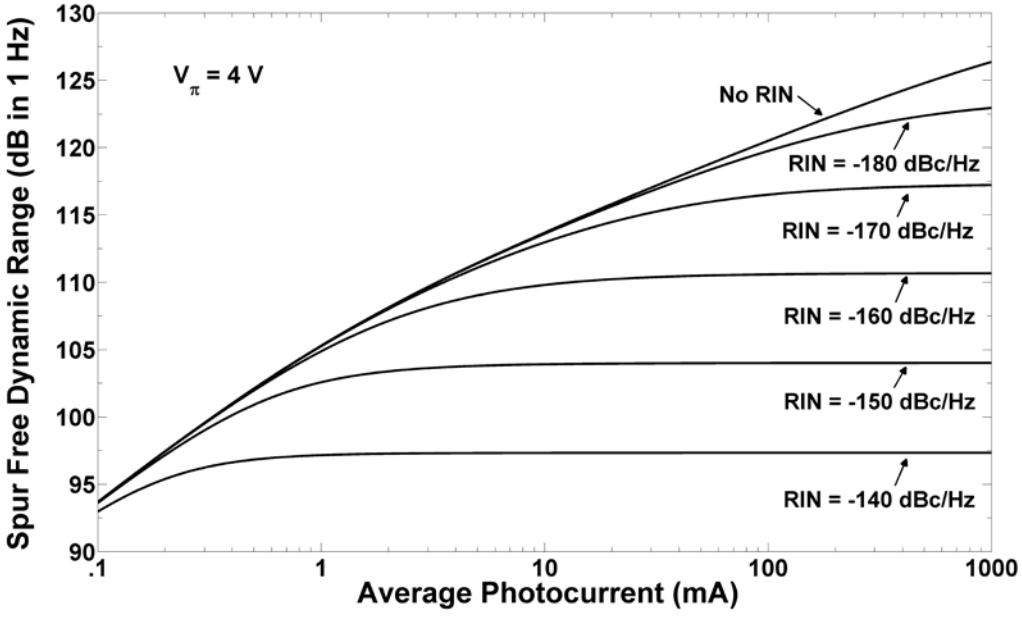

(b)

Fig. 5: Calculated third-order spur free dynamic range (17) as a function of I_{dc} (a) for three values of MZM half-wave voltage without any excess relative intensity noise (RIN) and (b) for six values of RIN with a fixed 4-V half-wave voltage.

2.2 Sources of Noise

The RF metrics NF, CDR and SFDR depend on the value of N_{out}, which has numerous contributing sources in an IMDD link. The most important equations for the basic sources of noise are provided here.

Thermal noise is one of two fundamental sources of noise considered here, the other being shot noise. The thermal noise power spectral density at the output of an IMDD link is given by

$$N_{th} = k_B T\left(g+1\right). \tag{18a}$$

The first term in (18a), gk_BT, is the thermal noise power spectral density at the output due to thermal noise at the input of the link. The second term in (18a), k_BT, is due to the output resistance. This latter output thermal noise takes the value of

$$N_{o\text{-}th} = -174.0 \text{ dBm/Hz} \tag{18b}$$

at T = 290 K. The first term in (18a) can be written as

$$N_{i\text{-}th}\left[\text{dBm/Hz}\right] = -196.1 + 20\log\left(I_{dc}\left[\text{mA}\right]\right) - 20\log\left(V_{\pi}\left[\text{V}\right]\right), \tag{18c}$$

where (6) was inserted for g with $R_{in} = R_{out} = 50\ \Omega$. Radio-frequency phase noise is an important issue in FODLs for radar testing applications. Because thermal noise is white, half of the noise power spectral density will contribute to intensity noise and the other half to phase noise. The single-sideband phase noise due to thermal noise is given by

$$\mathcal{L}_{th} = \frac{k_B T}{2P_{out}}. \tag{19}$$

Thermal-noise-limited signals as described by (19) seldom exist in practice. Rather, added noise defined by the system noise factor will increase the phase noise. If the system noise factor and gain are frequency-independent over the measurement bandwidth, (19) can be adjusted to yield $\mathcal{L}(f) = Fgk_BT/(2P_{out})$. Shown in Figure 6 is the measured phase noise for a 10.24 GHz oscillator with and without an RF amplifier, the former demonstrating a significant increase in noise that is described above. An Agilent E5500A/B phase noise test system was employed for the collection of these data. For both data sets, the RF output power was P_{out} = 5.3 dBm. The thermal noise limit in this case is given by (19) as -182 dBc/Hz. The oscillator's phase noise is shown by the grey curve and is well above the thermal-noise limit. The black curve is the measured phase noise after passing through an RF amplifier with G = 19.5 dB and NF = 6.3 dB at and around 10.24 GHz. The solid black line is the result of calculation with these parameters inserted, -156.5 dBc/Hz. The amplified oscillator phase noise does contribute to the black curve but the noise floor at -156.5 dBc/Hz is dominant from about 1-70 MHz offset frequency.

The second fundamental noise source in a photonic link considered here is shot noise. The shot noise power spectral density at the output of the IMDD architecture as described here is

$$N_{sh} = \frac{1}{2} qI_{dc}R_{out}, \tag{20a}$$

where q is the electronic charge constant. Inserting for q and R_{out} = 50 Ω, (20a) can be written

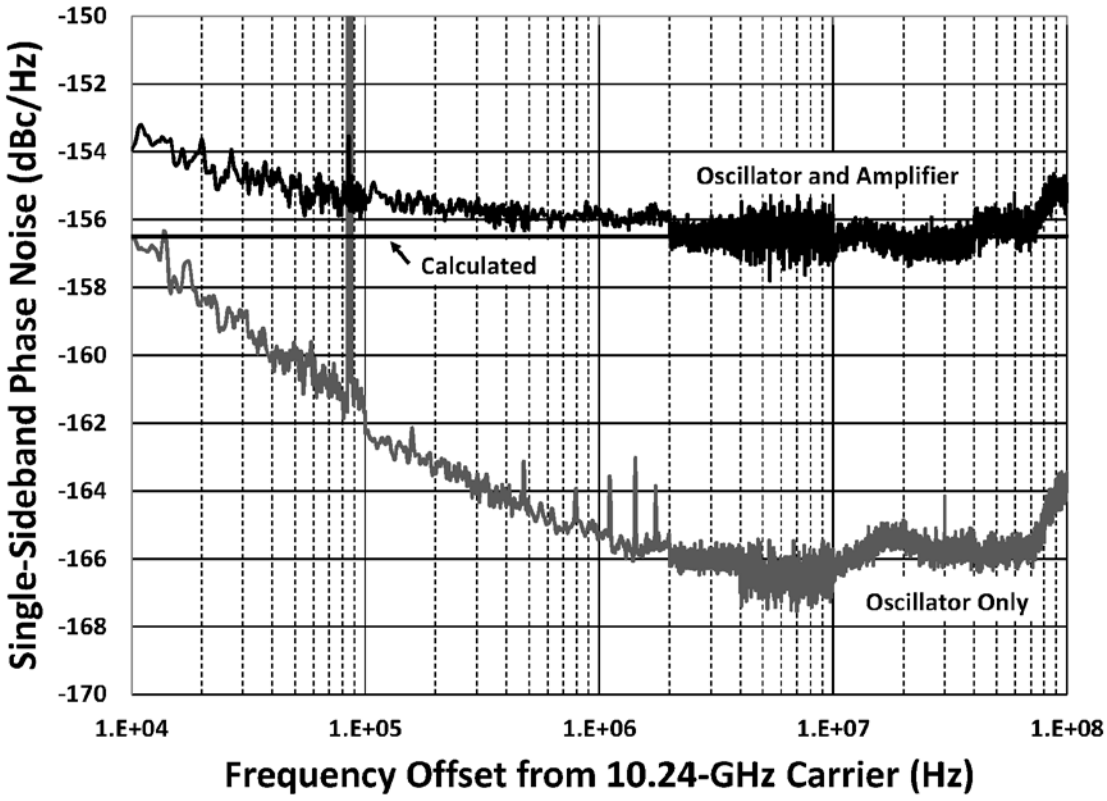

Fig. 6: Measured phase noise for an oscillator with (black) and without (grey) an RF amplifier in line. The calculated line is $\mathcal{L}(f) = Fgk_{\mathrm{B}}T/(2P_{\mathrm{out}}) = -156.5$ dBc / Hz for F = 4.3, g = 89.1, T = 290 K and P_{out} = 3.4 mW.

$$N_{\mathrm{sh}}\left[\mathrm{dBm/Hz}\right] = -174.0 + 10\log\left(I_{\mathrm{dc}}\left[\mathrm{mA}\right]\right). \tag{20b}$$

Measured shot noise is compared to that predicted by (20) in Fig. 7.

Because shot noise is often the reference for performance in IMDD links, it is worth providing equations for numerous performance metrics in the shot-noise-limit. The shot-noise-limited signal-to-noise ratio (SNR) is

$$\mathrm{SNR}_{\mathrm{sh}} = \frac{2P_{\mathrm{out}}}{qI_{\mathrm{dc}}R_{\mathrm{out}}B}. \tag{21}$$

Equation (3) can be inserted into (21) to obtain the shot-noise-limited SNR in the small-signal limit:

$$\mathrm{SNR}_{\mathrm{sh,ss}} = \frac{\pi^2 P_{\mathrm{in}}R_{\mathrm{out}}I_{\mathrm{dc}}}{2qV_{\pi}^2 B}. \tag{22a}$$

For R_{out} = 50 Ω, (22a) can be normalized to B = 1 Hz as

$$\mathrm{SNR}_{\mathrm{sh,ss}}\left[\mathrm{dB}\cdot\mathrm{Hz}\right]=151.9+P_{\mathrm{in}}\left[\mathrm{dBm}\right]+10\log\left(I_{\mathrm{dc}}\left[\mathrm{mA}\right]\right)-20\log\left(V_{\pi}\left[\mathrm{V}\right]\right). \tag{22b}$$

The shot-noise-limited SNR at 1-dB compression is given by (21) with (4a) inserted for P_{out},

$$\mathrm{SNR}_{\mathrm{sh,1dB}}=\frac{0.1794I_{\mathrm{dc}}}{qB}. \tag{23a}$$

Normalized to 1 Hz, (23a) is

$$\mathrm{SNR}_{\mathrm{sh,1dB}}\left[\mathrm{dB}\cdot\mathrm{Hz}\right]=150.5+10\log\left(I_{\mathrm{dc}}\left[\mathrm{mA}\right]\right). \tag{23b}$$

The maximum SNR in a shot-noise-limited IMDD link is obtained by inserting (2a) into (21) as

$$\mathrm{SNR}_{\mathrm{sh,max}}=\frac{0.3386I_{\mathrm{dc}}}{qB}, \tag{24a}$$

which can be written as

$$\mathrm{SNR}_{\mathrm{sh,max}}\left[\mathrm{dB}\cdot\mathrm{Hz}\right]=153.3+10\log\left(I_{\mathrm{dc}}\left[\mathrm{mA}\right]\right). \tag{24b}$$

As mentioned previously, the single-sideband phase noise is important for radar applications of FODLs. The shot-noise-limited single-sideband phase noise for an IMDD link is

$$\mathcal{L}_{\mathrm{sh}}=\frac{qI_{\mathrm{dc}}R_{\mathrm{out}}}{4P_{\mathrm{out}}}. \tag{25}$$

Measurements of single-sideband phase noise caused by shot noise are shown in Fig. 8 and are compared to (25). Equation (25) is one-half of the inverse of (21), owing to the fact that shot noise contributes equally to amplitude and phase noise. Therefore, expressions for the single-sideband phase noise similar to (22)-(24) can be written using the following expression:

$$\mathcal{L}_{\mathrm{sh}}\left[\mathrm{dBc/Hz}\right]=-\mathrm{SNR}_{\mathrm{sh}}\left[\mathrm{dB}\cdot\mathrm{Hz}\right]-3. \tag{26}$$

Three important RF metrics that depend on noise are F, CDR and SFDR. The shot-noise-limited F for an IMDD link is given by (9a) with (20a) inserted for N_{out}:

$$F=\frac{qV_{\pi}^{2}}{I_{\mathrm{dc}}\pi^{2}R_{\mathrm{in}}k_{\mathrm{B}}T}. \tag{27a}$$

For R_{in} = 50 Ω and at the standard noise measurement temperature T = 290 K, (27a) is

$$\mathrm{NF}_{\mathrm{sh}}\left[\mathrm{dB}\right]=22.1-10\log\left(I_{\mathrm{dc}}\left[\mathrm{mA}\right]\right)+20\log\left(V_{\pi}\left[\mathrm{V}\right]\right). \tag{27b}$$

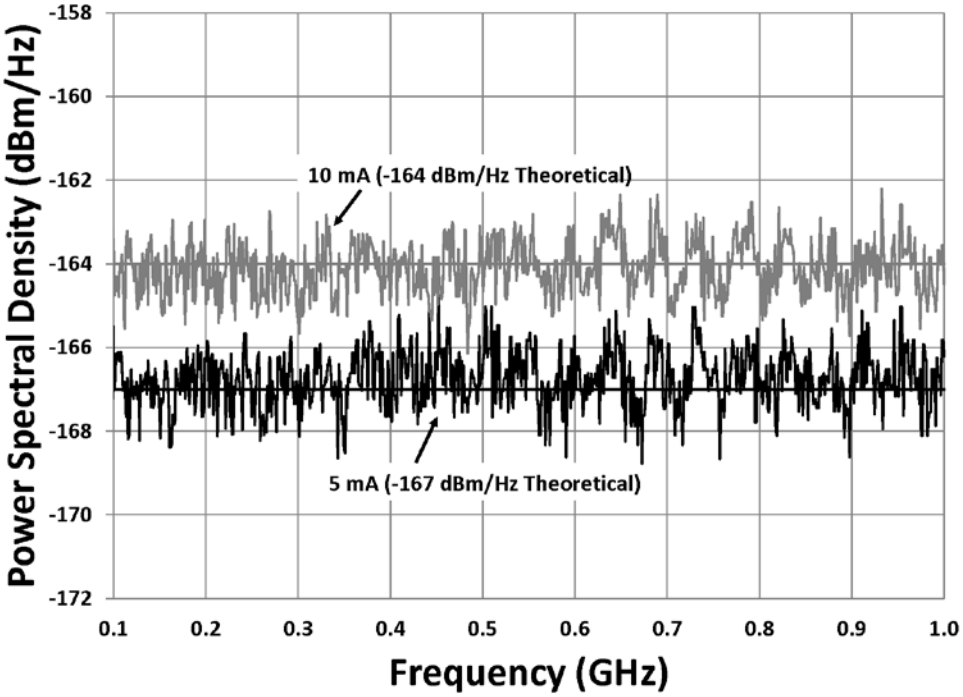

Fig. 7: Measured N_{sh} for I_{dc} = 5 and 10 mA and the calculation (20b) for each photocurrent. The data were obtained with a low-noise solid-state laser at 1.319 μm implemented in a crystal of $Y_3Al_5O_{12}$ doped with Nd^{3+} ions, commonly referred to as a Nd:YAG laser.

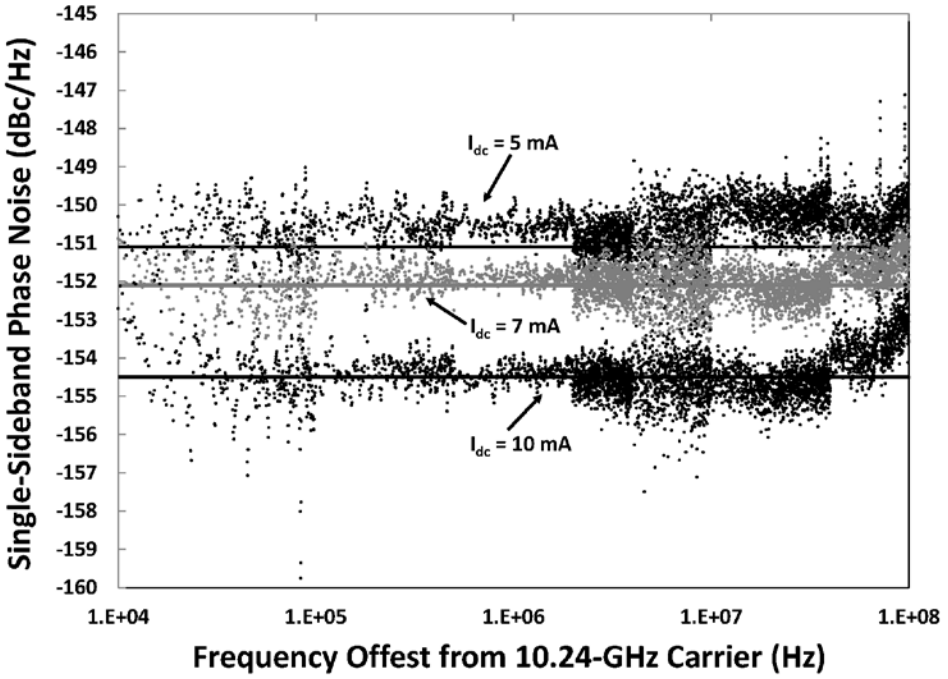

Fig. 8: Measured $\mathcal{L}_{sh}$ for I_{dc} = 5, 7 and 10 mA and the calculation (25) for each photocurrent.

Equation (20a) can be inserted for N_{out} into (12a) to obtain the following expressions for the shot-noise-limited CDR:

$$\mathrm{CDR}_{sh} = \frac{0.2258 \cdot I_{dc}}{qB} \tag{28a}$$

$$\mathrm{CDR}_{sh}\left[\mathrm{dB \cdot Hz}\right] = 151.5 + 10\log\left(I_{dc}\left[\mathrm{mA}\right]\right). \tag{28b}$$

Finally, the shot-noise-limited SFDR results from using (17a) with (20a):

$$\mathrm{SFDR}_{sh} = \left(\frac{2I_{dc}}{qB}\right)^{2/3} \tag{29a}$$

$$\mathrm{SFDR}_{sh}\left[\mathrm{dB \cdot Hz^{2/3}}\right] = 107.3 + \frac{20}{3}\log\left(I_{dc}\left[\mathrm{mA}\right]\right). \tag{29b}$$

It is unlikely that shot noise will limit the performance in long FODLs. Excess noise can be cast as relative intensity noise (RIN) and a noise penalty (NP) beyond shot noise [4] can be used. For purposes here, RIN is defined as

$$\mathrm{RIN} = \frac{4N_{out}}{I_{dc}^2 R_{load}}, \tag{30a}$$

the output noise power spectral density normalized to the DC power. For R_{out} = 50 Ω,

$$\mathrm{RIN}\left[\mathrm{dBc/Hz}\right] = 19.0 + N_{out}\left[\mathrm{dBm/Hz}\right] - 20\log\left(I_{dc}\left[\mathrm{mA}\right]\right). \tag{30b}$$

Thermal and shot noise can be expressed as RIN. The shot-noise-limited RIN is

$$\mathrm{RIN}_{sh} = \frac{2q}{I_{dc}} \tag{31a}$$

$$\mathrm{RIN}_{sh}\left[\mathrm{dBc/Hz}\right] = -154.9 - 10\log\left(I_{dc}\left[\mathrm{mA}\right]\right). \tag{31b}$$

Two important sources of RIN for FODL design are laser RIN and RIN due to optical amplifiers, usually erbium-doped fiber amplifiers (EDFAs).

Laser RIN is a major concern in analog photonics. Laser noise at the RF carrier frequency as well as up-converted baseband laser noise must be considered. It is beyond the scope of this report to provide a detailed description of the noise processes in the various laser options for FODLs. Rather, some data sets will be presented to give some background on laser noise. Shown in Fig. 9 are measured data for a Nd:YAG laser. Figure 9(a) depicts the measured noise power spectral density at the output of a photodiode illuminated with the laser at three average photocurrents. Laser noise dominates from 10 kHz to 1 MHz, which scales as I_{dc}^2. The laser is shot noise limited for the values of I_{dc} shown above 10 MHz, where the spectra scale as I_{dc}. When the same spectra are cast as RIN, the shot-noise-limited scaling goes as $1/I_{dc}$, whereas the laser RIN is independent of photocurrent.

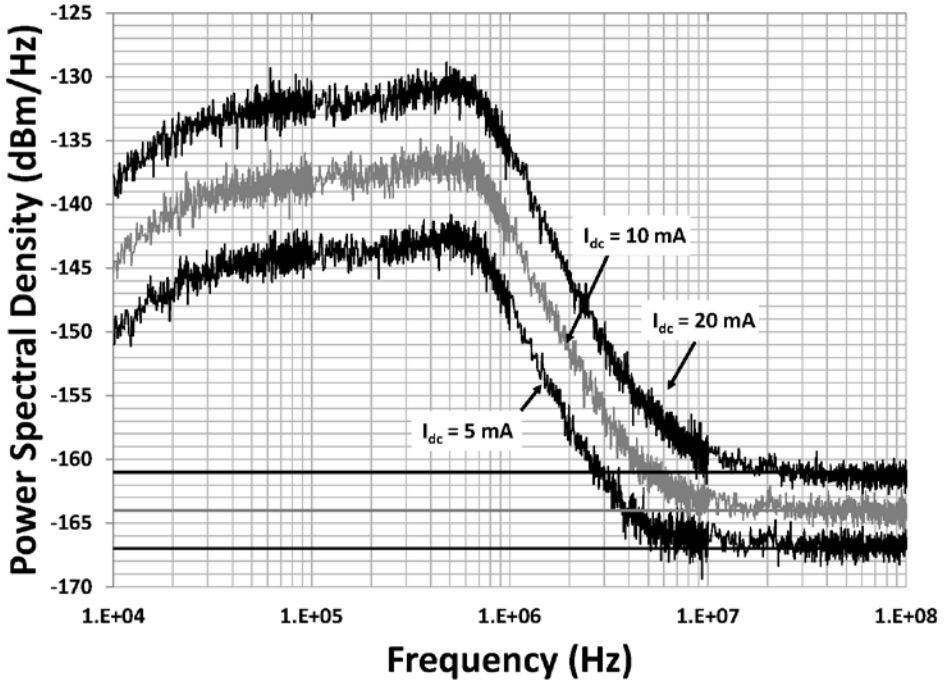

(a)

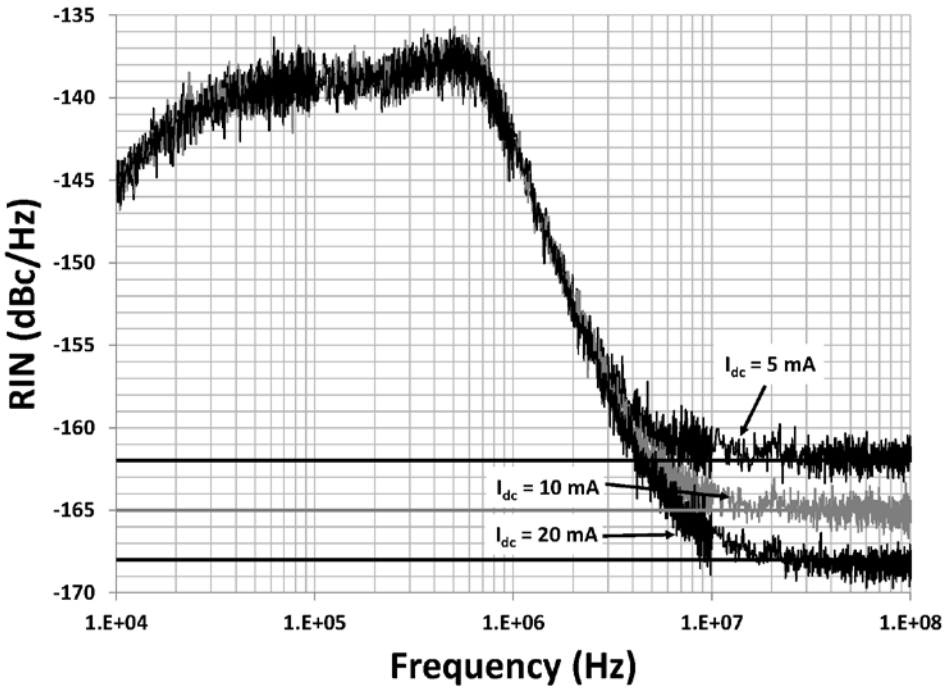

(b)

Fig. 9: Measured noise for a Nd:YAG laser at three photocurrents showing (a) power spectral density and (b) power spectral density relative to the DC power (RIN). The solid lines mark the shot noise limit for each curve.

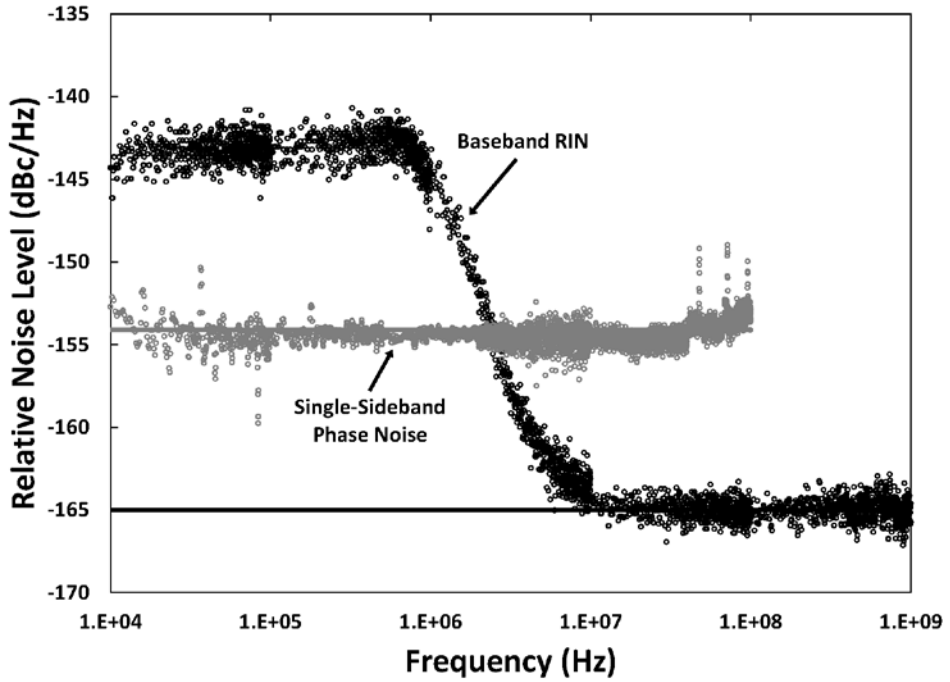

Fig. 10: Measurements for a Nd:YAG laser. Shown are the baseband relative intensity noise (RIN) and the single-sideband phase noise with respect to a 10.24 GHz carrier. The solid lines designate the shot-noise limit in each case.

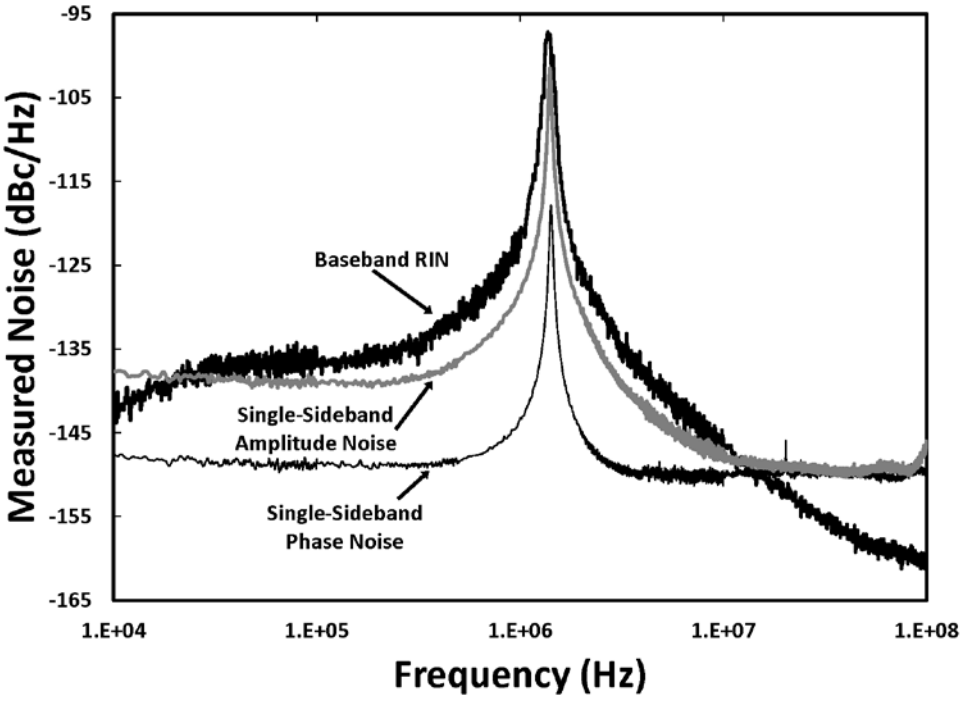

Fig. 11: Measurements for an erbium-doped fiber laser. Shown are the baseband relative intensity noise (RIN) as well as the single-sideband phase and amplitude noise with respect to a 10.24 GHz carrier.

The effects of up-converted baseband noise on a 10.24-GHz oscillator are shown in Figs. 10 and 11. Shown in Fig. 10 are the measured baseband RIN of a Nd:YAG laser and the single-sideband phase noise around 10.24 GHz for the output of a link using the same laser. In this case, the laser RIN produces intensity noise only in the RF domain and the single-sideband phase noise is limited by shot noise at the link output. The same is true and more explicitly shown for the data in Fig. 11. Shown there are the measured baseband RIN of an erbium-doped fiber laser as well as the amplitude and phase noise for a link using the laser. As expected for pure amplitude modulation, the single-sideband amplitude noise is 3 dB lower than the RIN peak. There is a peak in the phase noise spectrum that is 20-dB down from the peak in the amplitude domain. It is difficult to discern whether that noise is truly phase noise or an artifact of the limited rejection of amplitude noise in the measurement setup. Regardless, the two data sets in Figs. 10 and 11 suggest that laser RIN contributes primarily to up-converted amplitude noise, not phase noise.

Optical amplification will be required in long FODLs to maintain the signal level. The optical amplifier of choice is the EDFA. A classical work on EDFAs is provided by Desurvire [5]; treatments in terms of RIN [1] and noise penalty [4] are provided elsewhere. Data is presented here to give the reader an introduction to EDFA noise and the concept of EDFA noise penalty is applied to FODL design in Section 3. Shown in Fig. 12 is a data set for an EDFA. Plotted there are the measured optical noise figure and the measured RIN at the EDFA output as a function of input power into the EDFA. Shown also is the calculated RIN due to shot noise, which is the reference for the optical noise figure [1]. However, as shown in Fig. 12, the RIN at the EDFA output decreases with increasing input power. The concept of noise penalty (NP) [4] describes the performance relative to shot noise at the link output, which is not necessarily equal to optical noise figure at the EDFA output. The bandwidth of an EDFA is measured on optical scales and the noise from an EDFA is independent of frequency in the RF domain. Shown in Figs. 13 and 14 are the measured single-sideband (SSB) phase and amplitude noise, respectively, for 10.24-GHz photonic links employing EDFAs. In these plots, data are shown for a link with

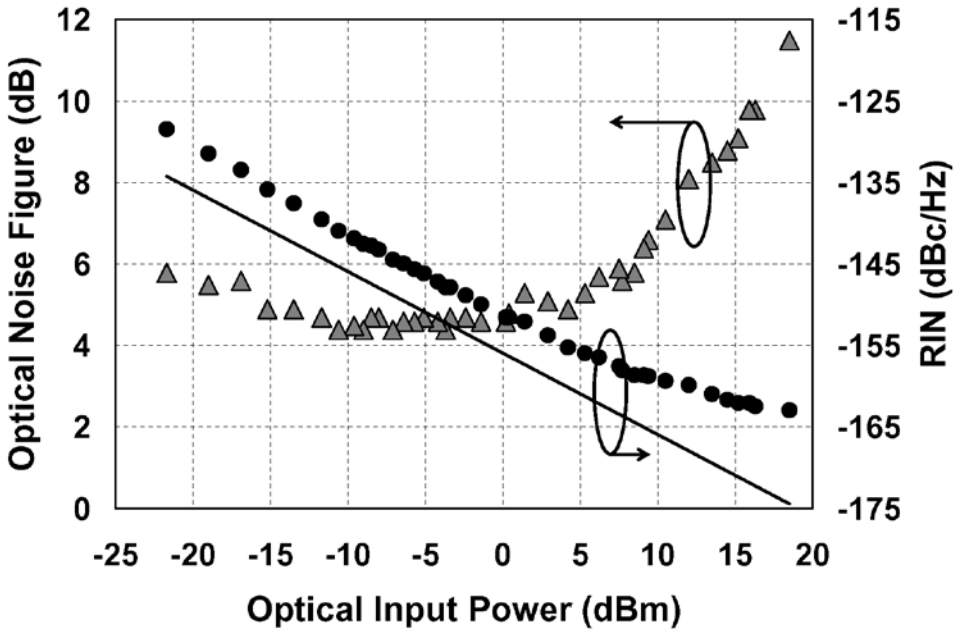

Fig. 12: Data set for an EDFA. Shown are the measured optical noise figure (triangles) and the measured RIN at the EDFA output (circles) as a function of input power into the EDFA. The solid line shows the shot-noise-limited RIN.

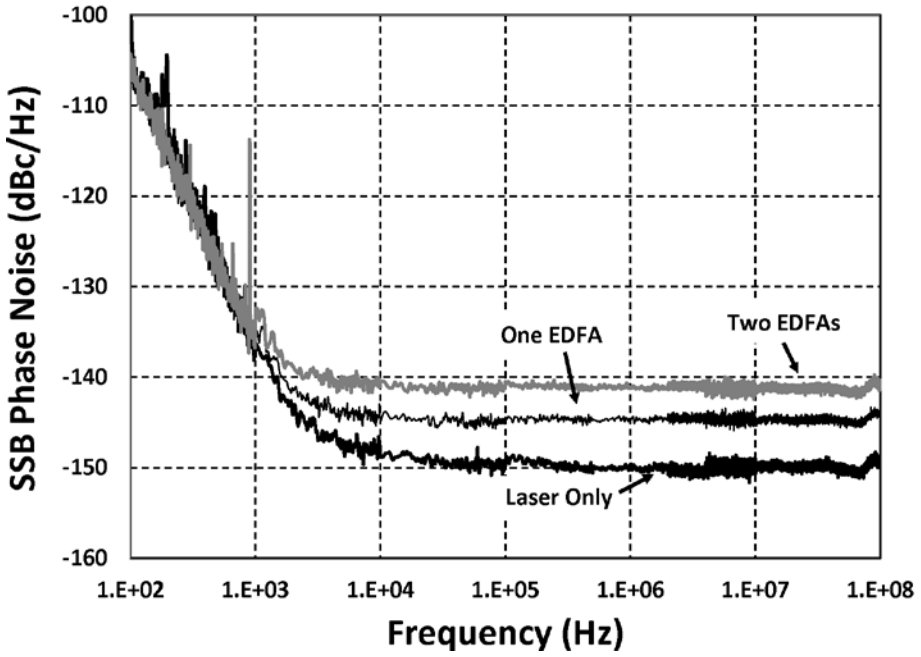

Fig. 13: The measured single-sideband (SSB) phase noise for three photonic links all at I_{dc} = 10 mA. Shown are data for a laser only and the same laser amplified with one and two erbium-doped fiber amplifiers (EDFAs). In both amplified cases, the EDFA gain is set to compensate a passive loss and therefore provides no net optical gain. The data are relative to an RF output of -15 dBm at 10.24 GHz. The theoretical shot noise level for these data is at -152 dBc/Hz.

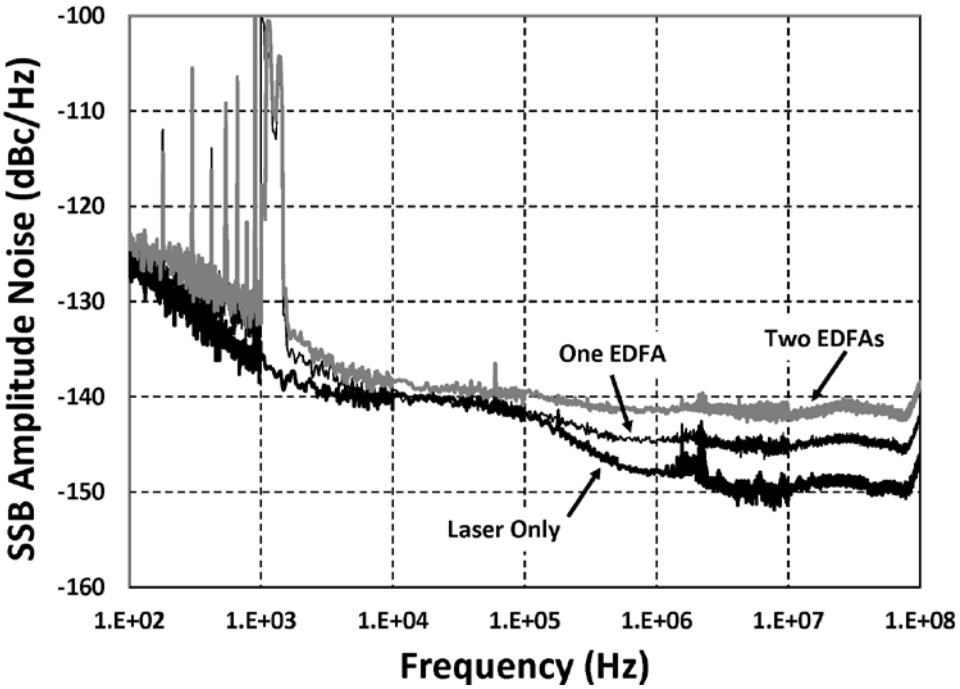

Fig. 14: The measured single-sideband (SSB) amplitude noise for the same circumstances as in Fig. 14.

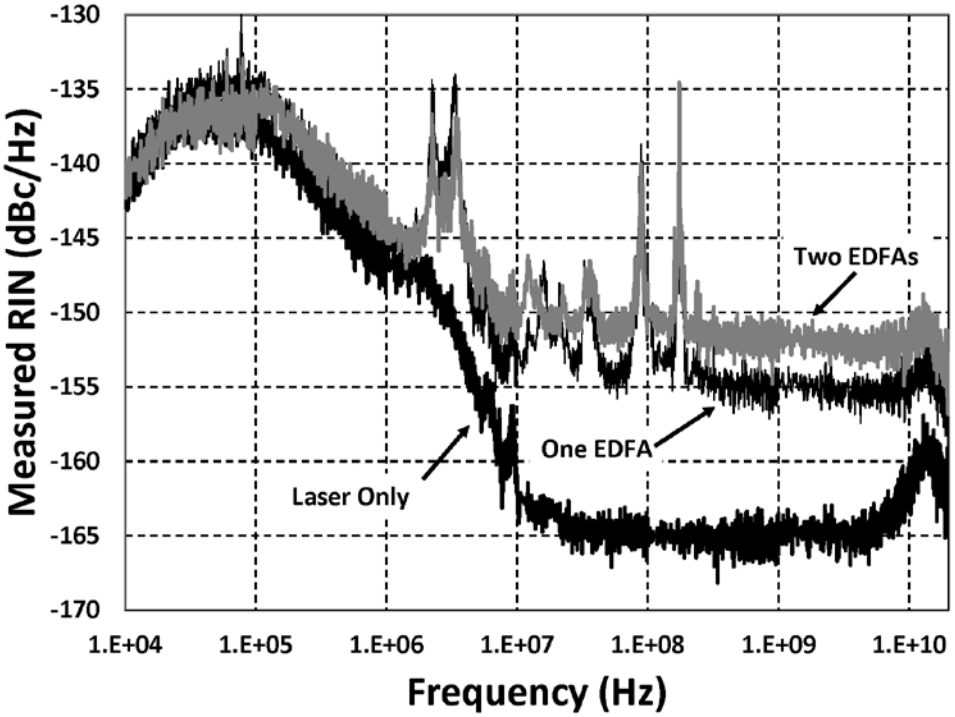

Fig. 15: The measured relative intensity noise (RIN) for three photonic links all at I_{dc} = 10 mA. Shown are data for a laser only and the same laser amplified with one and two erbium-doped fiber amplifiers (EDFAs). In both amplified cases, the EDFA gain is set to compensate a passive loss and therefore provide no net optical gain. The shot-noise limit for these data is -165 dBc/Hz. These data are not for precisely the same links as in Figs. 13 and 14.

the laser only, a loss-compensated link with one EDFA, and a loss-compensated link with two EDFAs. At frequencies above 100 kHz, the phase noise with the laser only is nearly shot-noise limited. A penalty of about 5 dB is incurred by using one EDFA with an additional 4 dB added with two EDFAs. For identical EDFAs in a symmetric loss compensated system, the change in noise penalty should be 3 dB for two EDFAs [6], close to the observed change. Similar trends are observed in the SSB amplitude noise data shown in Fig. 14. Measured RIN data for links similar, but not identical, to those in Figs. 13 and 14 are shown in Fig. 15. For these links, the laser-only configuration is shot-noise limited starting before 100 MHz. In this case, the penalty for adding one EDFA is 10 dB, with a second EDFA adding an additional 3 dB.

The effect of RIN on the RF performance of a FODL is significant, as demonstrated in Figs. 3(b), 4(b) and 5(b). In those plots, the curves labeled "No RIN" indicate that shot and thermal noise only are included in the calculation. When the plotted RF metrics become independent of I_{dc}, the RIN limit is reached. The previous equations for F, CDR and SFDR can be modified to give the performance in the RIN limit. Note, as described above, the effect of RIN on phase and amplitude noise can vary; it is best to conduct that analysis empirically.

The RIN-limited noise factor is given by inserting (30a) into (9a):

$$F_{\mathrm{RIN}} = \frac{V_\pi^2 \cdot \mathrm{RIN}}{\pi^2 R_{\mathrm{in}} k_{\mathrm{B}} T}. \tag{32a}$$

In dB-form,

$$\mathrm{NF}_{\mathrm{RIN}}\left[\mathrm{dB}\right] = 177.0 + 20\log\left(V_{\pi}\left[\mathrm{V}\right]\right) + \mathrm{RIN}\left[\mathrm{dBc/Hz}\right], \tag{32b}$$

For R_{in} = 50 Ω and T = 290 K. The compression dynamic range as a function of RIN only is obtained by inserting (30a) into (12a) as

$$\mathrm{CDR}_{\mathrm{RIN}} = \frac{0.4516}{\mathrm{RIN} \cdot B} \tag{33a}$$

$$\mathrm{CDR}_{\mathrm{RIN}}\left[\mathrm{dB \cdot Hz}\right] = -3.5 - \mathrm{RIN[dBc/Hz]}\,. \tag{33b}$$

Finally, the RIN-limited spurious free dynamic range is

$$\mathrm{SFDR}_{\mathrm{RIN}} = \left(\frac{4}{\mathrm{RIN} \cdot B}\right)^{2/3} \tag{34a}$$

$$\mathrm{SFDR}_{\mathrm{RIN}}\left[\mathrm{dB \cdot Hz}^{2/3}\right] = 4.0 - \frac{2}{3}\mathrm{RIN[dBc/Hz]}\,, \tag{34b}$$

as given by inserting (30a) into (17a).

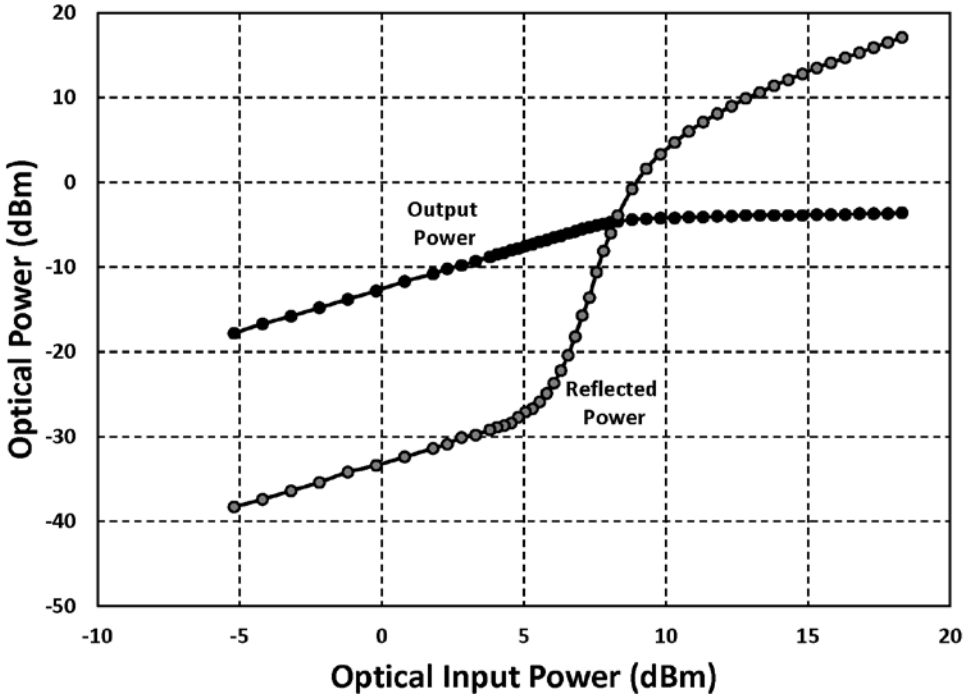

Fig. 16: The measured optical output power (black circles) and reflected optical power (grey circles) as a function of optical input power into 50 km of SMF-28 fiber [9].

2.3 Fiber Effects

Long lengths of fiber impact the performance of a FODL. Loss, stimulated Brillouin scattering (SBS) and chromatic dispersion are the initial concerns for single (optical) channel implementations. Loss is straight-forward and can be offset with EDFAs; as described in Section 1, a typical value is 0.2 dB/km optical loss. A brief description of the remaining issues, SBS and chromatic dispersion are provided here.

The performance of a FODL employing IMDD will increase with increased output optical power (increased I_{dc}). A dominant process that limits the power handling of an optical fiber, and hence the performance of a long-haul analog link, is SBS. Brillouin scattering in a crystal occurs when a photon is annihilated with the subsequent emission of a lower-frequency photon and an acoustic phonon (Stokes process) or a higher-frequency photon (anti-Stokes process) [7]. Stimulated Brillouin scattering is a fiber nonlinearity that occurs at a relatively low optical power when signal photons stimulate the Stokes process resulting in Stokes-shifted photons counter propagating in the fiber with respect to the signal [8]. As will be demonstrated below, the SBS process is problematic in that it limits the amount of signal power that can be transmitted to the end of a link and in that the Stokes signal will cause noise in the RF domain.

Shown in Fig. 16 is the response for a 50-km span of SMF-28 fiber demonstrating the SBS process [9]. The output optical power and backscattered optical power are linear functions of the input power below 4 dBm input optical power. The fiber loss in this regime, about -12 dB, is primarily due to Rayleigh scattering in the fiber and the backscattered level, about -33 dB, provides a measure of the counter-propagated Rayleigh-scattered light. As the SBS threshold is reached, the backscattered power increases and the output power saturates.

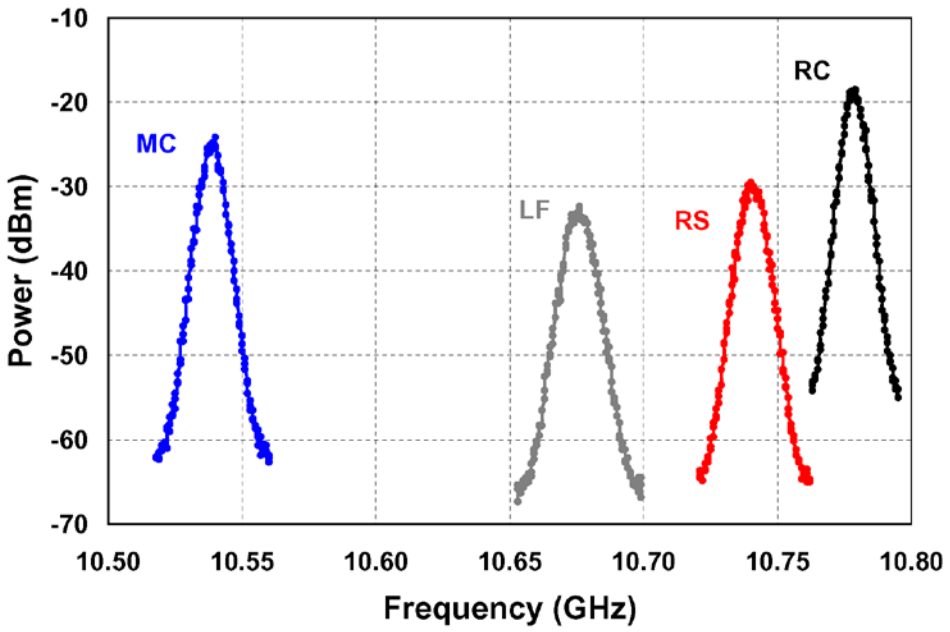

Fig. 17: Measured SBS frequencies for different fiber types [10]. Shown are data for Corning LEAF (LF), Corning Metrocor (MC), OFS TrueWave RS (RS) and OFS TrueWave Reach (RC).

In addition to the saturated output power and, hence, decreased RF performance, the SBS process adds significant noise around the acoustic phonon frequency associated with the scattering. The counter-propagating Stokes signal, which is down-shifted in frequency via the inelastic scattering, can elastically Rayleigh scatter to co-propagate with the signal. The Rayleigh-scattered Stokes signal and the original pump signal will then mix through photodetection resulting in a noise peak centered near the SBS frequency. This frequency is near 10 GHz for most telecommunications fiber. Shown in Fig. 17 are the measured SBS spectra resulting from this process for various fiber types [10]. Fibers exhibiting different SBS frequencies will be employed in the design presented in Section 3. Even if the limited optical output power such as shown in Fig. 16 can be tolerated, this noise will result in increased noise figure and decreased dynamic range for a FODL operating near the SBS frequency. Increased noise has also been observed at frequencies away from the SBS frequency [11] and increased phase noise has been observed through fiber [12], both of which must be examined in a FODL.

As quantified by its dielectric function, optical fiber will have a frequency-dependent index of refraction, which results in a frequency-dependent time delay when traversing a given length of optical fiber. For dual-sideband modulation formats, such as IMDD, the analog photocurrents generated by each sideband can destructively interfere due to this chromatic dispersion. Full and partial destructive interference via this phenomena causes frequency-dependent fading in the RF response. Such fading is demonstrated in Fig. 18, where measured and calculated data show the effect. The theoretical RF gain factor for an IMDD including dispersion is [13]

$$g = \pi^2 \left(\frac{I_{dc}^2}{V_\pi^2} \right) R_{in} R_{out} \cos^2 \left(\frac{DL\lambda_o^2 \pi f^2}{c} \right), \tag{35}$$

where D is the dispersion parameter for the fiber of length L, λ_o is the optical carrier wavelength, f is the electronic modulation frequency and c is the speed of light in vacuum.

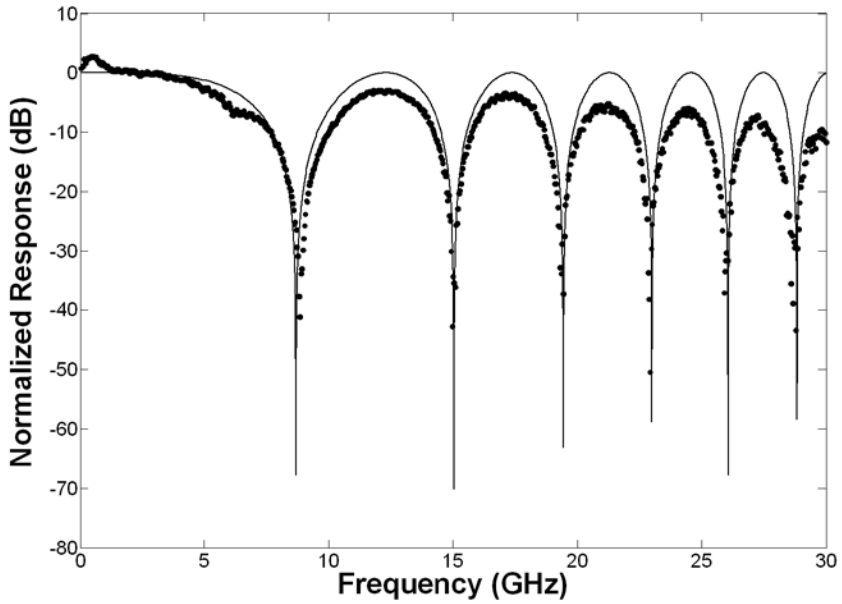

Fig. 18: The measured (circles) and calculated [line, (35)] normalized response for an IMDD link with D = 16.5 ps/(nm·km), L = 50 km and λ_o = 1551 nm. The roll off in the measured data is due to the frequency response of the modulator and photodiode—not chromatic dispersion.

There are some useful equations that can be derived from (35). First is the 3-dB frequency, the lowest frequency at which the response is 3-dB lower than the normalized response [1]:

$$f_{3\mathrm{dB}} = \left(\frac{c}{4\lambda_o^2 DL} \right)^{1/2} . \tag{36}$$

It is also useful to calculate the k^{th}-order null in terms of radio frequency, fiber length, or delay time as [14]

$$f_{\mathrm{null}}\left(\mathrm{GHz}\right) = 3.87\times 10^{5} \left(\frac{1+2k}{D\left(\dfrac{\mathrm{ps}}{\mathrm{nm}\cdot\mathrm{km}}\right) L\left(\mathrm{km}\right)\lambda_o^2\left(\mathrm{nm}\right)} \right)^{1/2} \tag{37}$$

$$L_{\mathrm{null}}\left(\mathrm{km}\right) = 1.50\times 10^{11} \left(\frac{1+2k}{D\left(\dfrac{\mathrm{ps}}{\mathrm{nm}\cdot\mathrm{km}}\right) f^2\left(\mathrm{GHz}\right)\lambda_o^2\left(\mathrm{nm}\right)} \right) \tag{38}$$

$$t_{\text{null}}\left(\mu\text{s}\right) = 7.34\times10^{11}\left(\frac{1+2k}{D\left(\frac{\text{ps}}{\text{nm}\cdot\text{km}}\right)f^{2}\left(\text{GHz}\right)\lambda_{\text{o}}^{2}\left(\text{nm}\right)}\right). \tag{39}$$

There are other deleterious effects of chromatic dispersion in a long-haul analog link that are beyond the scope of this report. These effects are covered in [1], such as increased even-order distortion and optical phase-to-intensity noise conversion. Likewise, there are numerous other fiber nonlinearities that can affect the performance of long delay lines. The work in [1] and the references therein provide a thorough description of other fiber effects. However, SBS and chromatic dispersion are the main considerations for the FODL designs to follow.

3 DESIGN OF A FIBER-OPTIC DELAY LINE

The initial design for an X-Band FODL with two delays is presented here. The final FODL architectures described in the following two sections deviate from this design due to modified project needs. However, it is instructive to describe the thought process of the original IMDD FODL design as shown in Fig. 19. A 18-dBm semiconductor distributed feedback (DFB) laser (JDSU CFQ-935) was used as the source. As shown in Fig. 20, this laser is essentially shot-noise limited for a photocurrent of I_{dc} = 10 mA. The MZM was a 40-GHz device with a V_{π} = 4.7 V at 8 GHz and V_{π} = 5.0 V at 12 GHz. The two 20-km fiber spans are customized such as to allow an SBS threshold > 10 dBm and to eliminate fading at 10 GHz due to chromatic dispersion. The MZM insertion loss at quadrature is much less than 8 dB and allows a 10 dBm launch power into the first span. With a loss of 0.35 dB/km through the custom span, an output power of 3 dBm is expected before the first EDFA (JDSU OA-400). A photocurrent of I_{dc} = 10 mA is desired, which sets the required power before the photodiodes at 11 dBm assuming a photodiode responsivity of nearly 0.8 A/W. With a 60%/40% fiber optic coupler at the first EDFA output, this dictates that the first EDFA must source 13 dBm of optical power. This sets the launch power into the second span at 9 dBm, which requires the second EDFA to source 11 dBm with a 2-dBm input.

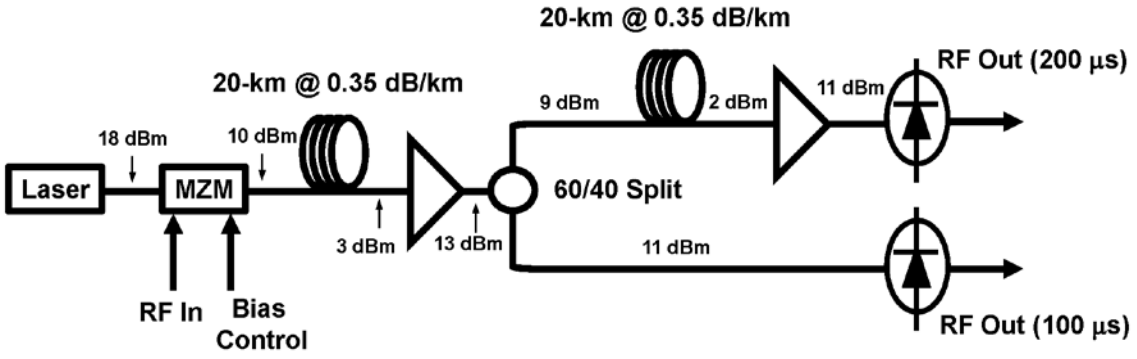

Fig. 19: Block diagram for the initial X-Band FODL design with optical power budget.

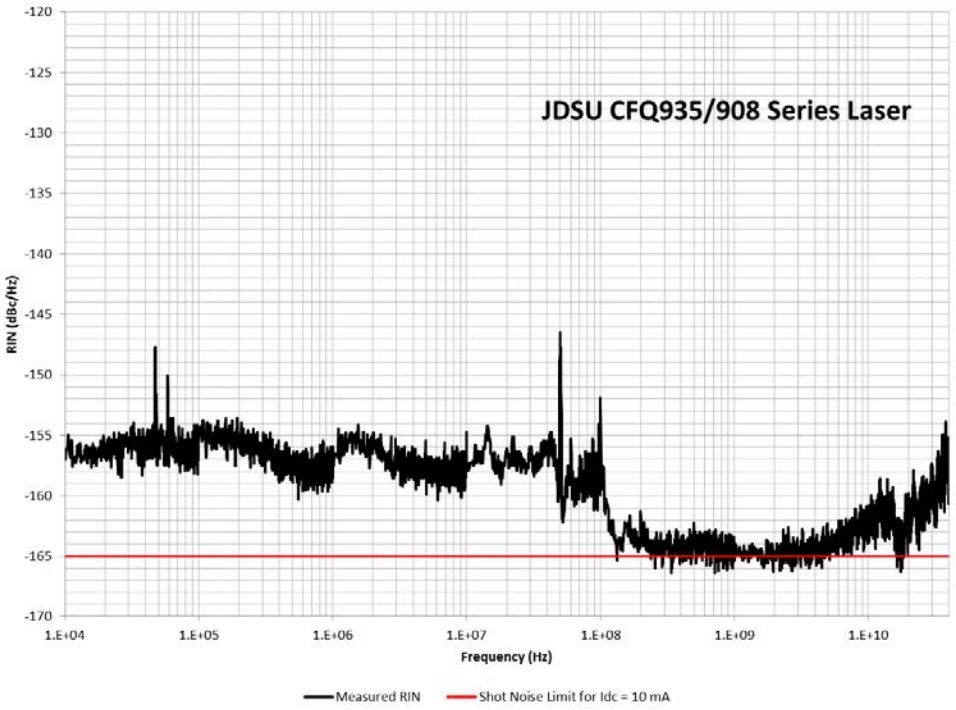

Fig. 20: Measured RIN spectrum for a JDSU semiconductor distributed feedback laser [15].

The remaining parameters required to estimate the performance are the noise added by the EDFAs. The JDSU OA-400 EDFAs have been characterized previously at NRL [16] and excerpts from that work are provided in Figs. 21 and 22. Shown in Fig. 21 are the measured optical output powers for an EDFA as a function of optical input power for two pump currents, 50 and 100 mA. From these data, we can deduce that a pump current between 50 and 100 mA, but closer to 100 mA, will be required for both of the EDFAs shown in Fig. 19. The noise penalties for the same pump currents are shown in Fig. 22. For one EDFA, the noise penalty will be somewhere near 4 dB; this is the expected noise penalty for the 100-μs channel. For two EDFAs in a loss-compensated system, the combined noise penalty should be 3-dB higher than that of a single EDFA [6]. Therefore, we expect the noise penalty for the 200-μs channel to be about 7 dB.

Given the estimated EDFA noise penalties, the performance of each channel can be approximated using the design equations in the previous section. Equation (6b) gives the gain as G = -15.5 dB for each channel at 8 GHz falling to G = -16.1 dB for each channel at 12 GHz. The noise figure is given by (27b) with the noise penalties above added. For the 100-μs channel, NF = 29.5 dB at 8 GHz rising to NF = 30.1 dB at 12 GHz. The expected NF for the 200-μs channel is 3-dB higher, NF = 32.5 dB at 8 GHz rising to NF = 33.1 dB at 12 GHz. The input power at 1-dB compression is the same for both channels as given by (7b), 13.0 dBm at 8 GHz and 13.6 dBm at 12 GHz. The OIP3 is also the same for both channels and is independent of frequency, OIP3 = 7.0 dBm, according to (15b). Finally, the $SFDR_3$ is given by (29b) with a correction of -2/3 times the noise penalty in dB. For the 100-μs channel, $SFDR_3$ = 111.3 $dB \cdot Hz^{2/3}$; $SFDR_3$ = 109.3 $dB \cdot Hz^{2/3}$ for the 200-μs channel. These are the specifications provided at the time of the initial design. Others can be calculated using the equations in Section 2.

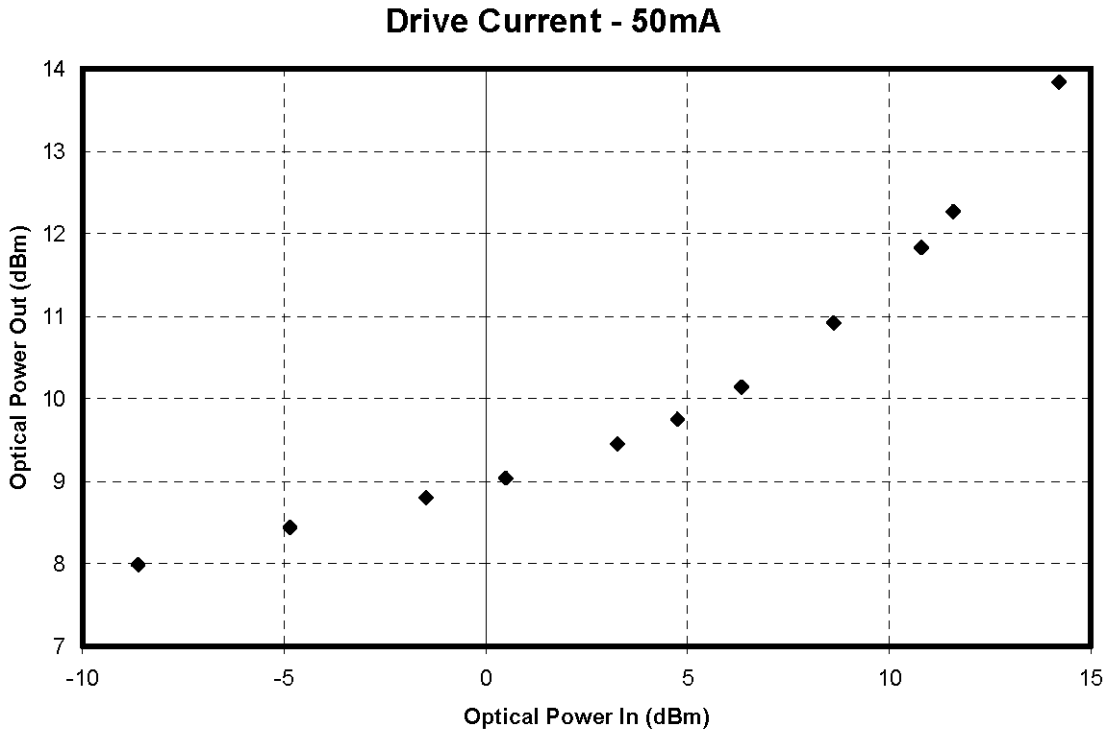

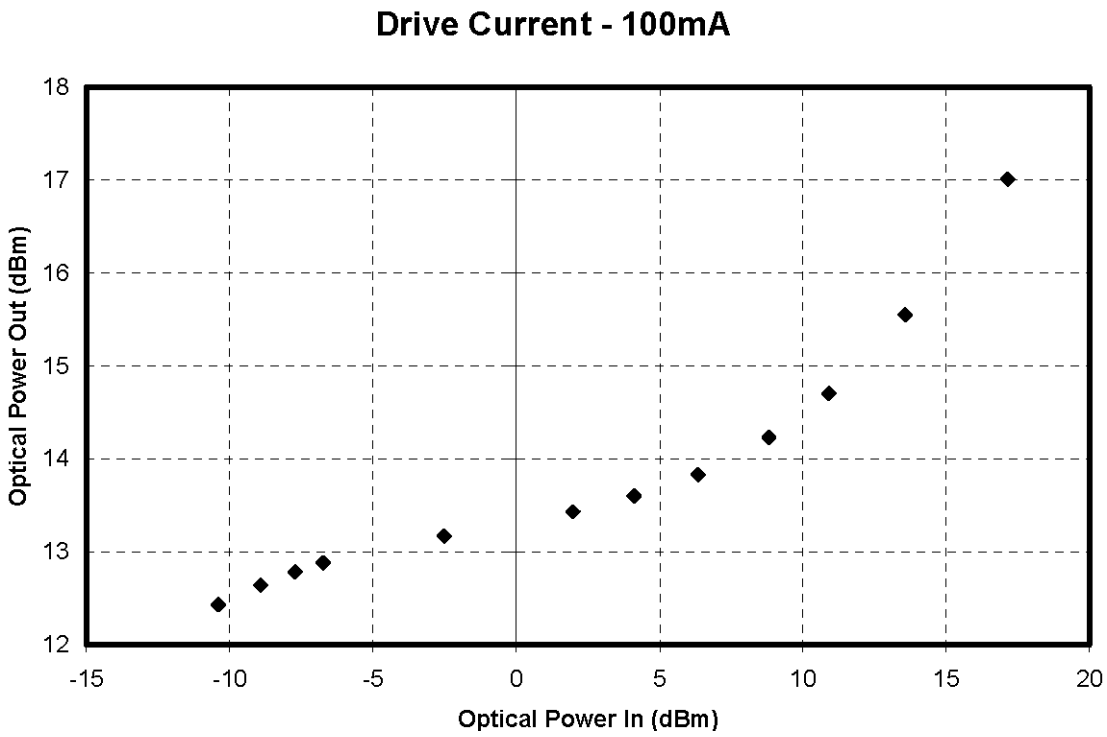

Fig. 21: Measured optical output power as a function of optical input power into a JDSU OA-400 EDFA for two different pump currents [16].

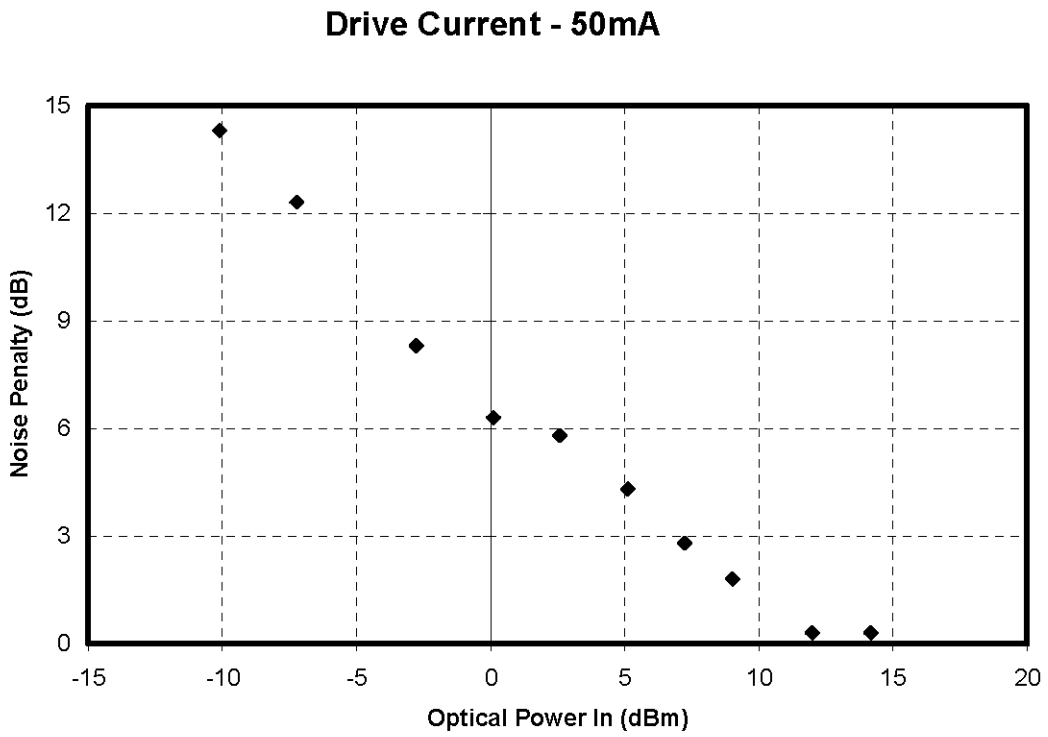

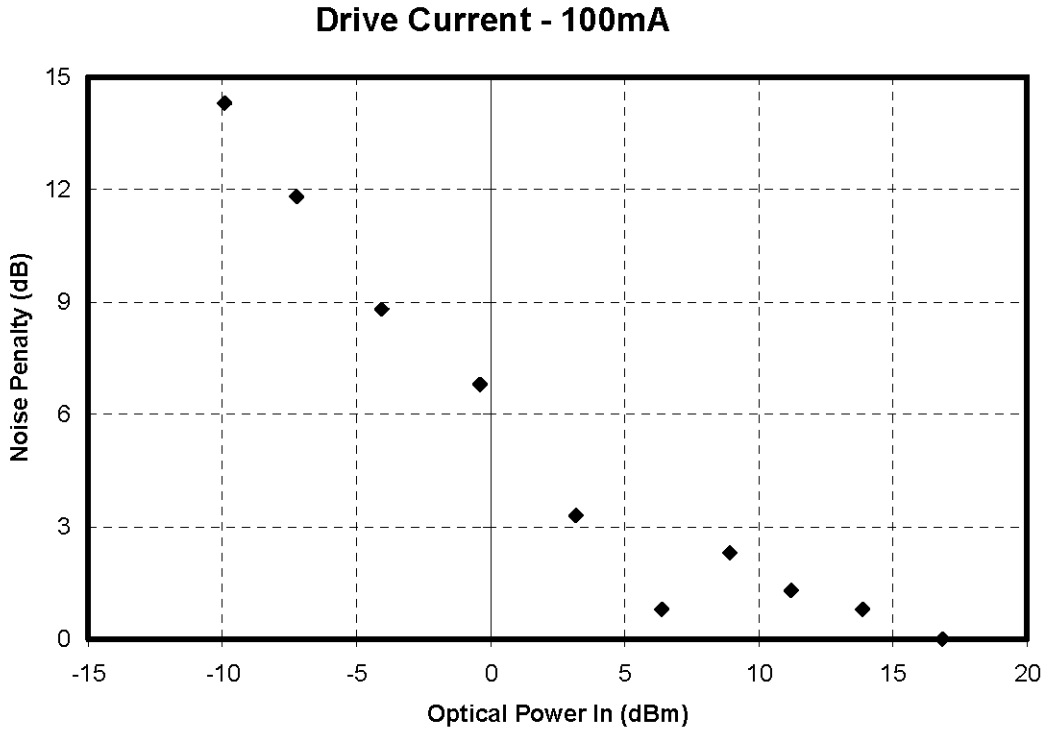

Fig. 22: Measured noise penalty relative to shot noise as a function of optical input power into a JDSU OA-400 EDFA for two different pump currents [16].

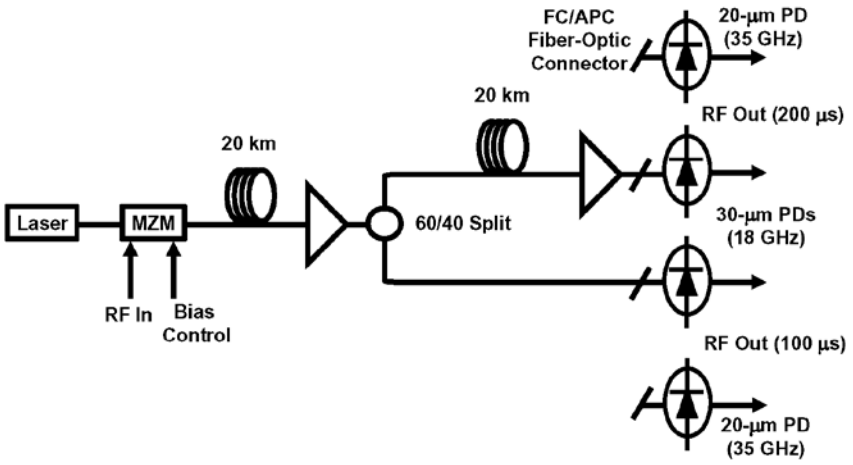

Fig. 23: Block diagram for FODL #1.

4 MEASURED PERFORMANCE

Two FODLs were designed following the procedure in Section 3 and are shown in Figs. 23 and 36. There are four modes for each FODL: short delay low band (18 GHz), short delay high band (35 GHz), long delay low band, and long delay high band. The short and long delays for FODL #1 are 100 and 200 μs, respectively; those for FODL #2 are 67 and 125 μs. In this section the measured performance for each FODL in all configurations is presented.

The custom fiber spans are detailed in the previous section but did exhibit unexpected noise in X-Band. Shown in Fig. 24 are spectra measured at the output of FODL #1 Span 1, showing a peak near the Brillouin frequency. Those data are shown as a function of launch power and the peak remains relatively constant, suggesting that the scattering is not stimulated. Rather, the noise is attributed to non-stimulated Brillouin scattering reflected to the output of the link. The source of the reflection was not precisely determined. One possible source is the splices between the two fiber types used (see Section 5). For both FODLs, the launch power into each span was set at approximately 9 dBm.

Shown in Figs. 25 and 26 are the S-Parameters for FODL #1. The RF gain ($|S_{21}|^2$) is a few dB below -16 at 10 GHz due to cable and connector loss on the packaged FODL. Shown in Figs. 27 and 28 are the measured noise power spectral densities at the output of the FODL. For these data, the shot noise level is around -164 dBm/Hz. More noise power is observed at the output and is due to a larger amount of noise from the EDFAs than expected. The ripple in the high-band data is due to impedance mismatch in the measurement apparatus. Furthermore, band breaks in the measurement system cause some discontinuities in the data, such as at 20 GHz in the 200-μs high-band channel. Shown in Figs. 29 and 30 are the measured SSB phase and amplitude noise for a 10.24 GHz carrier. These data are relative to a nominal output power of -15 dBm. The shot noise level at these levels is approximately -152 dBc/Hz. The calculated noise figures are shown in Fig. 31. For these data, a nominal noise level was determined across the band and the gain data were used to calculated noise figure. Features such as the peak near 10.53 GHz are therefore not included in Fig. 31. The compression characteristics are shown in Figs. 32 and 33, followed by OIP3 data in Figs. 34 and 35. The compression data were obtained with a single-tone excitation at 10.24 GHz and the OIP3s were measured using a two-tone test near 10.24 GHz. The $SFDR_3$ for FODL #1 at 10 GHz are as follows, Low Band 100 μs: 105 $dB \cdot Hz^{2/3}$, Low Band 200 μs: 103 $dB \cdot Hz^{2/3}$, High Band 100 μs: 107 $dB \cdot Hz^{2/3}$, and High Band 200 μs: 103 $dB \cdot Hz^{2/3}$.

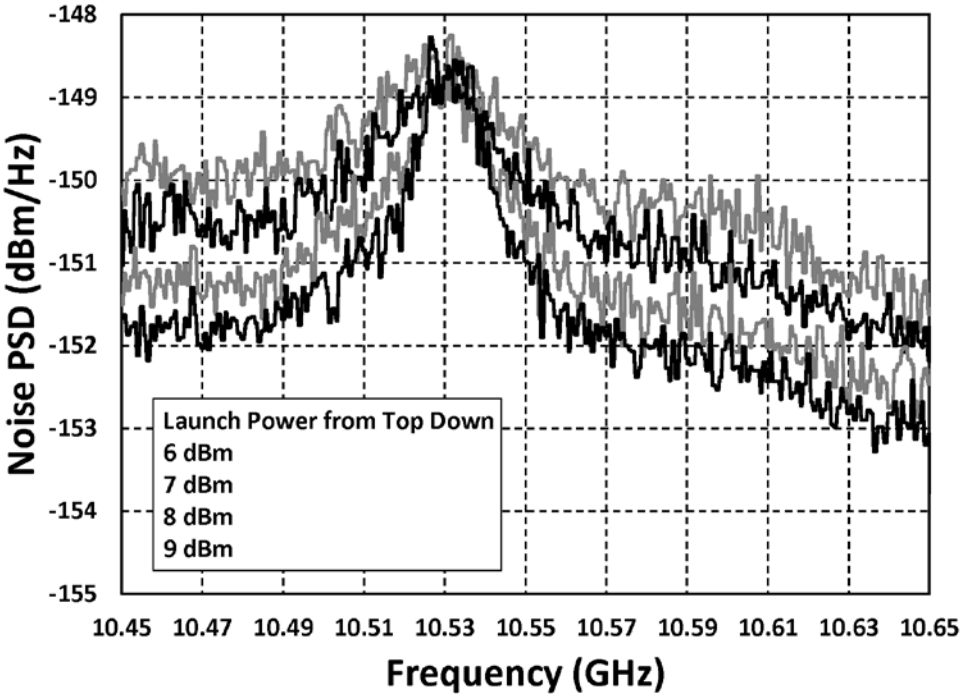

Fig. 24: The measured noise around the SBS frequency at the output of the first 20-km span of FODL #2.

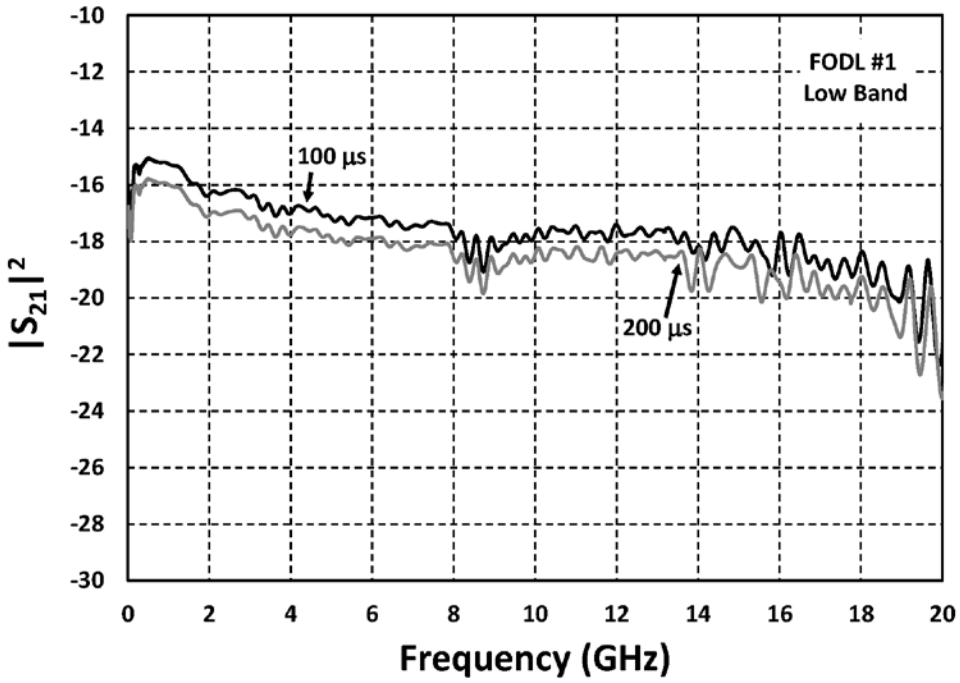
FODL #1
Low Band
100 µs
200 µs
|S21|2
Frequency (GHz)

(a)

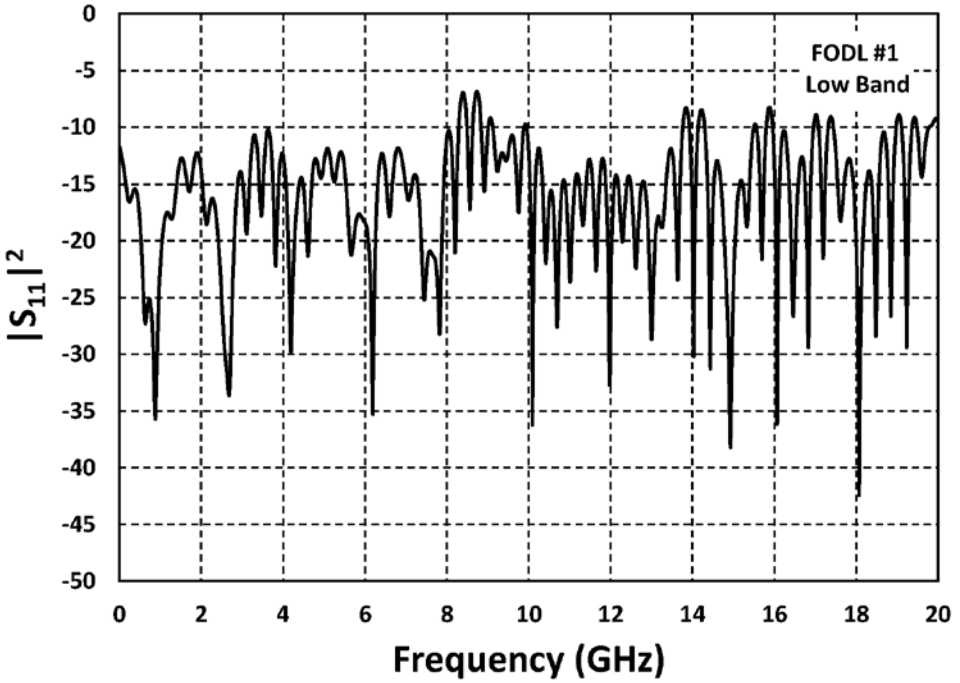
FODL #1
Low Band
|S11|2
Frequency (GHz)

(b)

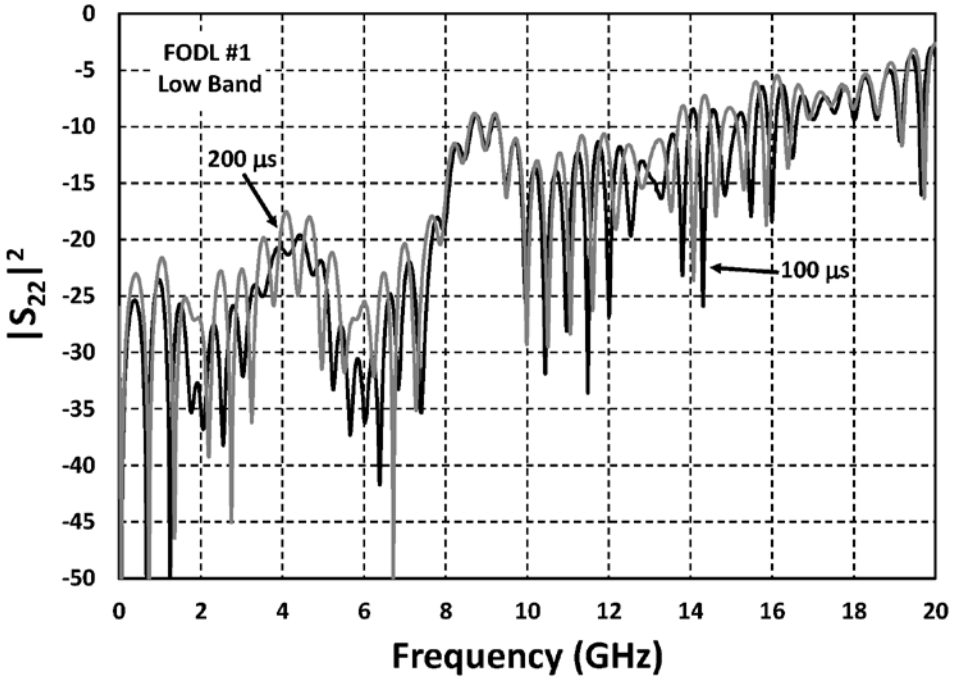

(c)

Fig. 25: Measured S Parameters for the Low Band of FODL #1 showing (a) gain, (b) reflection from the input and (c) reflection from the output.

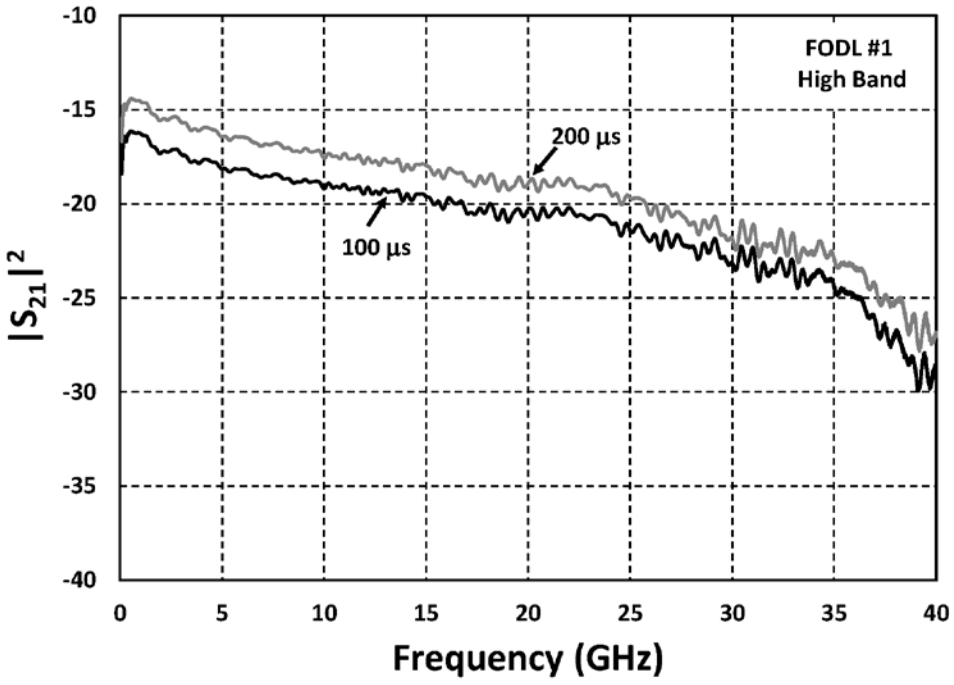

(a)

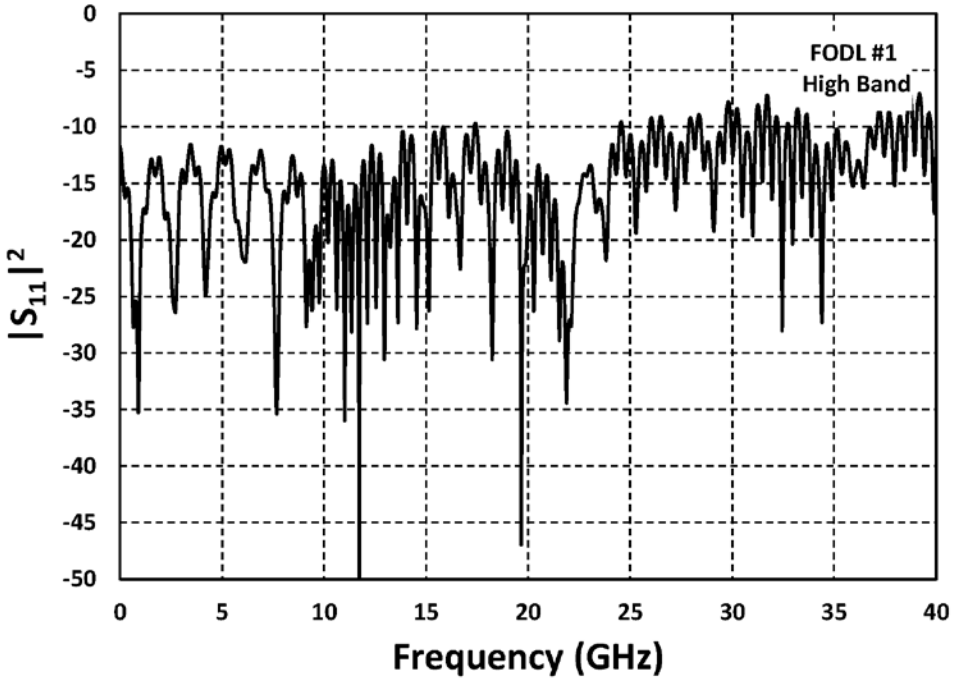

(b)

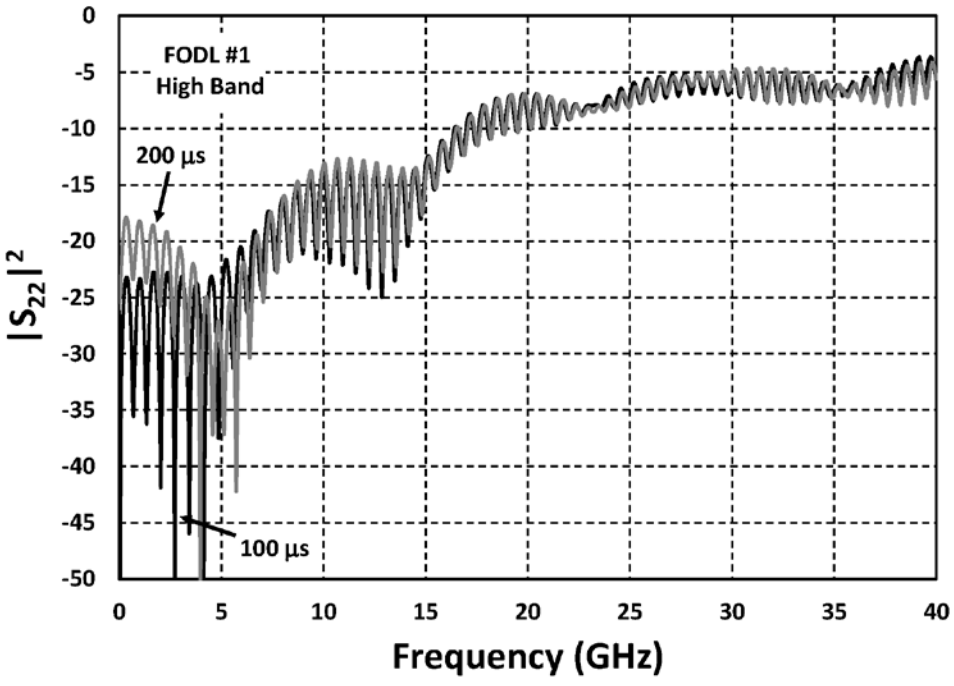

(c)

Fig. 26: Measured S Parameters for the High Band of FODL #1 showing (a) gain, (b) reflection from the input and (c) reflection from the output.

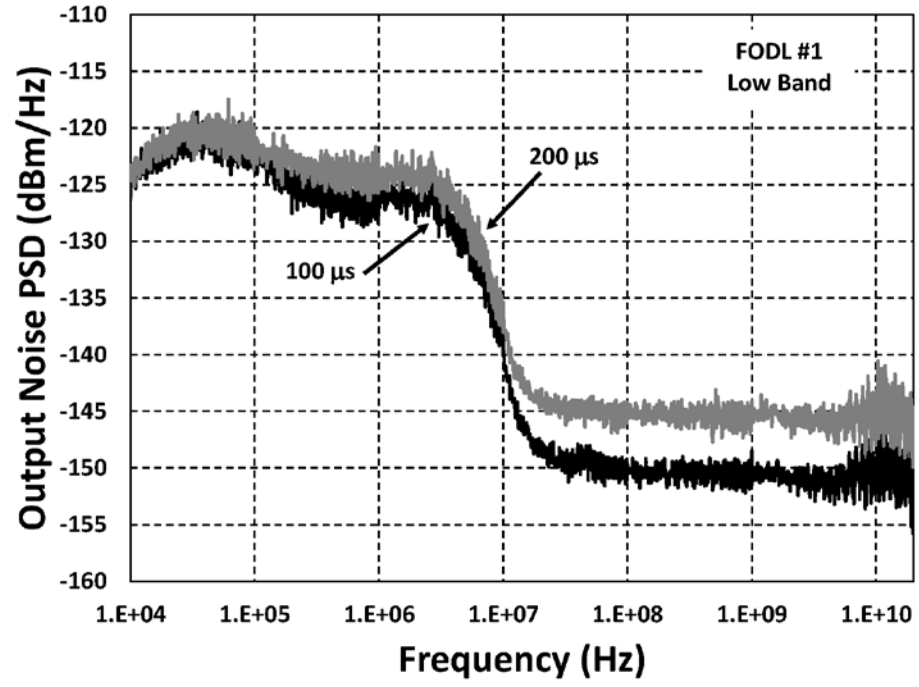

(a)

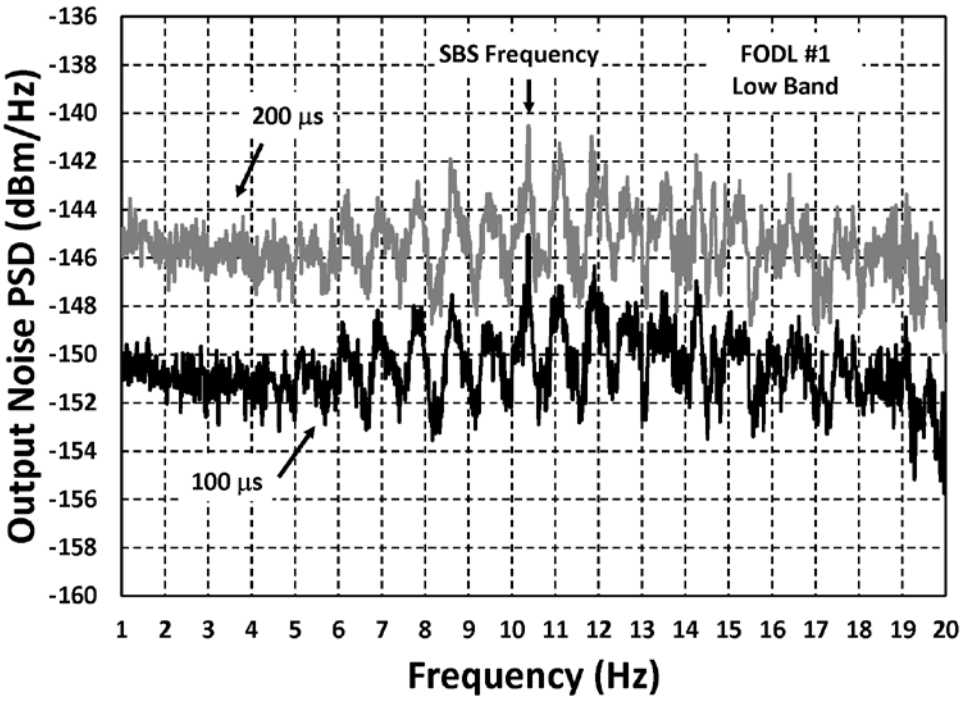

(b)

Fig. 27: Measured output noise power spectral density (PSD) for the Low Band of FODL #1.

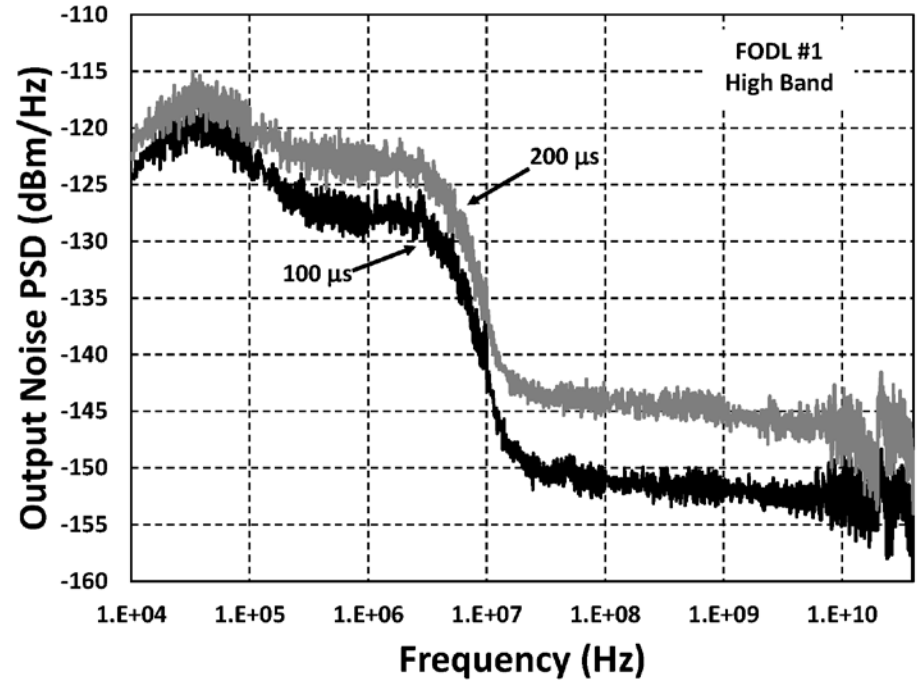

(a)

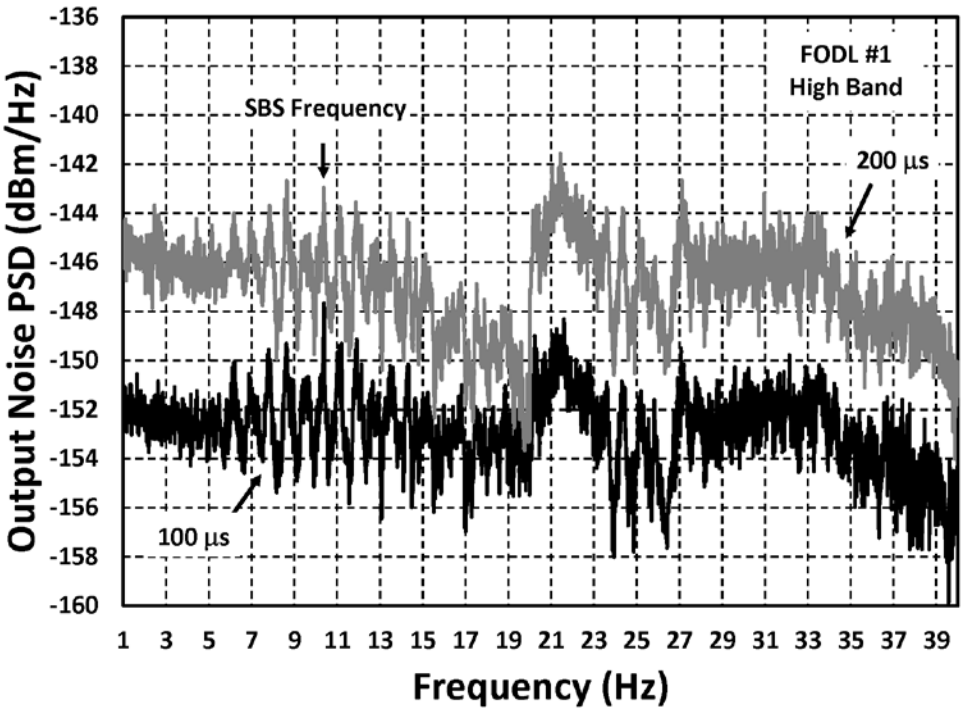

(b)

Fig. 28: Measured output noise power spectral density (PSD) for the High Band of FODL #1.

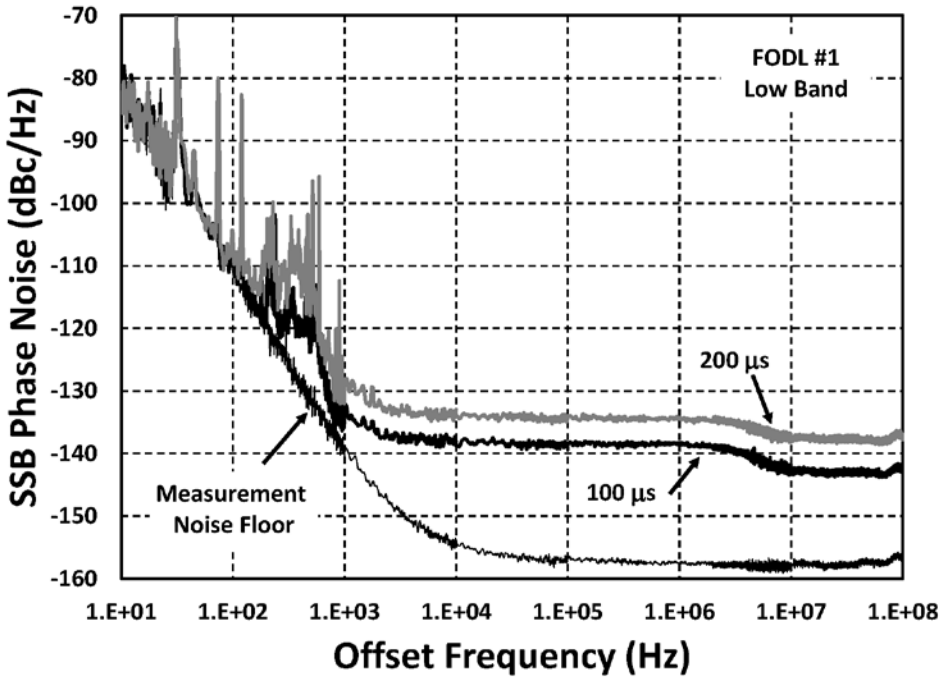

(a)

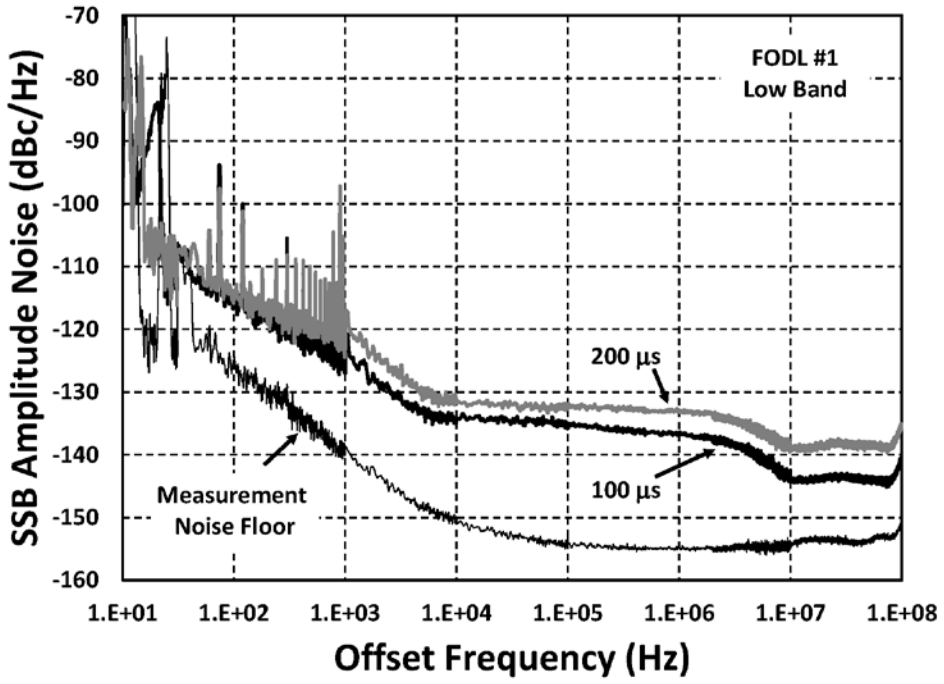

(b)

Fig. 29: Measured single-sideband (a) phase and (b) amplitude noise for a 10.24 GHz carrier using the Low Band of FODL #1.

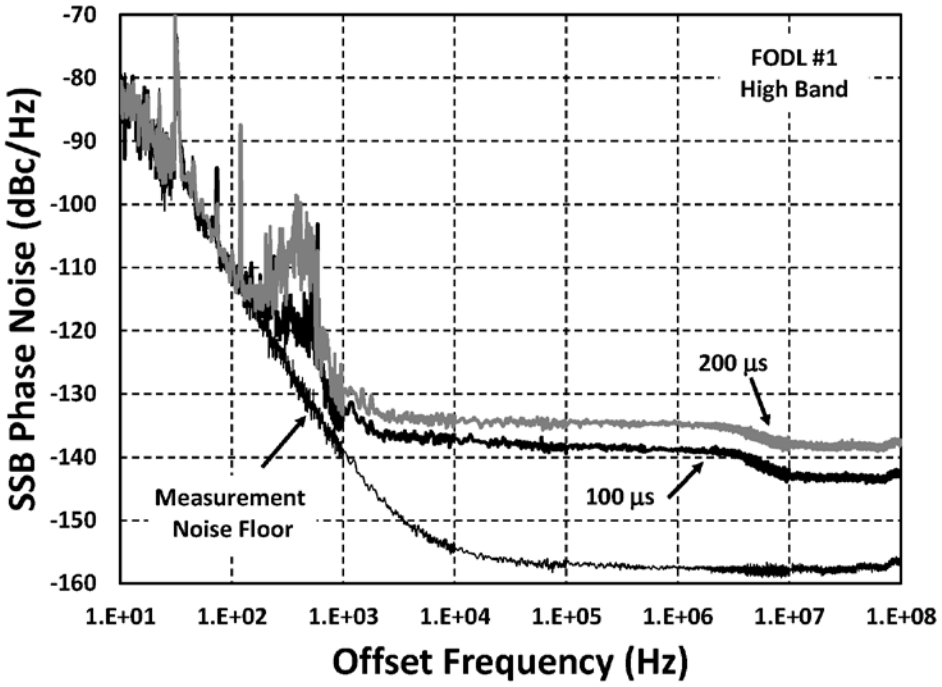

(a)

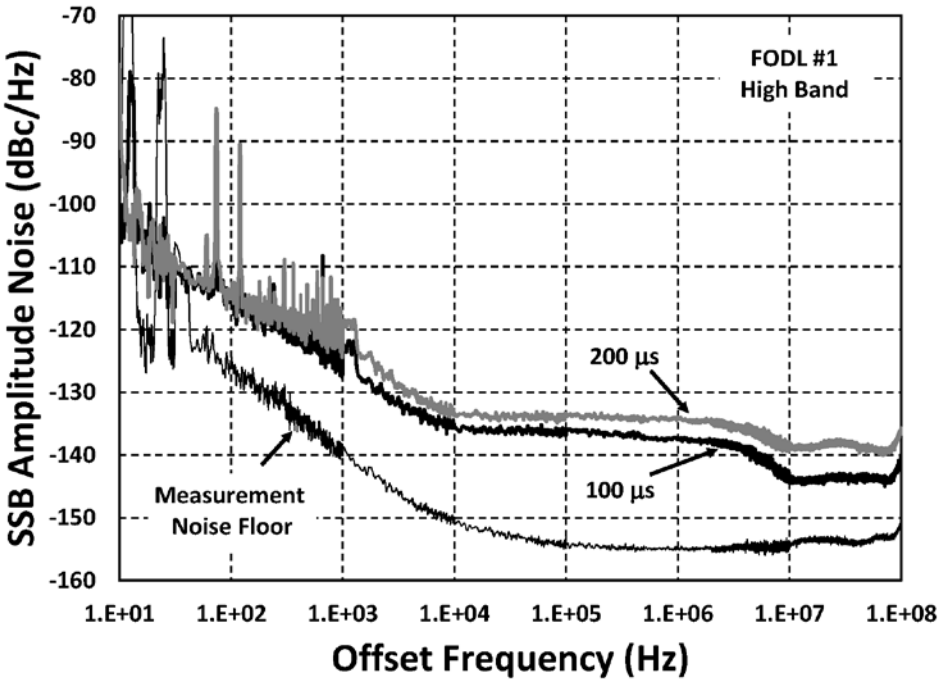

(b)

Fig. 30: Measured single-sideband (a) phase and (b) amplitude noise for a 10.24 GHz carrier using the High Band of FODL #1.

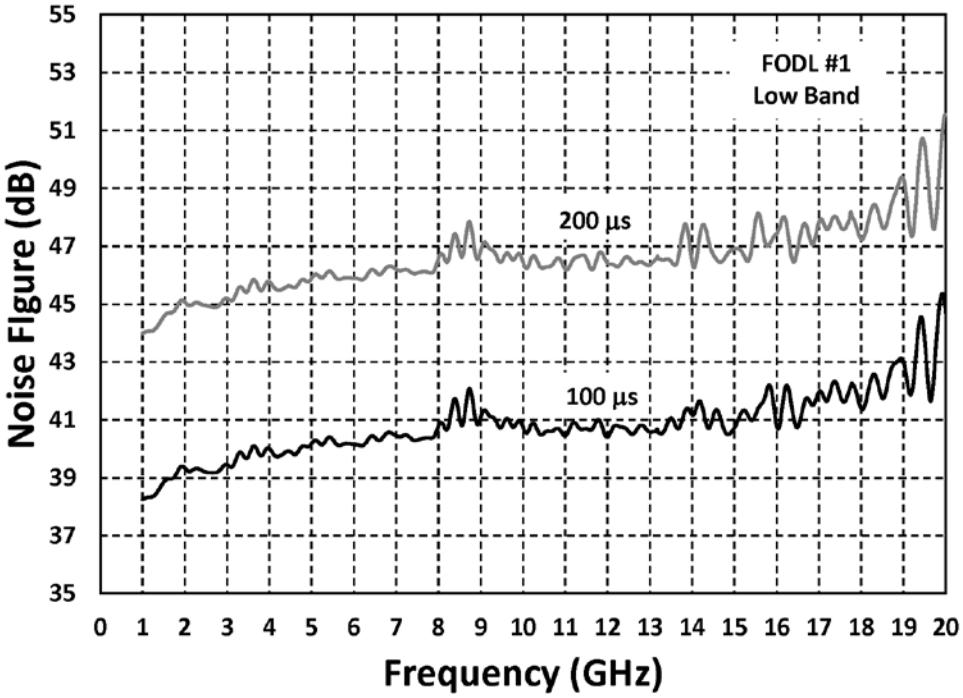

(a)

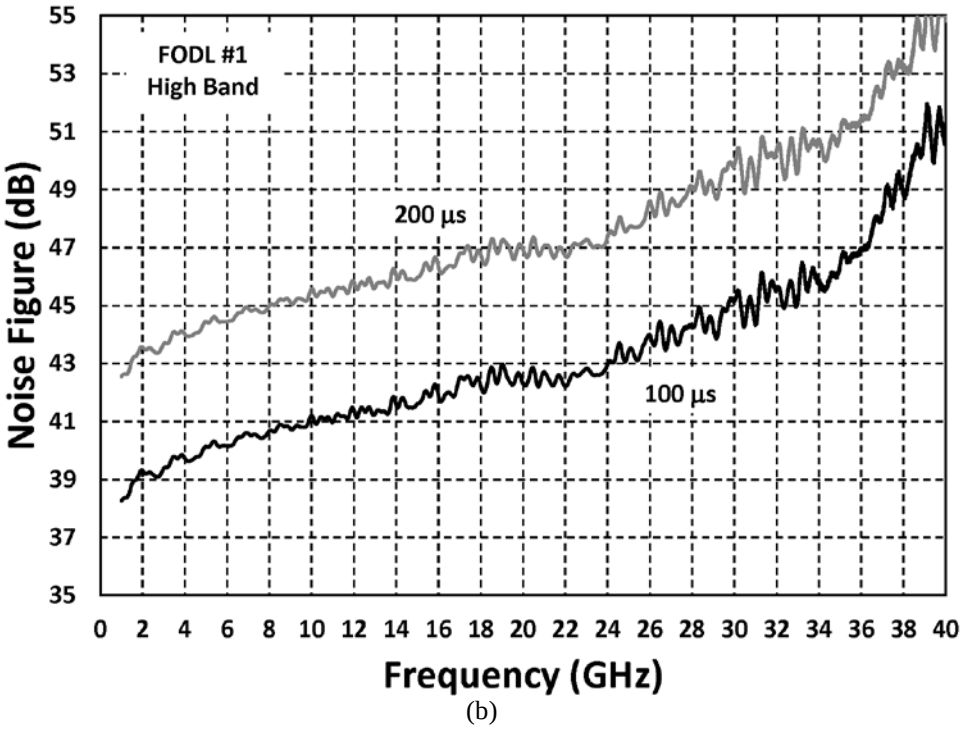

(b)

Fig. 31: Estimated noise figures for FODL #1.

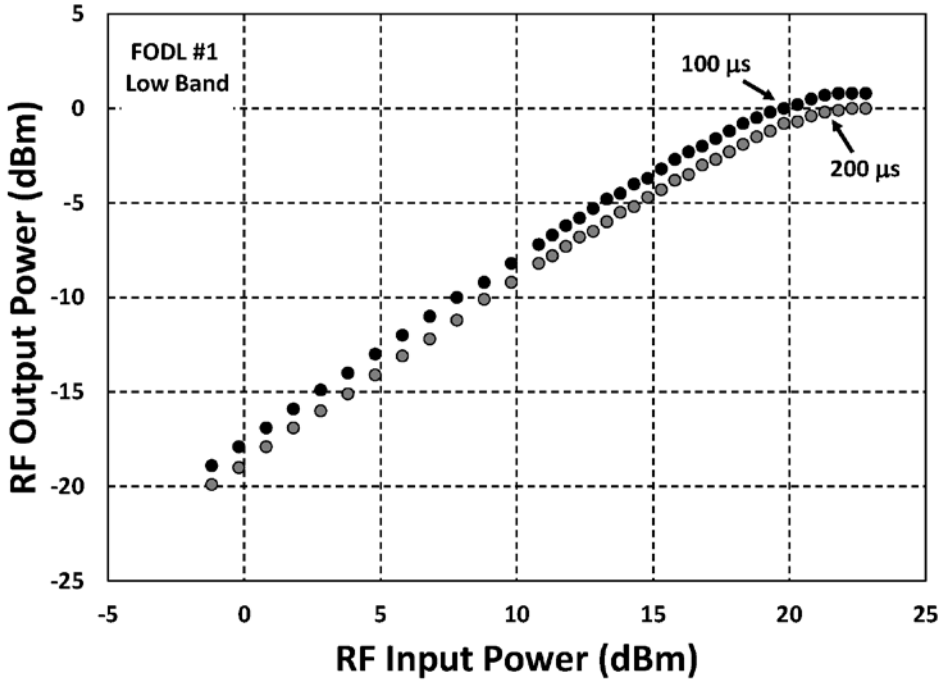

Fig. 32: The measured compression characteristic at 10.24 GHz for the Low Band of FODL #1.

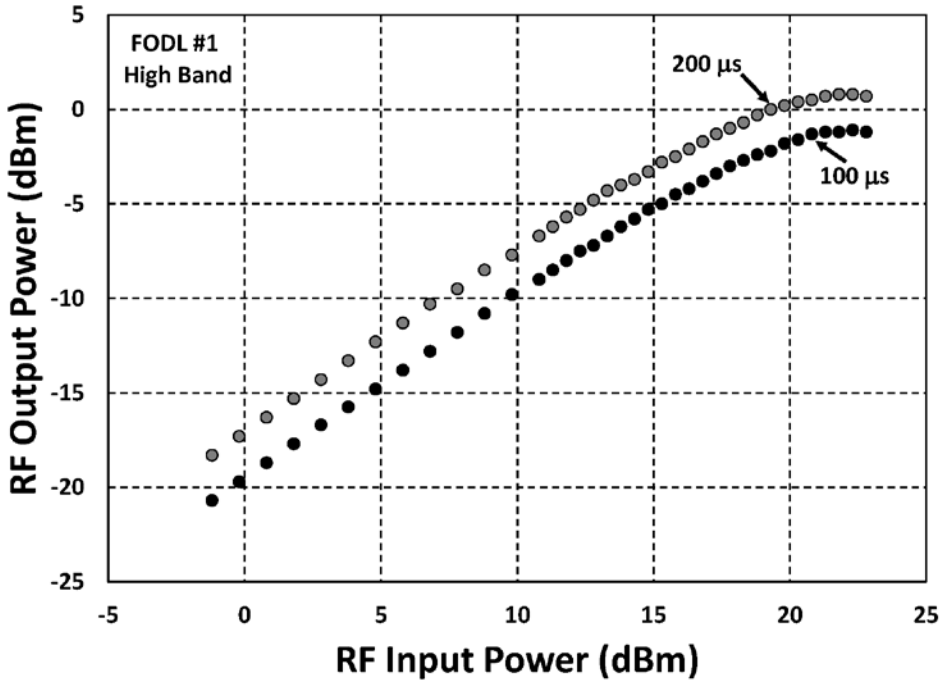

Fig. 33: The measured compression characteristic at 10.24 GHz for the High Band of FODL #1.

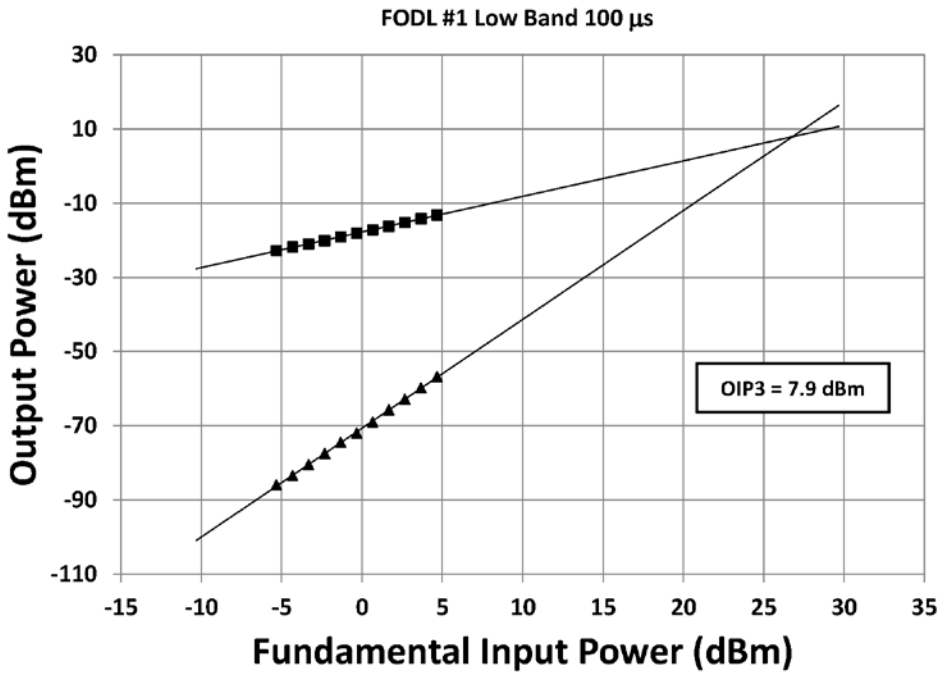

(a)

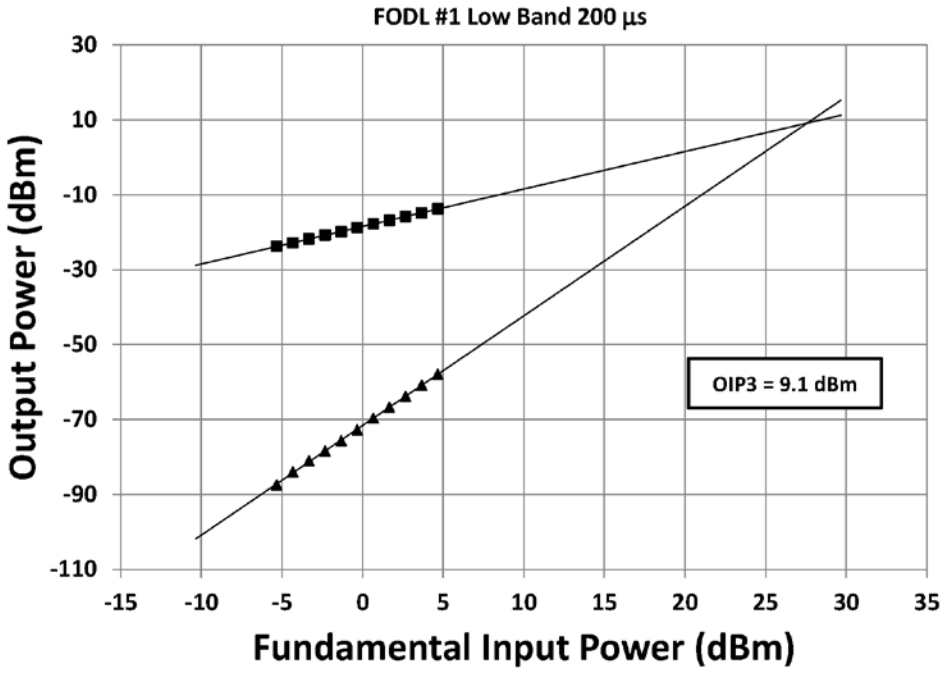

(b)

Fig. 34: Low-Band third-order output intercept point (OIP3) data for FODL #1 near 10.24 GHz. Shown are the fundamental response (squares) and the third-order intermodulation response (triangles).

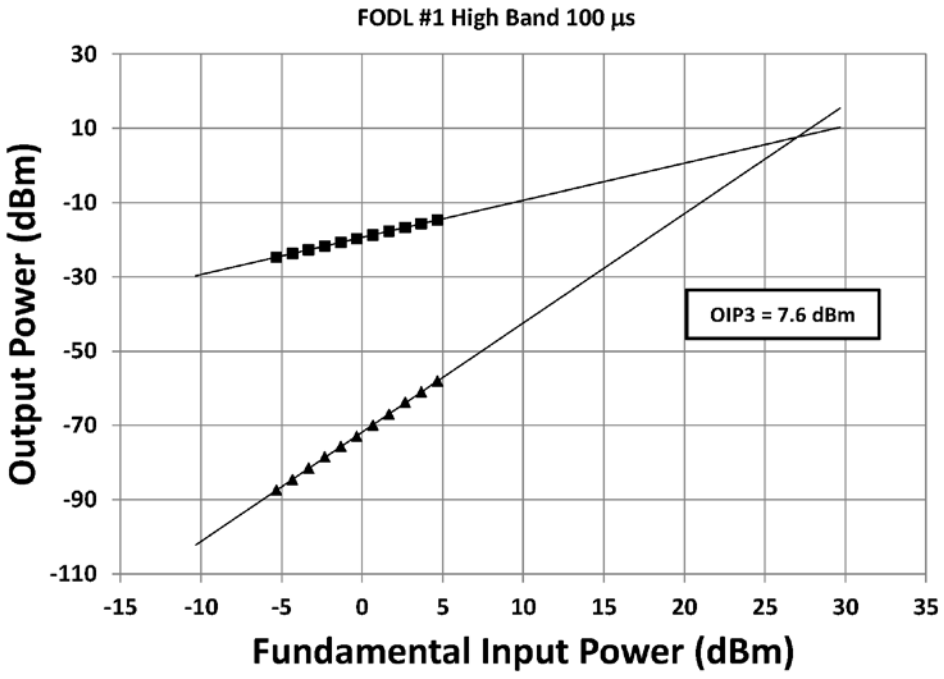

(a)

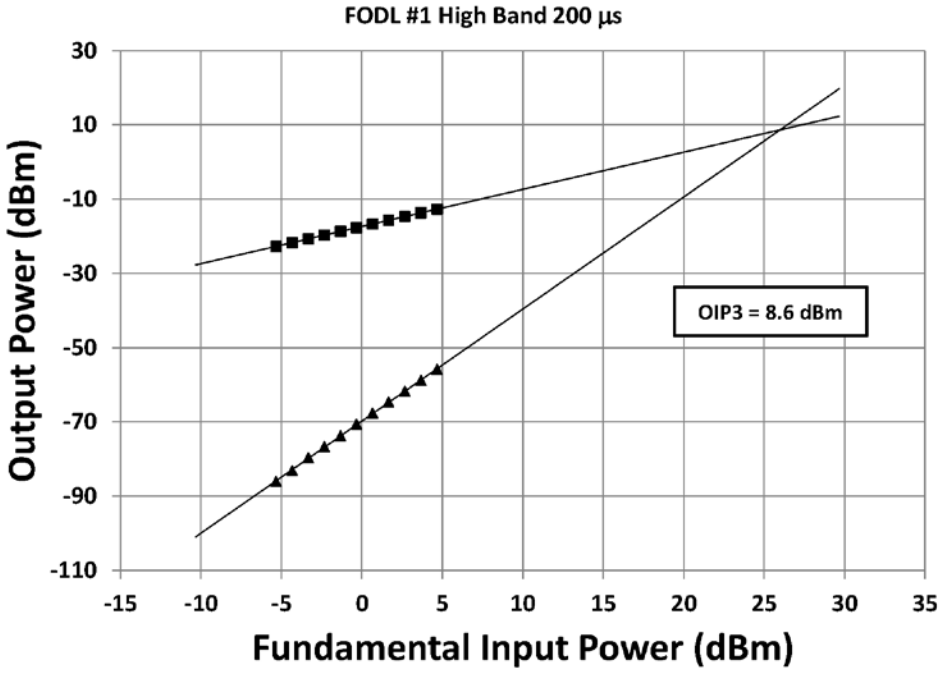

(b)

Fig. 35: High-Band third-order output intercept point (OIP3) data for FODL #1 near 10.24 GHz. Shown are the fundamental response (squares) and the third-order intermodulation response (triangles).

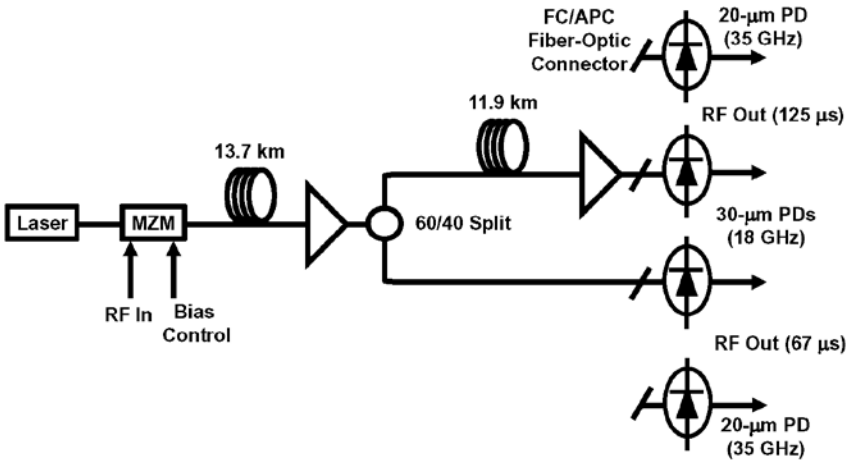

Fig. 36: Block diagram for FODL #2.

Shown in Figs. 37 and 38 are the S-Parameters for FODL #2. The RF gain ($|S_{21}|^2$considerably lower than the design and due to chromatic dispersion. Precise length trimming was traded for increased net dispersion in FODL #2. Shown in Figs. 39 and 40 are the measured noise power spectral densities at the output of the FODL. For these data, the shot noise level is around -164 dBm/Hz. More noise power is observed at the output and is due to a larger amount of noise from the EDFAs than expected. The ripple in the high-band data is due to impedance mismatch in the measurement apparatus. Furthermore, band breaks in the measurement system cause some discontinuities in the data, such as at 20 GHz in the 200-μs high-band channel. Shown in Figs. 41 and 42 are the measured SSB phase and amplitude noise for a 10.24 GHz carrier. These data are relative to a nominal output power of -15 dBm. The shot noise level at these levels is approximately -152 dBc/Hz. The amplitude noise data go below the measurement noise floor; this is due to imperfect setting of the nominal -15 dBm output power. The calculated noise figures are shown in Fig. 43. For these data, a nominal noise level was determined across the band and the gain data were used to calculated noise figure. Features such as the peak near 10.53 GHz are therefore not included in Fig. 31. The compression characteristics are shown in Figs. 44 and 45, followed by OIP3 data in Figs. 46 and 47. The compression data were obtained with a single-tone excitation at 10.24 GHz and the OIP3s were measured using a two-tone test near 10.24 GHz. The $SFDR_3$ for FODL #2 at 10 GHz are as follows, Low Band 67 μs: 107 $dB \cdot Hz^{2/3}$, Low Band 125 μs: 105 $dB \cdot Hz^{2/3}$, High Band 67 μs: 107 $dB \cdot Hz^{2/3}$, and High Band 125 μs: 106 $dB \cdot Hz^{2/3}$.

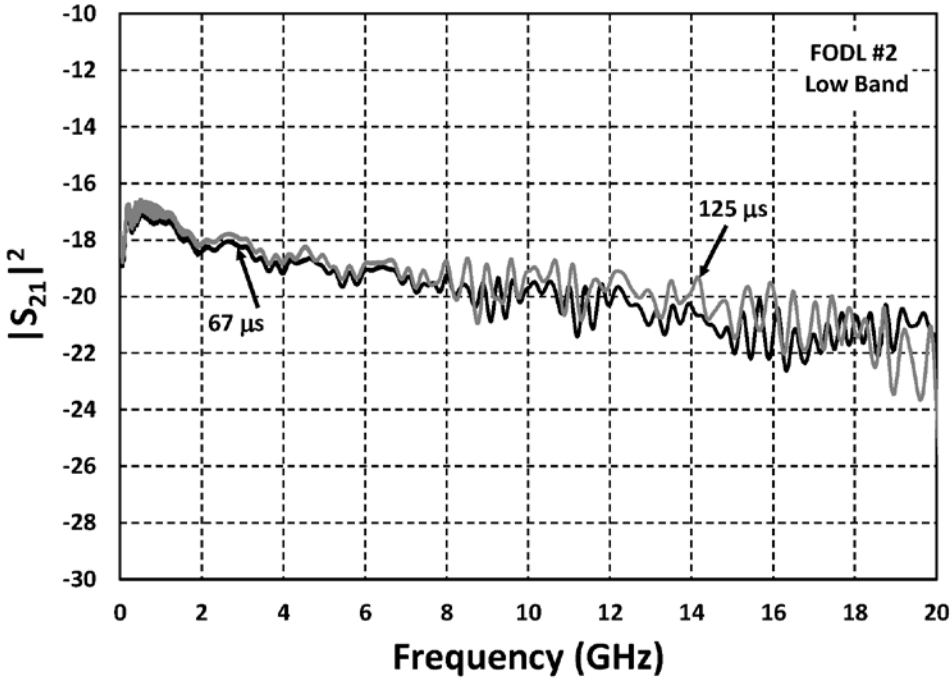
FODL #2
Low Band
125 µs
67 µs
$|S_{21}|^2$
Frequency (GHz)

(a)

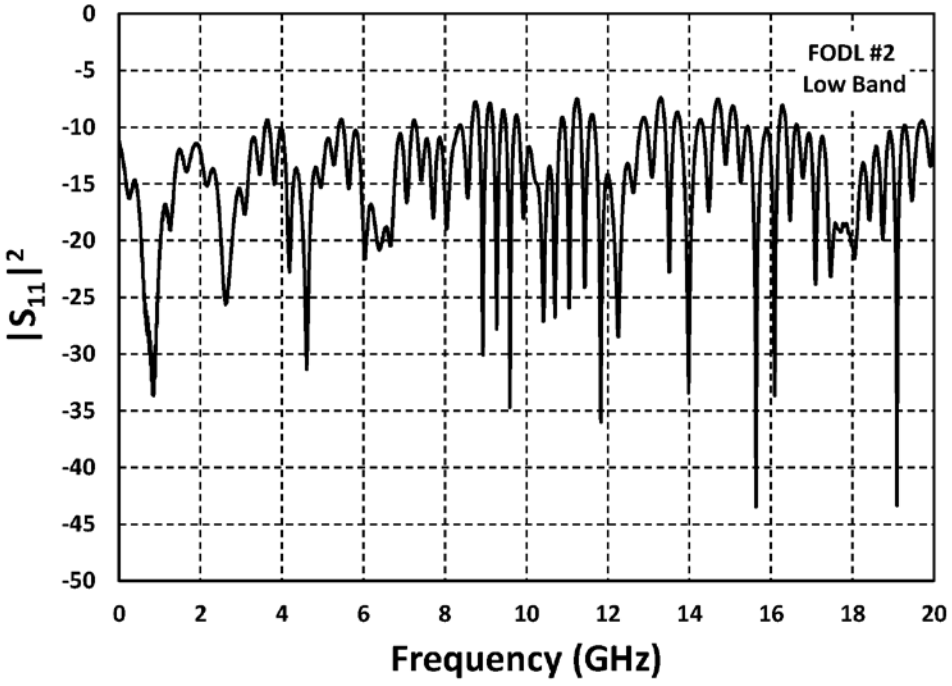
FODL #2
Low Band
$|S_{11}|^2$
Frequency (GHz)

(b)

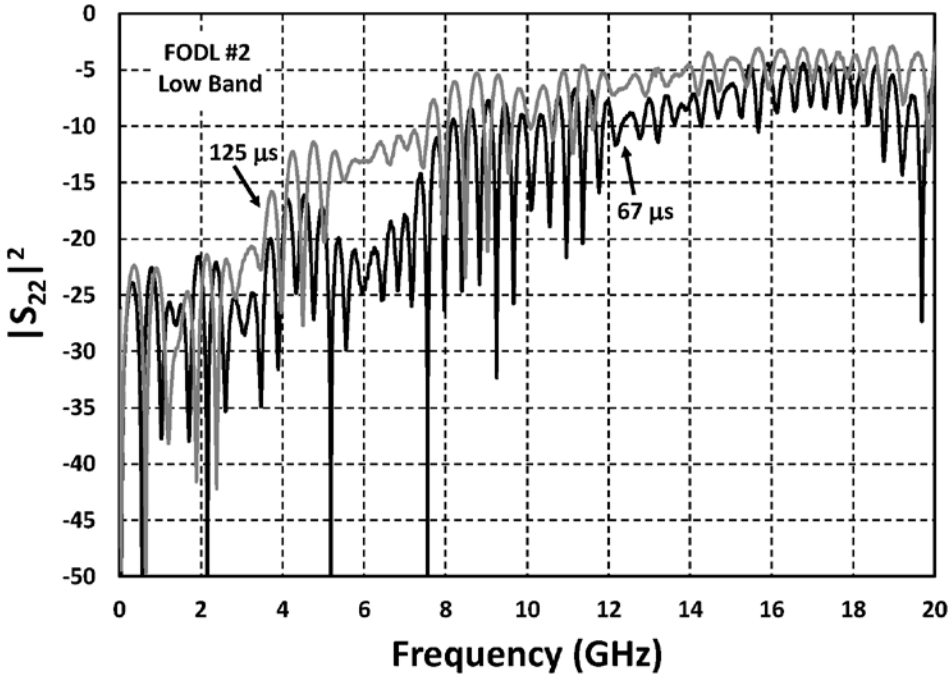

(c)

Fig. 37: Measured S Parameters for the Low Band of FODL #2 showing (a) gain, (b) reflection from the input and (c) reflection from the output.

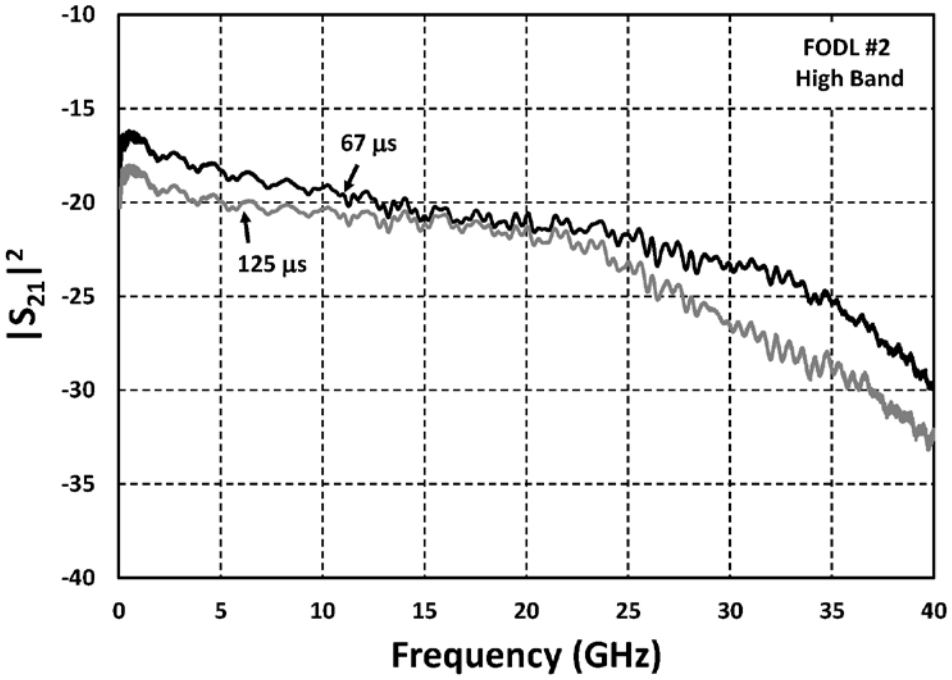

(a)

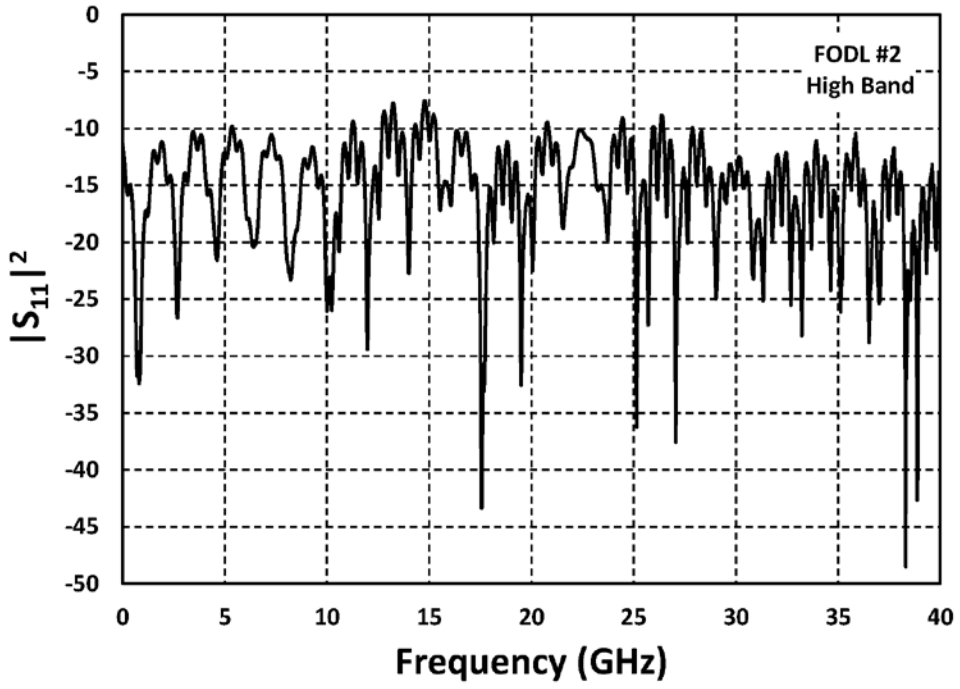

(b)

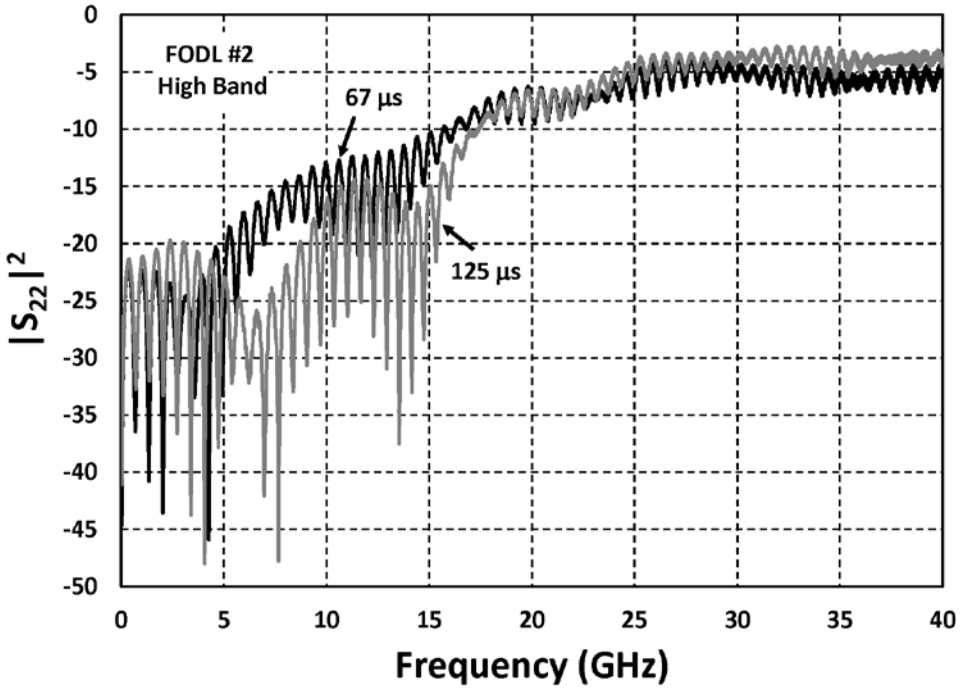

(c)

Fig. 38: Measured S Parameters for the High Band of FODL #2 showing (a) gain, (b) reflection from the input and (c) reflection from the output.

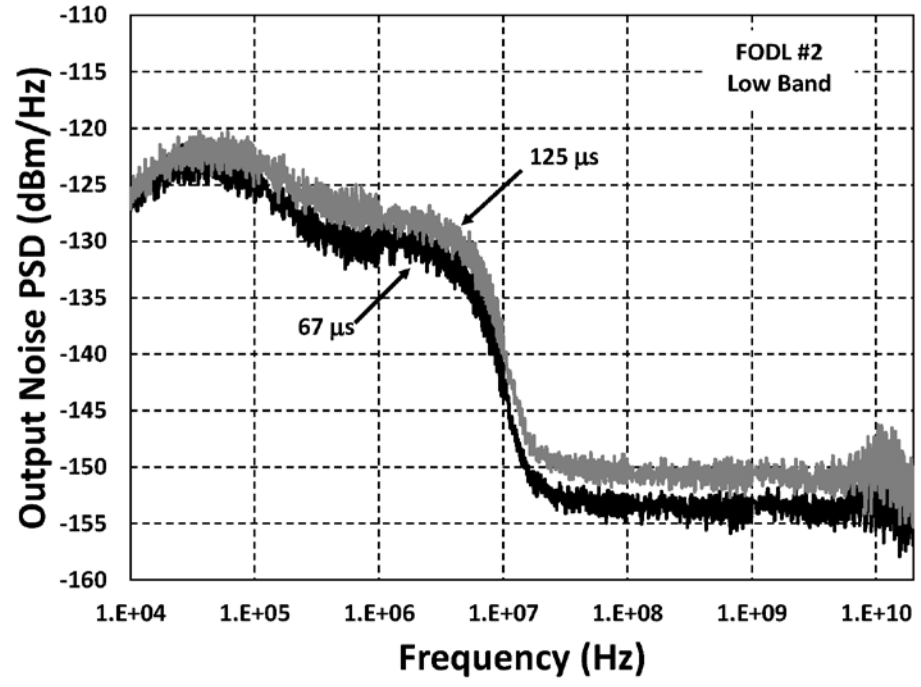

(a)

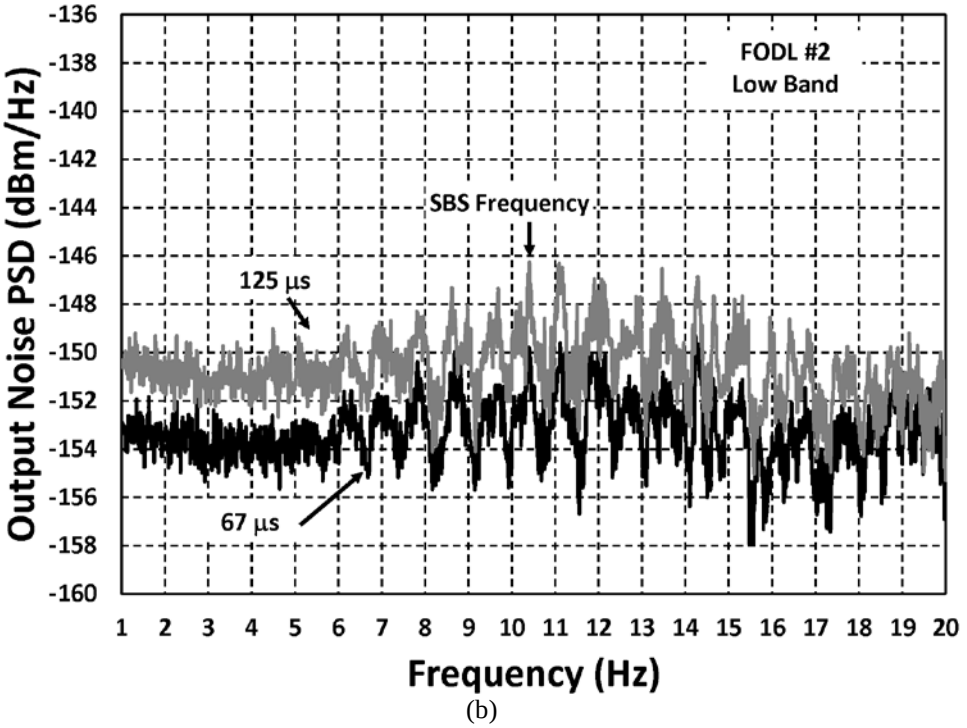

(b)

Fig. 39: Measured output noise power spectral density (PSD) for the Low Band of FODL #2.

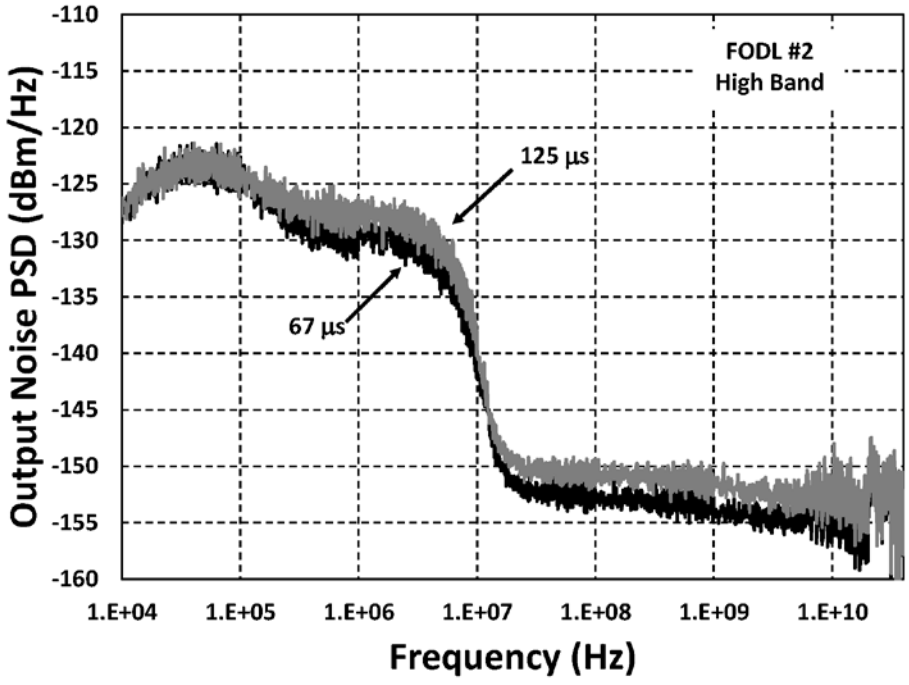

(a)

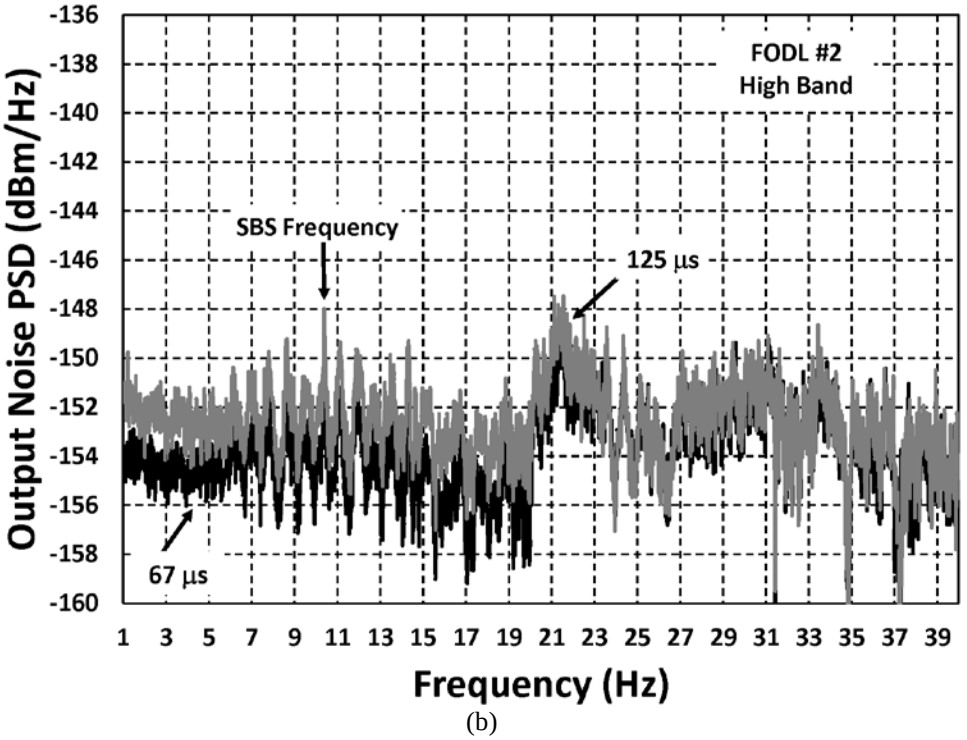

(b)

Fig. 40: Measured output noise power spectral density (PSD) for the High Band of FODL #2.

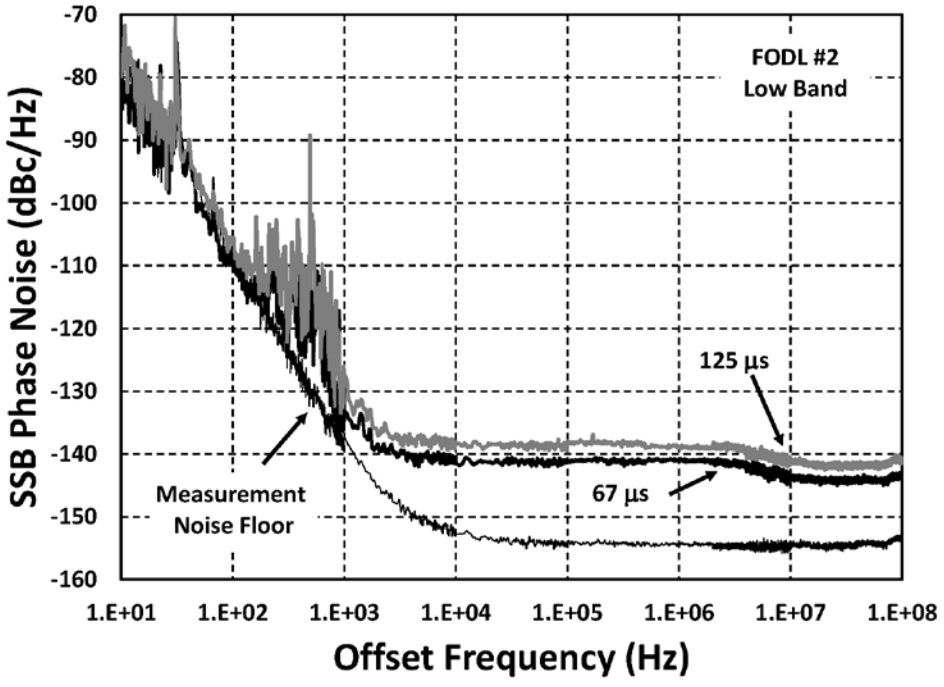

(a)

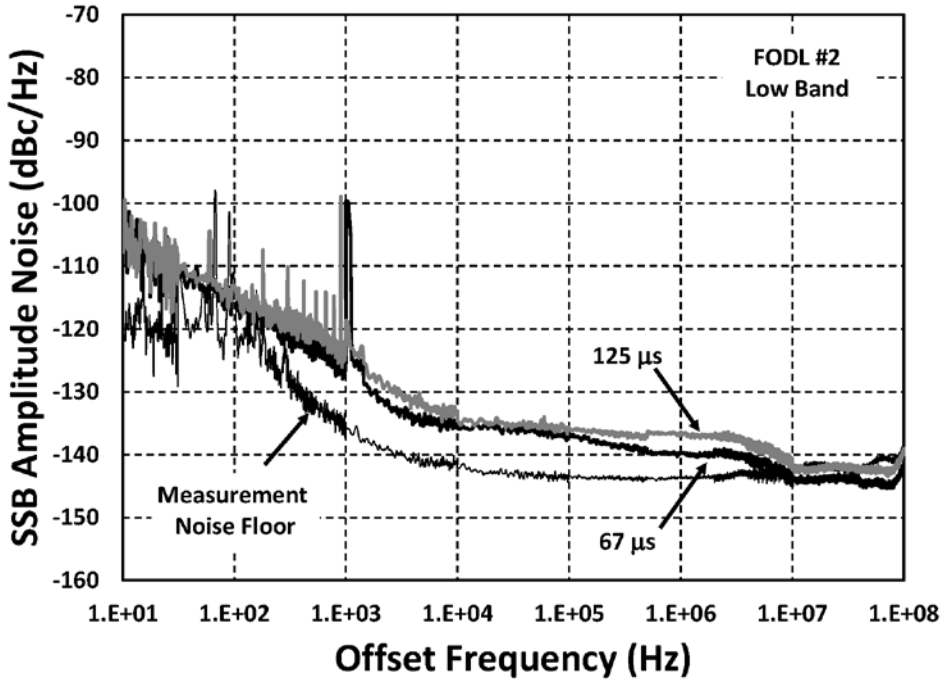

(b)

Fig. 41: Measured single-sideband (a) phase and (b) amplitude noise for a 10.24 GHz carrier using the Low Band of FODL #2.

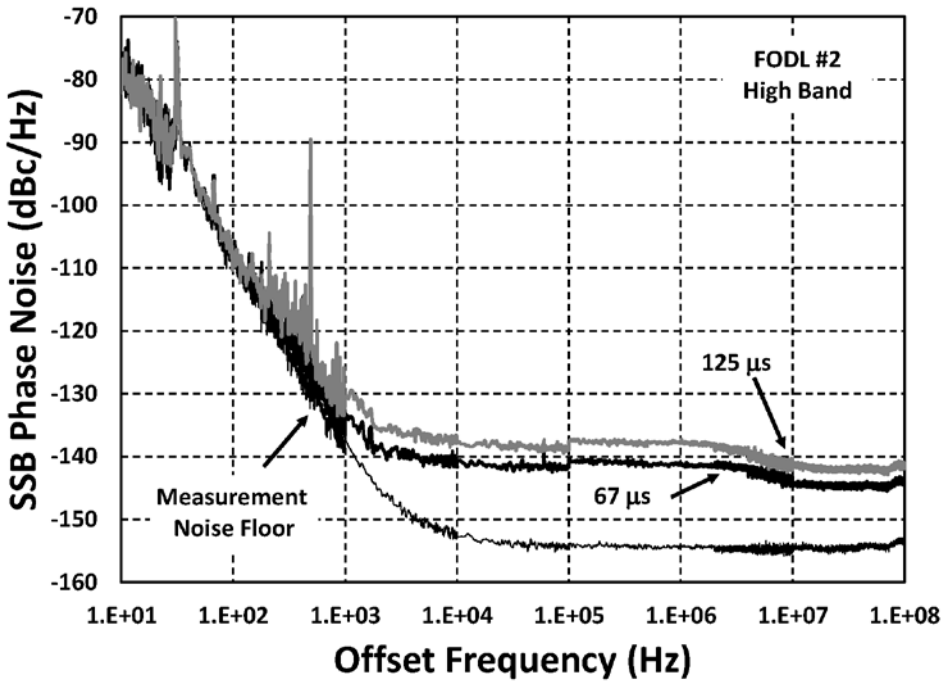

(a)

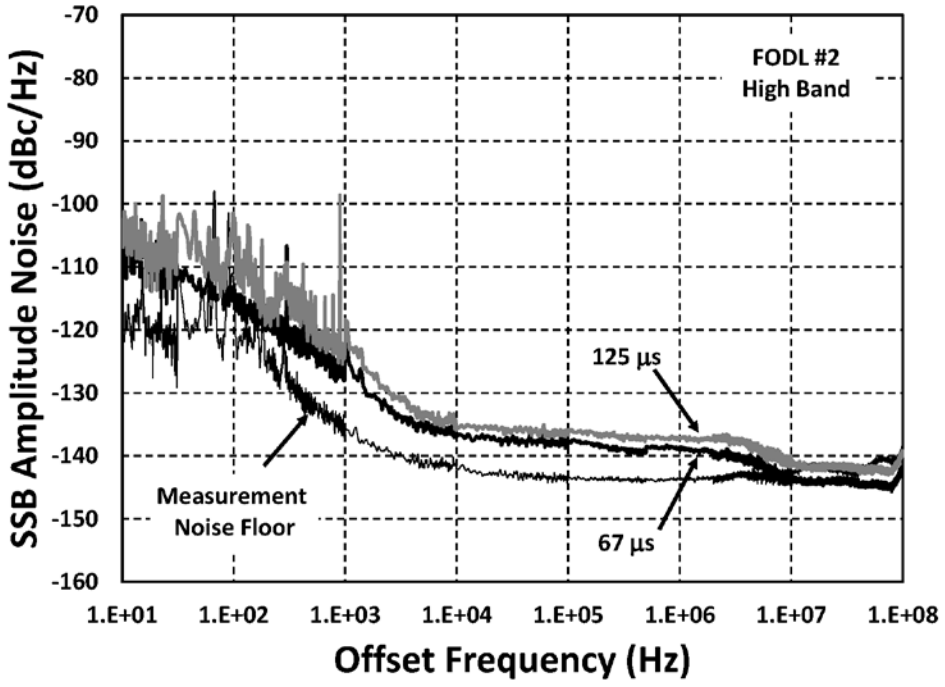

(b)

Fig. 42: Measured single-sideband (a) phase and (b) amplitude noise for a 10.24 GHz carrier using the High Band of FODL #2.

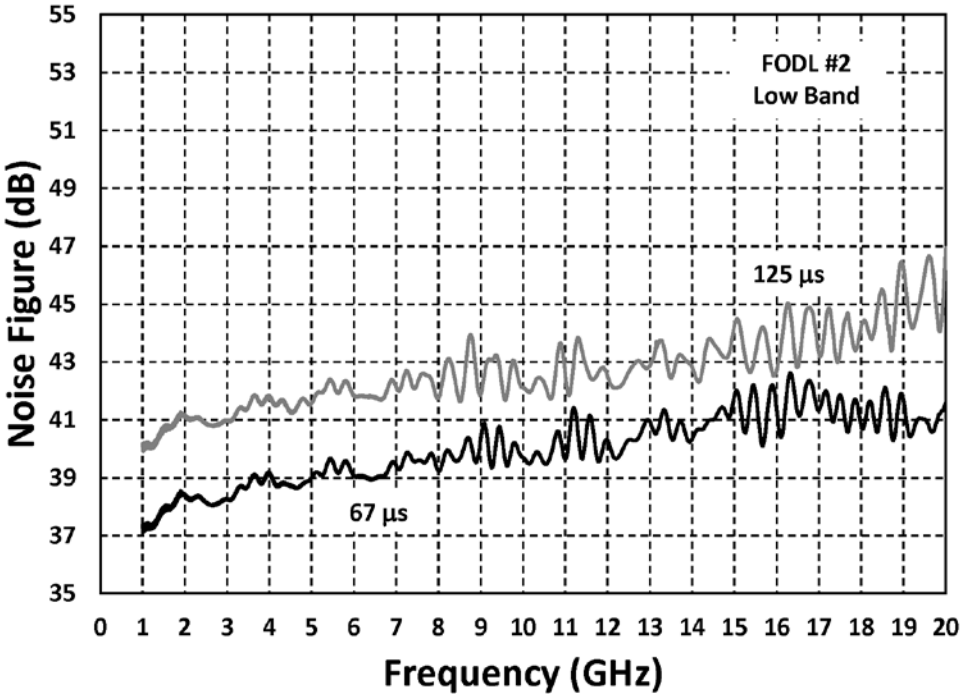

(a)

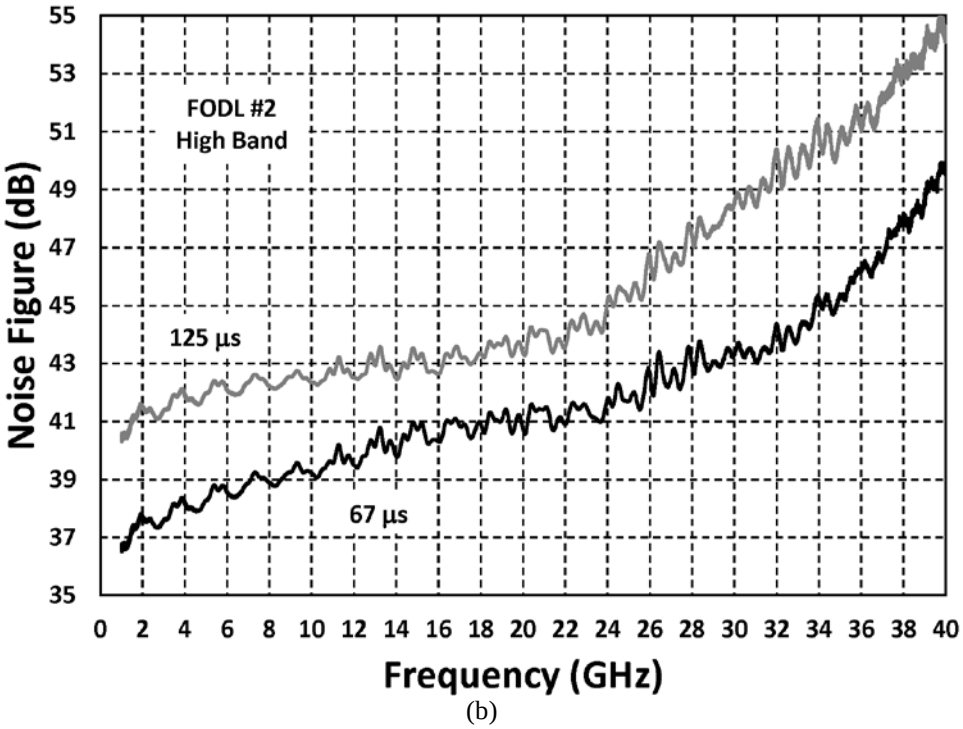

(b)

Fig. 43: Estimated noise figures for FODL #2.

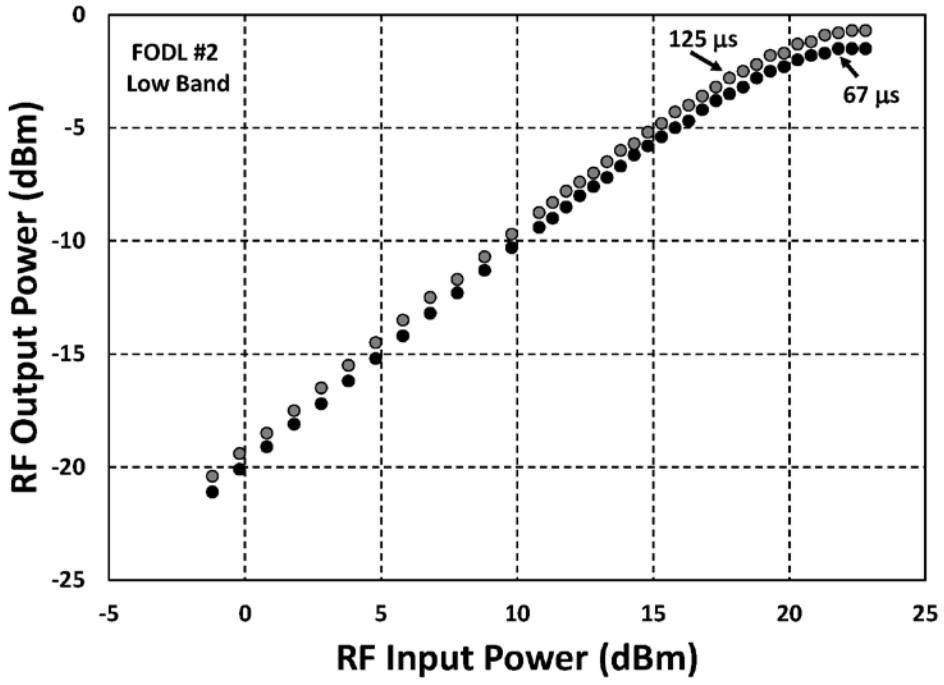

Fig. 44: The measured compression characteristic at 10.24 GHz for the Low Band of FODL #2.

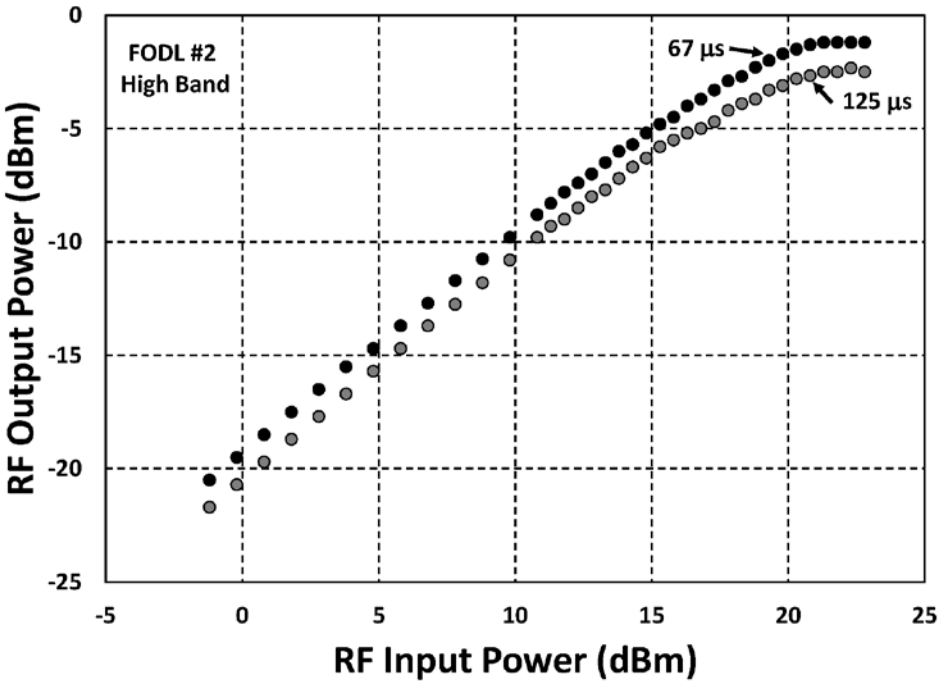

Fig. 45: The measured compression characteristic at 10.24 GHz for the High Band of FODL #2.

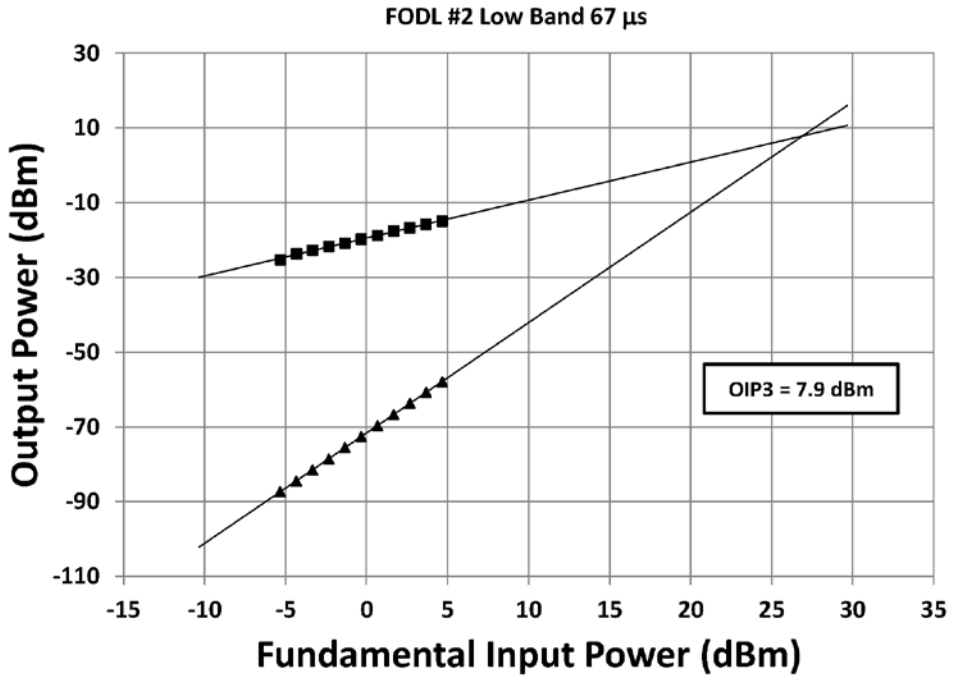

(a)

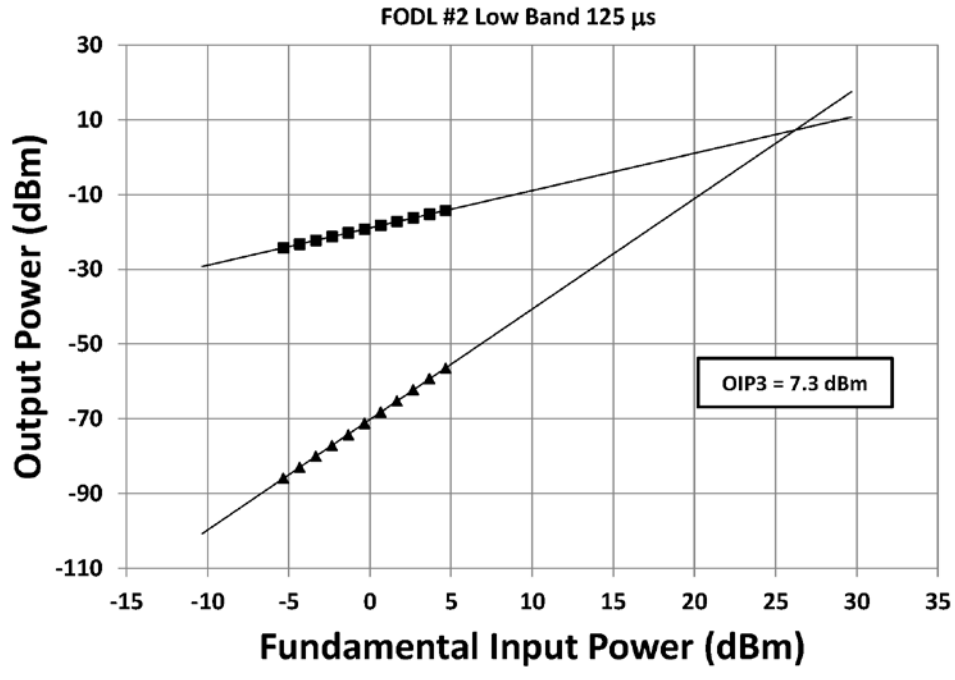

(b)

Fig. 46: Low-Band third-order output intercept point (OIP3) data for FODL #2 near 10.24 GHz. Shown are the fundamental response (squares) and the third-order intermodulation response (triangles).

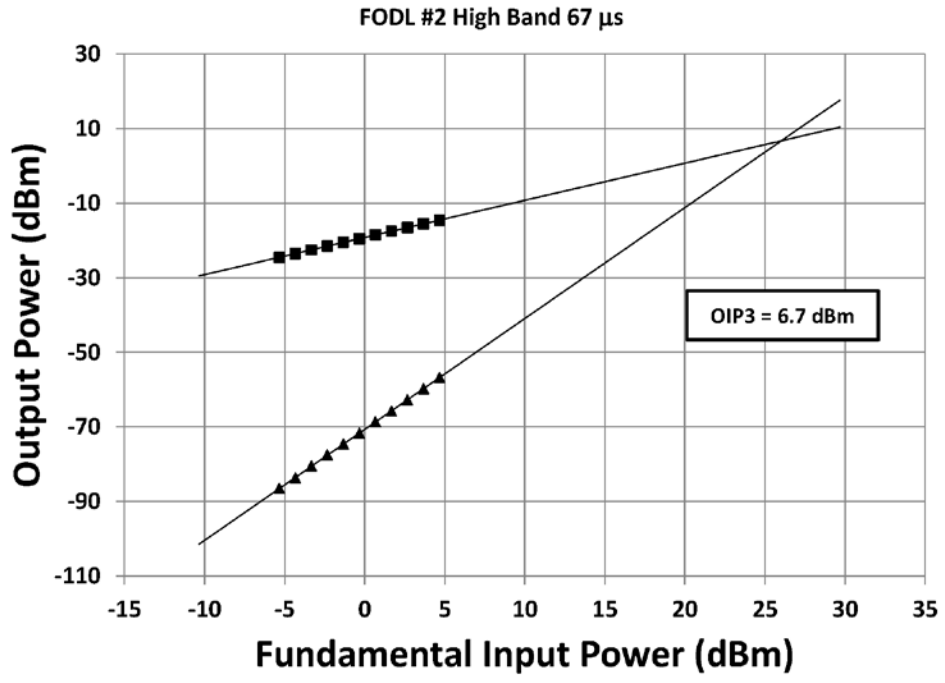

(a)

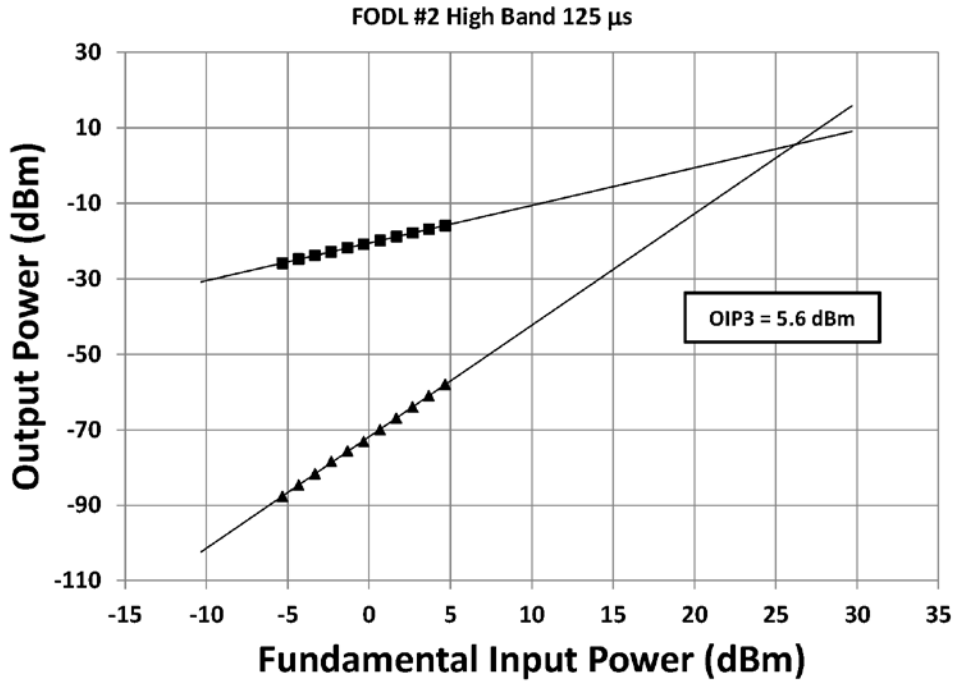

(b)

Fig. 47: High-Band third-order output intercept point (OIP3) data for FODL #2 near 10.24 GHz. Shown are the fundamental response (squares) and the third-order intermodulation response (triangles).

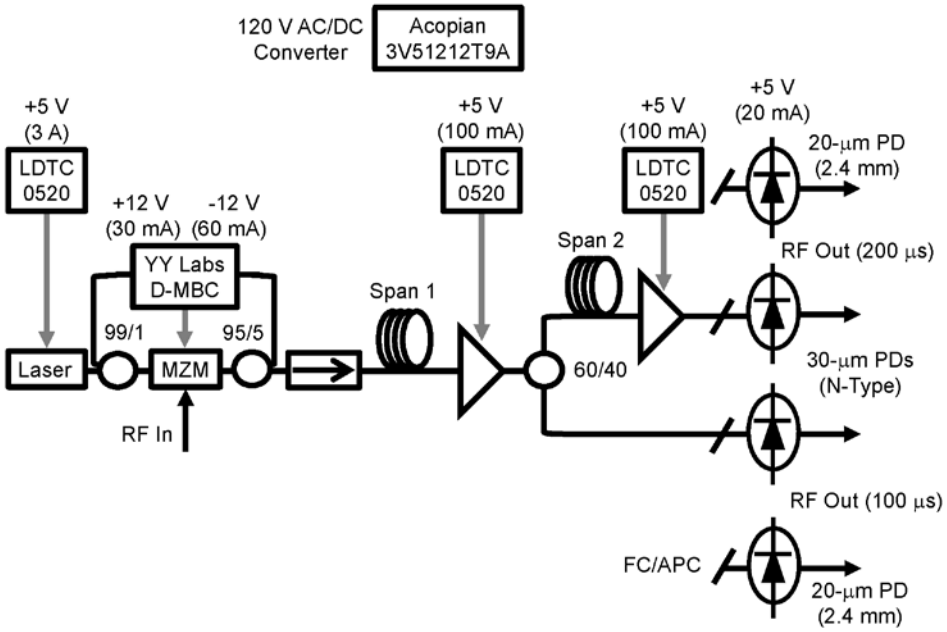

Fig. 48: A block diagram with electrical information for the FODLs.

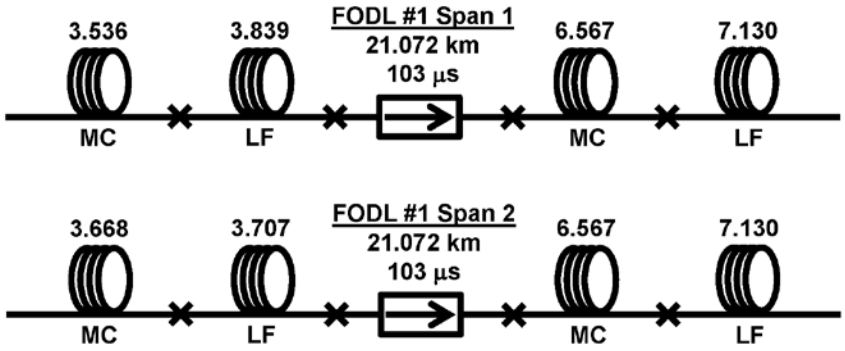

Fig. 49: Fiber layout for FODL #1. Lengths are shown in km. MC: Metrocore, LF: LEAF, Arrow: isolator.

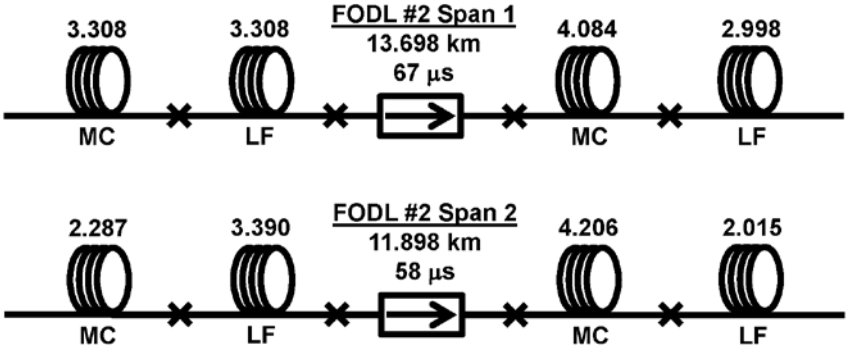

Fig. 50: Fiber layout for FODL #2. Lengths are shown in km. MC: Metrocore, LF: LEAF, Arrow: isolator.

5 HARDWARE DESCRIPTION

A block diagram including electrical connections for the FODLs is shown in Fig. 48. Both FODLs are very similar from a hardware point of view with the only major exception being the fiber layout. Detailed fiber spans for FODL #1 and FODL #2 are shown in Figs. 49 and 50, respectively. The FODL units are built to 19" rack-mount standard and measure 21"×19"×7" (length×width×height). Most of the weight of the units is distributed toward the back half of the box, though it is well balanced left to right. The AC power entry module is located on the rear panel of the units. This module includes a plug for the 120 Volt AC line, a rocker switch and 250 V 3 A fuse. The 120V AC input powers a linear DC power supply that outputs 5 V and ±12 V. The laser controllers make use of the 5 V and the modulator bias controller (MBC) uses the ±12 V. Under normal operating conditions in a room temperature environment the total power consumption is approximately 17 W. Figure 48 depicts typical current draw for the FODLs. If the units are in a warmer or outdoor environment the power consumption will climb significantly. The maximum power the FODLs can consume is 30 W. The front panel (Fig. 51) includes a latching button for activating the laser drivers, an indicator light for AC power, and sets of N-type and 2.4-mm RF bulkheads. There is one input on the left of each set and two outputs on the right, with the shorter delay output above the longer. The two types of RF bulkheads are connected to their respective cables in different manners. The N-type are simply screwed on by hand until the connection feels tight and secure. The 2.4-mm connectors require the use of a 5/16" torque wrench set at 8in-lbs. Care should be taken to not over tighten any of the RF connections.

5.1 Power-Up Procedure

1. Check to see that there is a fuse (250V, 3A) inserted into the fuse tray on the AC power entry module.
2. After checking that the switch is in the open position, as indicated by the "O" symbol on the rocker, connect the 120 AC power cord from a wall plug to the FODL unit.
3. Connect the RF input and output cables to the front panel, without any power on the RF input.
4. Close the switch and the AC power indicator light will come on. At this point the AC line is powering the internal power supply which in turn powers the MBC, the TEC for the laser, and the photodiodes.
5. Press the laser power button on the front panel. The ring illuminator on the button will light. This button activates the current drivers for the laser and the EDFAs.
6. Wait 5 minutes. During this time the laser and modulator will warm up and the MBC will lock the modulator at the appropriate bias point.
7. Turn on the RF input power.

5.2 Power-Down Procedure

1. Turn off the RF power.
2. Disable the laser power button.
3. Switch off the AC power and remove power cord.
4. Remove the RF cabling.

Fig. 51: Photograph of the front panel for one of the FODLs.

5.3 Changing RF Bands

Changing from Low Band to High Band requires moving fiber optic connectors. Before attempting to move these connectors please read the following information.

WARNING: ONLY PERSONNEL WITH EXPERIENCE IN HANDLING FIBER-OPTIC COMPONENTS SHOULD PERFORM THIS TASK

WARNING: POWER MUST BE TURNED OFF TO THE UNIT AND LINE VOLTAGE DISCONNECTED AT THE POWER INLET TO PERFORM THIS PROCEDURE TO PREVENT EXPOSURE TO HIGH VOLTAGE COMPONENTS INSIDE

WARNING: DO NOT REMOVE BOX LID WITH LASER ENABLED

Although the fibers within the box are protected by an outer jacket they are still very fragile and must be handled with care. Optical fiber has a very low tolerance to shear forces; therefore, tight bends in the fiber should be avoided as this can break the glass within the jacketing. When moving the connectors they should be handled only by their metal parts; they should not be moved or handled by the green boots attached to the connectors. The covers on the bulkheads should remain on the unused optical bulkheads at all times. Every time a fiber is disconnected the end face must be cleaned. Any dust or other particulates that may be on the end face of the fiber can result in excess optical loss or damage to the fiber itself necessitating the replacement of the connector. The end face of the connector should never be directly touched. Fiber optic connector cleaners have been supplied with the FODL units. To operate the cleaners press on the blue button and hold it down, which will expose two strips of the cleaning reel. Place the fiber connector end on one of the cleaning strips at right angles to the surface and lightly press it into the material. Then twist and pull the fiber along the strip. Repeat this procedure on the other strip. Once finished, release the blue button.

When inserting a connector into the bulkhead please take note of the alignment. All of the bulkheads have a slot which is made for the key on the connector. The key must be inserted into the slot before the connector is screwed on. Failure to do so will cause loss of optical signal and can cause damage to either or both of the connector/bulkhead pair. The connectors in the FODL are the FC/APC standard. The connectors are screwed onto the bulkhead with a standard right-

hand thread. Do not over tighten the connectors as this can cause misalignment of the fibers and damage to the connectors.

The FODL units are set up to work from 1 MHz to 18 GHz (Low Band) or 1 MHz to 40GHz (High Band). In order to switch between these two bands the following procedure should be followed.

1. Follow the power-down procedure.
2. Remove the box lid.
3. Remove the covers from the fiber bulkheads (see Fig. 52).
4. Disconnect one of the optical fibers on the side farthest away from the front of the box, clean the connector end face with the fiber cleaner, and connect fiber to appropriate bulkhead.
5. Repeat (4) with the remaining fiber.
6. Place the covers on the unused optical bulkheads.
7. Replace box lid.
8. Follow the power-up procedure.

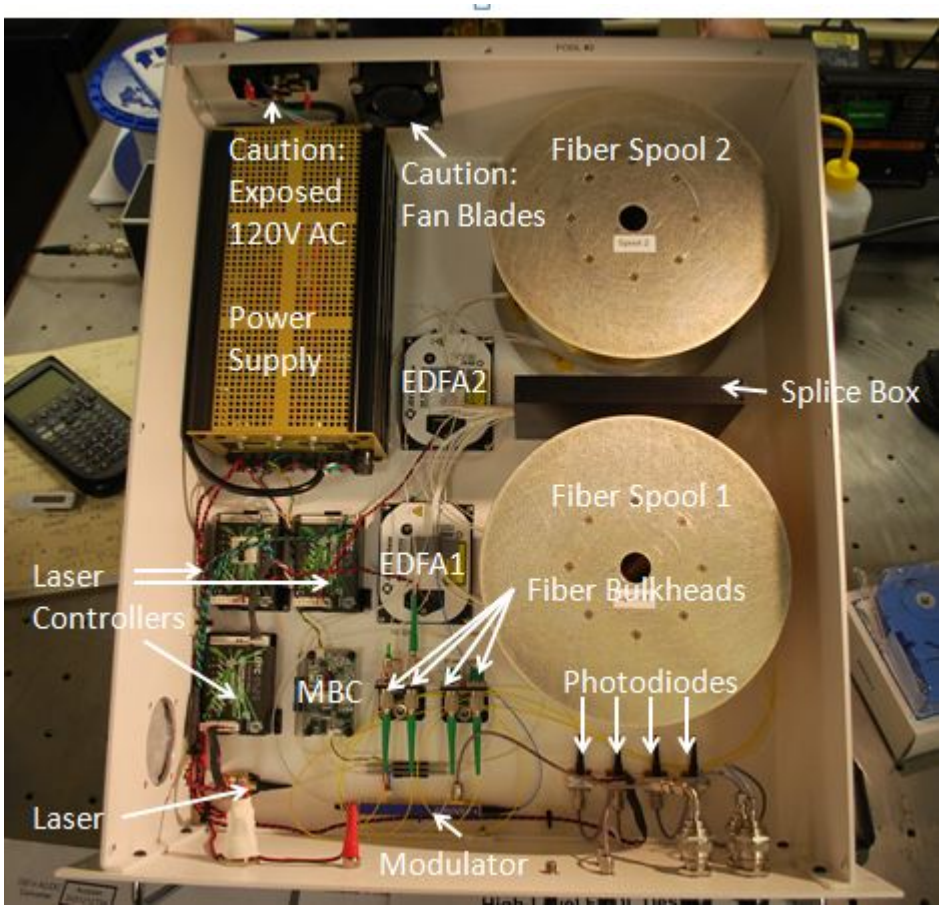

Fig. 52: Photograph of the inside of one of the FODLs.

6 CONCLUDING REMARKS

The design and performance of two FODLs for radar testing applications has been provided. Both delay lines provide 20-GHz (low band) and 40-GHz (high band) channels with delays of 67 μs or 125 μs (FODL #1) and 100 μs or 200 μs (FODL #2). The designs of both FODLs employ COTS parts and therefore can be implemented by others. The designs were geared towards providing wideband solutions at useful delays for radar testing. However, the tools to design variants of the FODLs presented here have also been provided in this report, which should allow for those with differing requirements to conceive a FODL to fit their needs.

The RF performance at the delay times and bandwidth of the FODLs in this report could be improved in two ways. First, the electro-optic front end (laser and modulator) and/or back end (photodiode) could be improved. State-of-the-art components were employed in these designs; however, custom or specialty components could be procured to increase the RF performance of these FODLs. The tradeoffs would be a considerable increase in cost, less reliability and a difficult transition path for a large quantity of FODLs. A second option for increasing the performance of the FODLs presented here would be a more complicated optical transmission span. Tradeoffs for this route include increased cost, size and complexity. The designs implemented here minimized cost, size and complexity in reliable all-COTS units to provide unrivaled RF bandwidth and performance.

Longer delays can be achieved with designs similar to those presented here at the cost of decreased performance. The fiber effects would need to be managed more carefully at longer delays to maintain bandwidth. Conversely, the bandwidth at the present FODL delay times could be increased with more attention on the fiber spans. Beyond fiber effects, the bandwidth limitation is due to the electro-optic modulators and photodiodes. Presently, there are COTS photodiodes available to 110 GHz and modulators to about 67 GHz. There are research-grade modulators presently available to 110 GHz. Such components could be employed but would cost considerably more and not quite reach the RF performance of the FODL units detailed in this report. Narrowband mitigation of fiber effects is also a solution where high carrier frequencies at low fractional bandwidth are required and down-conversion is not desirable.

A high-performance FODL such as those presented in this report will remain a useful technology in applications where digital options for wideband RF memory are lacking. Bandwidth, power consumption, size, scalability and cost are areas where analog FODLs remain ahead of digital approaches. For example, a digital implementation of the FODLs in this report would be costly and consume a large amount of power. The benefits of analog solutions at bandwidths beyond 40 GHz become even more drastic. Therefore, analog FODLs will remain a viable technology for radar testing and other applications for the foreseeable future.

REFERENCES

[1] V. J. Urick, F. Bucholtz, J. D. McKinney, P. S. Devgan, A. L. Campillo, J. L. Dexter, and K. J. Williams, "Long-Haul Analog Photonics," *J. Lightwave Technol.*, vol. 29, no. 8, pp. 1182-1205, Apr. 2011.

[2] V. J. Urick, J. D. McKinney, John F. Diehl, and K. J. Williams, "Wideband Analog Photonic Links: Some Performance Limits and Considerations for Multi-Octave Implementations," *Proc. SPIE*, vol. 8259, Feb. 2012.

[3] Haus, H. A., "IRE standards on methods of measuring noise in linear twoports, 1959," *Proc. of the IRE*, vol. 48, no. 1, pp. 60-68, Jan. 1960.

[4] V. J. Urick, F. Bucholtz, and K. J. Williams, "Optically-amplified short-length analog photonic links," *IEEE Topical Meeting on Microwave Photonics*, Grenoble, France, paper W2.2, Oct. 2006.

[5] E. Desurvire, *Erbium-Doped Fiber Amplifiers Principles and Applications*. Hoboken, NJ: Wiley, 2002.

[6] P. S. Devgan, V. J. Urick, J. D. McKinney, and K. J. Williams, "Cascaded noise penalty for amplified long-haul analog fiber-optic links," *IEEE Trans. Microwave Theory Tech.*, vol. 55, no. 9, pp. 1973-1977. Sept. 2007.

[7] C. Kittel, *Introduction to Solid State Physics*. New York: Wiley, 1996.

[8] G. P. Agrawal, *Nonlinear Fiber Optics*. San Deigo: Academic, 2001.

[9] J. D. McKinney, V. J. Urick, and J. Birguglio, "Optical comb sources for high dynamic range single-span long-haul analog optical links," *IEEE Trans. Microwave Theory Tech.*, vol. 59, no. 12, pp. 3249-3257, Dec. 2011.

[10] A. L. Campillo, F. Bucholtz, K. J. Williams, and P. F. Knapp, "Maximizing optical power throughput in long fiber optic links," NRL Memorandum Report, NRL/MR/56560-06-8946, Apr. 2006.

[11] J. Zhang and M. R. Phillips, "Modeling intensity noise caused by stimulated Brillouin scattering in optical fibers," *Conference on Lasers and Electro-Optics Digest*, paper CMH6, pp. 140-142, May 2005.

[12] P. S. Devgan, J. F. Diehl, V. J. Urick, and K. J. Williams, "Transmission of ultra-low-jitter RF signal with high output power using all-photonic gain and saturated photodetector," in *OFC Technical Digest*, San Diego, paper OTuE4, Mar. 2009.

[13] H. Schmuck, "Comparison of optical millimeter-wave system concepts with regard to chromatic dispersion," *Electron. Lett.*, vol. 31, no. 21, pp. 1848–1849, Oct. 1995.

[14] V. J. Urick, J. Diehl, A. Hastings, C. Sunderman, J. D. McKinney, P. S. Devgan, J. L. Dexter, and K. J. Williams, "Analysis of fiber-optic links for HF antenna remoting," NRL Memorandum Report, NRL/MR/5650-08-9101, Mar. 2008.

[15] J. M. Singley, V. J. Urick and J. F. Diehl, "Characterization of lasers for use in analog photonic links," NRL Memorandum Report, NRL/MR/5650-11-9370, Nov. 2011.

[16] J. F. Diehl, *JDS Uniphase OA-400 Information Sheet*, Internal NRL Document, June 2009.